

# POLITECNICO DI TORINO

Department of Mechanical and Aerospace Engineering

Class LM-33 (DM270)



**Politecnico  
di Torino**

Master's Thesis

in

Automotive Engineering

## **Design of the Upright Assembly of a Formula Student Prototype**



**SQUADRA | CORSE**  
**POLITO**

**Tutors:**

**Prof. Andrea Tonoli**

**Eng. Stefano Favelli**

**Candidate:**

**Riccardo Pastorino**

Academic Year 2022/2023



***Dedicata a...***

*In primis alla mia famiglia, se sono qui oggi è solamente grazie a loro, a loro che mi hanno sostenuto e spronato in ogni momento, a loro che mi hanno insegnato a crescere e a farmi strada.*

*Ai miei amici, di vecchia data e recenti, il percorso universitario è difficile e tortuoso ma è proprio vero che i viaggi volano se si è in compagnia.*

*Ai colleghi ed amici di Squadra Corse, senza il vostro aiuto questa Tesi non sarebbe stata possibile, ricordate che l'unione fa la forza, non mollate mai.*

*Per ultimi ma, certamente, non per importanza, ci tengo a ringraziare Stefano: una vera e propria guida durante questi due anni di esperienza nel Team e in questi mesi di stesura della tesi; ed il Professor Andrea Tonoli, per la fiducia dimostrata all'inizio del mio percorso da Team Leader ed in questo lavoro.*

***Grazie ancora a tutti,***

*Piccolo*





# Contents

<b>Contents</b>	<b>4</b>
<b>Abstract</b>	<b>6</b>
<b>1. Introduction</b>	<b>7</b>
1.1. Formula Student	8
1.2. Squadra Corse PoliTO	10
1.3. Unsprung Masses Division	13
1.4. Thesis Outline	16
<b>2. 2021 Upright assembly analysis</b>	<b>17</b>
2.1. 2021 Production technology and material	18
2.2. Boundary condition and load application	24
2.3. Topology optimisation and FEM analysis	27
2.4. Final component outcomes	33
2.5. Track testing failure	40
<b>3. Design Specifications</b>	<b>42</b>
3.1. What was to be changed from 2021?	43
3.2. Static load cases	43
3.3. Targets: weight, reliability, stiffness	45
<b>4. 2022 Solution analysis</b>	<b>47</b>
4.1. 2022 Production technology and material	47
4.2. 2022 Boundary conditions	51
4.3. FEM Model	52
4.4. Topology optimisation	66
<b>5. Results and testing</b>	<b>71</b>
5.1. FEM results	74
5.2. Production-CAD discrepancies	81
5.3. Assembly and testing	82
5.4. Setup shims and flip chip	84
<b>6. Fatigue analysis</b>	<b>87</b>
6.1. Load spectrum	88
6.2. Fatigue analysis setup	93
6.3. Fatigue analysis results	97
<b>7. Conclusions and future works</b>	<b>99</b>
<b>References</b>	<b>101</b>

<b>List of Figures</b>	<b>102</b>
<b>List of Tables</b>	<b>105</b>
<b>Abbreviations</b>	<b>105</b>

# Abstract

The upright assembly is a key structural element in the wheel assembly of any car, especially in high performance vehicles in which the suspension assembly has a lot of distinct elements. Differently from common passenger cars, in this study the main goal is focused on lowering the weight and maximise the stiffness of the components. Doing so it is possible to increase the overall performances of the vehicle both in terms of longitudinal and lateral accelerations.

This study has been carried out on a Formula Student prototype, a 4-Wheel-Drive (4WD) fully electric racing vehicle. In particular the vehicle on which the assembly has been designed is the one of Squadra Corse PoliTO, the racing Team of Politecnico di Torino, in which I had the opportunity to work as a Mechanical Designer in the Unsprung Masses division in the first year and as Team Leader in the second year of my experience.

This work aims to provide a tested and reliable workflow to follow when performing the design of a bespoke upright assembly. In particular the main aspects that will be delighted are the Topology Optimization and the Finite Element Method (FEM) Analysis. Of course, many other topics will be explained and discussed such as the production method, the material and the after-treatments. Another aspect of study will be a brief fatigue analysis performed using Altair HyperLife.

The software used in this study are CATIA V5, Altair HyperMesh and Altair Inspire apart from the obvious Microsoft Office Suite.

Comparative analysis have been performed between the solution studied for the 2022 season prototype (SC22), detailed in this work, and the 2021 vehicle (SC21). In particular the two solution have a lot of differences despite being the same assembly of two vehicles which have not be overturned from one year to the next.

The results obtained marked a significant improvement in terms of safety factor, especially in critical load cases; instead, from the stiffness point of view, the new solution isn't impressive also due to the intrinsic properties of the production process adopted.

This work highlights a lot of aspects that could be detailed in future studies both strictly related to upright assemblies and to production methods and materials.

# 1. Introduction

The design process of a racing prototype is focused on maximizing the performances while maintaining a sufficiently high reliability of the system. The overall performance of a race car is constituted by its longitudinal and lateral dynamic characteristics.

One of the key factors is the weight, especially the one constituted by the unsprung masses which are in general all the components connected to the wheels. For the majority of the cases, in a Formula Student prototype, the car adopts outboard motors directly connected to the transmission inside the upright; this increases even more the weight of the unsprung masses and so their impact on performance.

The Upright assembly is mainly constituted by the upright himself and some other pieces useful to link it to the suspension and brake assembly. In particular the solution adopted by Squadra Corse PoliTO relies on a double wishbone suspension scheme, inside the upright there is a two-stage planetary gear set linked to the motor on vehicle side and to the wheel hub on the other side of the upright.

Before to start the proper thesis work, it is dutiful to introduce the Formula Student championship and the characteristics that lead it to be, every year, more and more important for the Automotive world and manufacturers. After that, a glimpse of my Team, Squadra Corse PoliTO.

## 1.1. Formula Student

Formula Student is an international engineering competition for university students that challenges teams to design, build, and race a formula-style race car. Formula Student provides a platform for students to apply their theoretical knowledge in a real-world setting, and to develop skills in teamwork, communication, leadership, innovation, and entrepreneurship.



*Figure 1 – Formula Student Germany 2022 Panoramic Picture*

The goal of Formula Student is to foster the next generation of engineers, innovators, and leaders in the automotive and motorsport industries, and to promote sustainability, safety, and affordability in motorsport. The competition involves a series of static and dynamic events, which test the performance, reliability, and cost-effectiveness of the cars. The events are:

### Static events:

- **Engineering Design Event:** teams present their car design to a panel of judges, who evaluate the car's design, innovation, and feasibility. The judges can ask questions to test the team's knowledge of the car's design, validation and engineering principles.
- **Cost and Manufacturing:** In this event, teams present a cost report detailing the cost of materials and manufacturing processes used in the car's design and production.
- **Business Plan presentation:** here all the teams present a business case for their car, detailing the marketing and sponsorship strategies, financial planning, and sustainability aspects of their project.

### Dynamic events:

- **Acceleration:** a simple straight-line acceleration over a 75 meter track, the fastest car wins. Traction and low aerodynamic drag are the key factors to win this event.
- **Skidpad:** in this event the car needs to complete a figure of eight pattern, doing 2 laps of the right circle and 2 laps of the left one. The second lap of

each circle will be timed and their average, plus penalties, if any, will be the total time of the run. This event tests the car's cornering grip and stability.

- **Autocross:** this event is like a qualifying session of F1. Drivers go through a technical track full of tight turns, chicanes, and slaloms. The event tests the car's handling, agility, and driver skill.
- **Endurance & Efficiency:** the endurance event evaluates the car's durability and reliability by testing its performance over a long distance race, the track has the same characteristics of the Autocross one and the total event is around 22 km long. After the course is completed, the total energy consumption, taking into account also the regenerated amount as a negative contribution, is calculated and so the efficiency event leader board is established.

To participate in Formula Student, each team must design and build a single-seater, open-wheeled, formula-style race car that complies with a set of technical regulations and safety standards. To take part in dynamic events the Team must pass a series of technical inspections and tests such as the electrical inspections, mechanical inspections, the brake test and the rain test.

The future of Formula Student is promising, as the competition continues to evolve and adapt to the changing landscape of motorsport and mobility. The competition is expected to embrace new technologies, such as autonomous driving, electric and hybrid powertrains, and advanced materials and manufacturing methods. Overall, Formula Student is an exciting and rewarding program that offers students a unique and valuable experience in the world of engineering and motorsport.

## 1.2. Squadra Corse PoliTO

Squadra Corse is the Formula Student team of the Politecnico di Torino. It was born in 2004, as the first ever Team of the Turin university, with the objective of competing in the Formula Student championships. In 2005 the first prototype was produced and competed, of course featuring an Internal Combustion Engine.



*Figure 2 - Squadra Corse PoliTO 2005 Prototype (SC05)*

In 2009 the first hybrid prototype was developed by the Team and won the world championship, in the hybrid category, in 2010. The car was named SC08H and was an evolution of the already good performing, and victorious, 2008 car.



*Figure 3 - Squadra Corse PoliTO 2009/10 Prototype (SC08H)*

In 2012 Squadra Corse was the first Italian team to participate in the Electric category and so the first fully electric prototype was designed, the SC12e.



*Figure 4 - Squadra Corse PoliTO 2012 Prototype (SC12e)*

The 2022 car has been the tenth fully electric prototype of the Team, the most recent and sophisticated of the history of Squadra Corse, named 'Aurora'. It has the following technical characteristics:

- ✍ Mass without driver 211 kg
- ✍ Full carbon fibre monocoque
- ✍ 4WD outboard AMK electric motors independently controlled
- ✍ Front mass repartition 47.5 %
- ✍ Wheelbase length 1.525 m
- ✍ Track width 1.2 m
- ✍ 185/40 R13 slick tires on 13" OZ Racing magnesium-aluminium alloy rims
- ✍ Aerodynamic  $Cl^*A$  4.8
- ✍ Aerodynamic efficiency 3.1
- ✍ Maximum power 80 kW (limited by the rules)
- ✍ 0-100 km/h 2,6 s



*Figure 5 - Squadra Corse PoliTO 2022 Prototype (SC22, 'Aurora')*



During the 2022 Season the team participated to 3 events: Formula SAE Italy (FSATA), Formula Student Germany (FSG) and Formula Student Alpe Adria (FSAA) and collected very good results in terms of overall performances. The main downside of the year has been the electric reliability that forced the prototype to not complete the Endurance events.

At FSATA the Team gained 2<sup>nd</sup> place in the Engineering Design as well as in both the Skidpad and Autocross event. In Croatia (FSAA) we got 3<sup>rd</sup> place in Cost and Manufacturing and 4<sup>th</sup> place in the Acceleration event, scoring 3.56 seconds: the overall record of the Team!



*Figure 6 - FSAA Award ceremony and celebration*

To conclude this section dedicated to the Team, I'm proud to say that for the current 2023 season, I served as the Team Leader of this extraordinary reality. An incredible group of 65 students from 10 different degree courses. Despite the fact that we were unable to produce a new prototype and participate in the 2023 events due to financial constraints, it was a fantastic year full of unforgettable experiences. We took advantage of the enforced shutdown year to re-organize the Team, with the hope and objective to come back stronger in 2024!



*Figure 7 - Squadra Corse 2023 Team*

### 1.3. Unsprung Masses Division

For the Season 2021/22 I was part of the Unsprung Masses division, which, despite the obvious name wasn't responsible only for specifically not sprung masses components but also driver interface sub-systems. The division was composed of 8 members guided by the Division Leader. Unsprung masses is a really important division of the Team because it is responsible for the large part of the mechanical subsystems. Suffice it to say that the division handles 28% of the total weight of the prototype.



*Figure 8 - Unsprung Masses 2021/22 Division*

In particular the Division was in charge of the design of:

- ✍ **Anti-roll Bar:** the mechanical system that regulates the car behaviour in roll conditions.
- ✍ **Brakes:** callipers and master cylinders are OEM components but the disks are made by the team starting from scratch.
- ✍ **Suspensions:** double wishbone layout with carbon fibre tubes and aluminium inserts.
- ✍ **Pedal box:** one of the driver main interfaces with the prototype, very important sub-system to allow the driver to have the perfect feeling to push continuously, especially on the brake pedal.
- ✍ **Steering:** critical subsystem in terms of tolerances and free play, another driver interface component. It has similar solution to the suspensions assembly in terms of materials and production technology.
- ✍ **Upright:** the assembly which will be explained in this thesis work. It is needed to connect brakes and suspensions to the rim and consequently to the tire itself; passing through the transmission assembly.

**Rims:** the term speaks for itself. Currently the focus is all on the development and design of custom carbon fibre rims, to lower the weight and increase stiffness with respect to the magnesium alloy ones adopted until now.

Here below a 3D view of all the components designed, ordered and assembled by the Division.

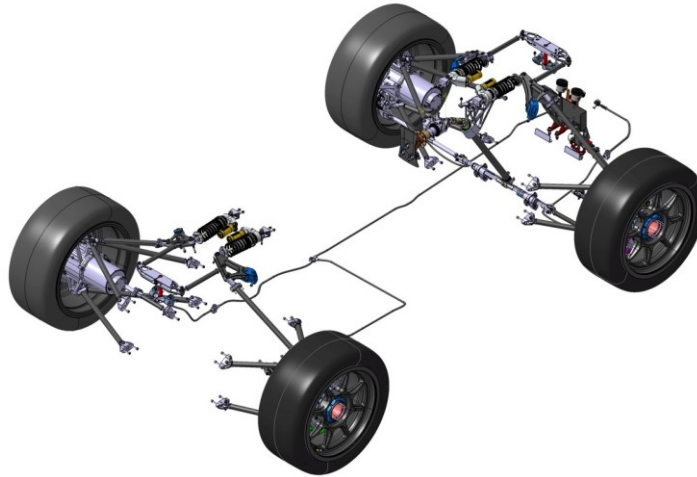


*Figure 9 – SC22 Unprung Masses Assembly*

To better understand the focus of this work it's important to have a clear view of the wheel assembly of our car. Here below there is a detailed view of the front right wheel assembly, the upright is marked in fuchsia colour just to highlight it.

Formula Student paddock is entirely focused on using very small rims: 13 inches are the most adopted, we also use them, 10 inches rims are increasing in number and only 1 pioneer Team is using 8 inches ones as crazy as it may sound. Either way, in a Formula Student prototype the space is always a big issue, especially inside the rims with the large number of subsystems that are needed to be placed there.

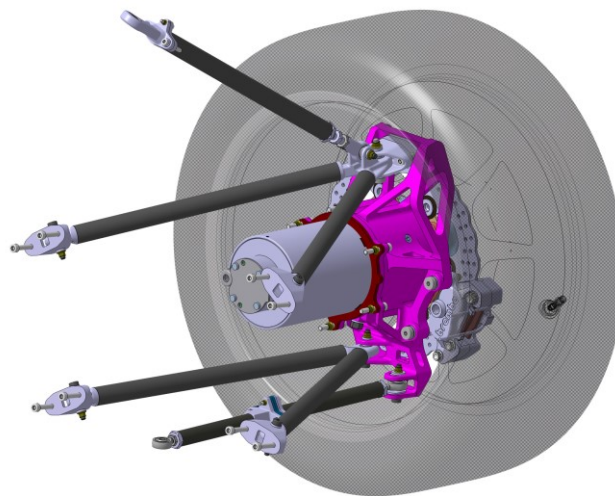


*Figure 10 – SC22 Front Wheel Assembly*

The suspension scheme adopted is double wishbone coupled with a push-rod and a tie-rod; of course both camber and toe are adjustable as well as the ride height. The electric motor is placed in outboard position with its output shaft directly connected to the transmission by means of a grooved profile. The transmission, a two stage planetary gear set, with a fixed ratio of 14.69 is mounted inside the upright itself. A fixed calliper made by Brembo, 4 pistons for the front axle and 2 pistons for the rear one, is mounted on the upright using two M7 bolts.

The upright has to comply to many geometrical constraints taking into account not only the external envelope but also the several mounting points and holes to connect all the subsystems explained here above. The upright assembly is made up of very few components and the upright itself is the bigger, more critical and more complicated one. As a result, in this work, we will focus mainly on the upright, while the other components and elements will be covered in a separate chapter.

## 1.4. Thesis Outline

This thesis work is structured in 6 chapters as detailed here:

1. **Chapter 1: Introduction**
2. **Chapter 2: 2021 Upright assembly analysis.** In this chapter the solution adopted by the Team, for the previous season, will be explained.
3. **Chapter 3: Design Specifications.** Here there will be listed and detailed the 2022 design targets: starting from the improvement that were needed to achieve compared to the 2021 solution, all the load spectrums used for the design and finally the performance targets (weight, stiffness and reliability).
4. **Chapter 4: 2022 Solution analysis.** The main chapter of this thesis work in which all the 2022 Upright assembly design will be explained: material choice, production technology, FEM model and topology optimisation.
5. **Chapter 5: Results and testing.** Final component FEM results, production-CAD discrepancies and assembly on the prototype.
6. **Chapter 6: Fatigue analysis.** This is a chapter dedicated to the post-design fatigue verification using HyperLife.
7. **Chapter 7: Conclusions and future works**

## 2. 2021 Upright assembly analysis

After the 2020 Season stop, forced by the well-known pandemic situation, in 2021 the Team decided to experiment a new production technology and material solution for the Upright assembly.

The 2021 prototype (SC21) has been a big step-forward for the Team in terms of monocoque design, wheel assembly and suspension subsystem. The upright design has been guided by the change in the transmission assembly and motor-plate attachment geometry.

The main targets that led to the testing of a new production technology were to increase the rigidity and reduce the mass, both achievable thanks to the 3D printing method. This innovative project has been carried out in collaboration with Prima Additive, a Team's Gold Sponsor.

I want to specify that I was not part of the Team during the 2021 Season and I was not involved in any design decision or process for that year's solution. In this chapter I will present and analyse it from the perspective of myself being the designer of the 2022 solution. This was done to understand the starting point of my 2022 design phase and to set the comparison between the SC21 Upright assembly and the SC22 one.

## 2.1. 2021 Production technology and material

The production technology chosen was the additive manufacturing, in particular, Laser Powder Bed Fusion (LPBF). LPBF uses a laser beam to selectively melt fine metal powder and build up fully-dense parts layer-by-layer.

The building process starts with the deposition of a layer of metal powder on the building platform by a re-coater blade. The laser beam melts the powder according to the slice geometry tracing the cross-section. After irradiation, the platform is lowered by a vertical distance equal to the layer thickness and the sequence is repeated until completion of the part. At the end of the building process, the un-melted powder is removed from the platform with the part, which is then removed from the platform. The entire process is performed in an inert environment thanks to a continuous gas smoke flowing in the machine. Because it is made from compressed air and is relatively inexpensive, the gas used today is primarily molecular nitrogen (N<sub>2</sub>).

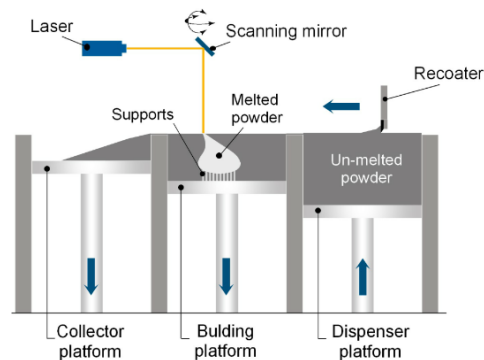


*Figure 11 – LPBF Printing Process*

The machine produced and proposed to the team by Prima Additive is the Print Sharp 250: a medium-volume machine for powder bed fusion applications, developed for the industrial production of complex components.



*Figure 12 – Print Sharp 250 Prima Additive*

In the following table are listed all the technical specs of the machine. It is interesting to notice the laser power of 500 W, which is exactly in the middle range of LPBF machines, and the printing volume of 250 x 250 x 300 mm. Because of the limited construction capacity,



only one upright could be printed at a time by rotating it 45° around the machine's z-axis, thus 2D nesting was not feasible.

<b>Dimensions (LxWxH)</b>	3500mm (L) x 1100mm (W) x 2450mm (H)
<b>Weight</b>	2000 kg
<b>Power Supply</b>	380 V / 50 Hz / 8 kW
<b>Type of Laser</b>	Laser Yb (Ytterbium) IR single mode
<b>Laser Power</b>	500 W
<b>Laser Focus Diameter</b>	70 – 100 µm
<b>Beam Wavelength</b>	1060 – 1080 nm
<b>Building Volume</b>	250 x 250 x 300 mm
<b>Beam Deflection Speed</b>	8 m/s
<b>Positioning Speed</b>	10 m/s
<b>Build Rate</b>	12 – 30 cm <sup>3</sup> /h
<b>Layer Thickness</b>	0,02 – 0,1 mm
<b>Layer Width</b>	0,1 mm (single line width)
<b>Re-coater specs</b>	Travel: 650 mm
<b>Building platform z-axis</b>	Travel: 300mm / Speed: max 6mm/s / Res: 0,01 mm
<b>Heating platform</b>	Up to 200° C
<b>Monitoring of O<sub>2</sub> level</b>	Below 100 ppm (0,01%)
<b>Permissible room temperature</b>	15 – 30° C
<b>Gas (Consumption – running/filling)</b>	7 l/min (running)
<b>System Fill Consumption</b>	20 l/min (up to filling)
<b>CAM Software</b>	Materialise Magics
<b>Control &amp; Other software</b>	Eplus control software (EPC)
<b>Industrial interfaces</b>	Ethernet

*Table 1 – Print Sharp 250 Prima Additive Technical Specifications*

The material proposed and chosen was an aluminium alloy very commonly adopted in additive manufacturing: AlSi10Mg. It has good mechanical properties and relatively low density, this is why is largely used in aerospace and automotive applications.

Here below, both the chemical composition and mechanical properties of the material provided by Prima Additive are listed.

Chemical Composition (% - Weight)										
Si	Fe	Cu	Mn	Mg	Ni	Zn	Pb	Sn	Ti	Al
9 - 11	≤ 0,55	≤ 0,05	≤ 0,45	0,2-0,45	≤ 0,05	≤ 0,1	≤ 0,05	≤ 0,05	≤ 0,15	Res.
Mechanical Data										
<b>Particle Size Distribution</b>										20 – 63 µm
<b>Density</b>										2,65 g/cm <sup>3</sup>
<b>Part Accuracy</b>										≤ 0,1 mm
<b>Thinnest wall</b>										0,3 – 0,4 mm
<b>Layer thickness</b>										30 µm
<b>Roughness</b>										6 – 10 R <sub>a</sub> [ µm ]
<b>Tensile Strength</b>										460 ±20 (XY) / 460 ±20 (Z) R <sub>m</sub> [ MPa ]
<b>Yield Strength</b>										270 ±20 (XY) / 270 ±20 (Z) R <sub>p0,2</sub> [ MPa ]
<b>Young Modulus</b>										75 ±10 (XY) / 70 ±10 (Z) E [ GPa ]
<b>Elongation at break</b>										8 ±2 A [ % ]
<b>Hardness</b>										55 ±5 HRB

*Table 2 – AlSi10Mg Prima Additive Characteristics*

It's important to underline that the AlSi10Mg, thanks to its high percentage of silicon (10% in weight) has a near eutectic composition, this will result in a low range of solidification that helps preventing the formation of cracks. The presence of silicon is helping by lowering the



CTE (Coefficient of thermal expansion) and solidification shrinkage; moreover, it improves laser absorption.

Conventionally, the components produced by casting of this alloy are thermally treated to improve mechanical properties, in particular a T6 heat treatment is usually applied. This heat treatment process involves solution heat treatment, quenching, and artificial aging:

During the **solution heat treatment** stage, the alloy is heated to a high temperature (typically between 500°C to 540°C for AlSi10Mg) to dissolve any alloying elements clusters or compounds that have been formed during the alloy's manufacturing process. This process improves the alloy's ductility, allowing it to be formed into the desired shape.

The next stage of the T6 heat treatment process is **quenching**, where the alloy is rapidly cooled using a suitable quenching medium, such as water or oil. This process "freezes" the alloy's microstructure in place, which helps to retain the desirable properties obtained during the solution heat treatment process.

Finally, the **artificial ageing** stage involves heating the alloy to a lower temperature (typically between 160°C to 180°C for AlSi10Mg) to allow the alloying elements to precipitate and form a more stable microstructure. This process enhances the alloy's strength and hardness.

A big difference of LPBF compared to casting is that the laser melting process is characterized by a rapid fusion and re-solidification, this results in a micro-structure very similar to T6 heat treated casted components, for this reason, it is not necessary a further ageing treatment.

The rapid heating and cooling of the material and the continuous repetition, layer after layer, of this fast process may results in high residual stresses in the finished component. Therefore, a stress relief treatment is much needed in AlSi10Mg parts fabricated by LPBF.

To perform this heat treatment the material is heated to a temperature below its solution heat treatment temperature, typically around 200 – 300 °C for AlSi10Mg, and held at this temperature for 2 – 4 hours. The heat treatment helps to relax the material, reducing residual stresses and improving its overall dimensional stability. However, it's important to note that this process can also lead to a slight reduction in the material's mechanical properties.

Prima Additive provided us with some specimens to test the material properties and compare the results with the datasheet. The specimens have been designed following the normative DIN50125, in particular a Type A d12 test has been performed. In this method, a test specimen with a diameter (d) of 12 mm having circular cross-section with cylindrical ends is subjected to a tensile load until it fractures.

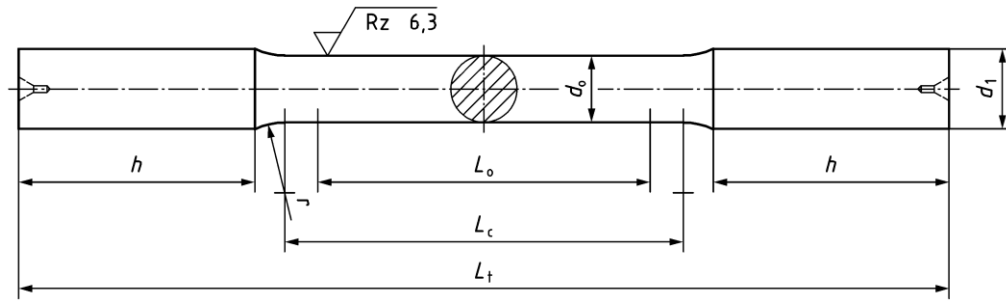


*Figure 13 – DIN50125 Type A Specimen geometry*

During the test, the load and elongation of the specimen are continuously measured and recorded. The results have been used to extract the Young's modulus ( $E$ ), Yield strength ( $R_{p0,2}$ ), Ultimate strength ( $R_m$ ) and strain at failure ( $A$ ).

It is fundamental to put in evidence that there were some issues during the CAD design of the specimens that led to an incorrect fillets radius and position. This error was clearly noticeable in the experimental results, in particular 3 out of the 4 components tested had the rupture line in the proximity of the fillet and not in the middle zone of the specimen, as expected. Here below the specimens picture after the tensile tests.



*Figure 14 – AlSi10Mg wrong specimens test results*

Therefore the mechanical properties extrapolated by these 3 specimens were completely inconsistent and meaningless.

The only test that showed significant results, by achieving its rupture in the middle of the specimen, showed also a good ductility characteristic despite its brittle failure.

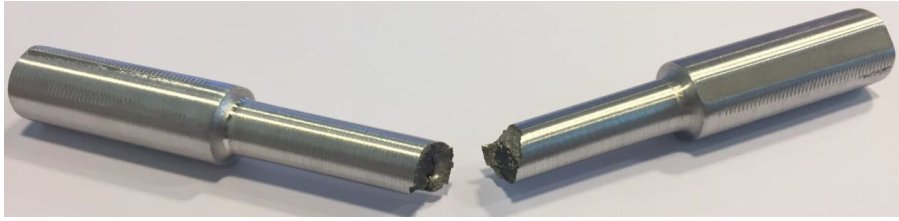


*Figure 15 – AlSi10Mg specimen with correct rupture position*

Elongation at break was more than double the one resulting from the other 3 specimens as well as the Young's modulus was significantly higher. This results are the closest to the theoretical values so they might be representative of the properties of a component with good surface quality and very few imperfections.

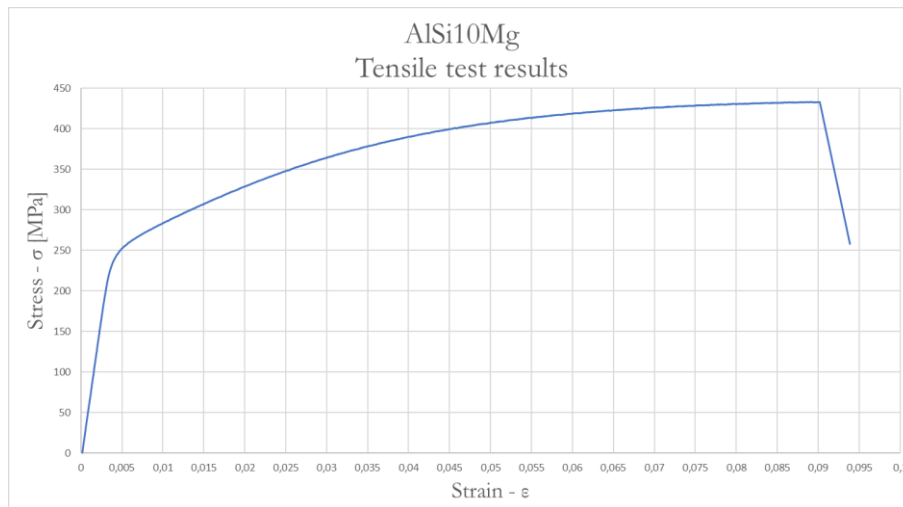


*Figure 16 – AlSi10Mg Stress Strain plot*

The mechanical properties obtained by this specimen were the following.

<b>Tensile Strength</b>	433,3 $R_m$ [ MPa ]
<b>Yield Strength</b>	255,9 $R_{p0,2}$ [ MPa ]
<b>Young Modulus</b>	71,5 $E$ [ GPa ]
<b>Elongation at break</b>	9,02 $A$ [ % ]

*Table 3 – AlSi10Mg Experimental Mechanical Properties*

Of course, the overall results are not sufficient to validate the datasheet provided and they show also the current limitations in the repeatability of additive manufacturing techniques which, having a vast set of parameters to calibrate, result in being a very complex production method.

Due to its linkages with other suspension and powertrain sub-assemblies the finished upright need to have some specific geometric and dimensional tolerances, detailed in the engineering drawing of the component. The tolerances requested are impossible to reach with the only use of LPBF technology and Additive Manufacturing techniques more in general, this is why a CNC-Milling procedure is needed to refine the component in some spots. This production method has been adopted for the 2022 solution and will be detailed in section 4.1 of this work.

In particular the chip removal process is possible thanks to the material allowance imposed before the 3D printing process. The locations that needed this other machining were the suspension attachments, the transmission and bearings mounting surfaces and, of course, all the holes which are present in the upright.

## 2.2. Boundary condition and load application

The design process of any mechanical component needs to start by defining the boundary conditions, both in geometrical terms and of external load application. In particular, speaking of the upright assembly, the first things to define are the overall maximum dimensions of the final component.

These dimensions have to be set taking into account all the sub-assemblies involved in the wheel area of the prototype such as: the rim size, the transmission geometry, the brake calliper, the motor and suspension attachment surfaces. The hardpoints of the suspension and brake calliper are defined by the Vehicle Dynamics division of the Team.

It is fundamental to analyse also the wheel movement and steering action, these two effects will force the upright to have a lot of free space around the suspensions linkage points.

To do so a kinematic cad is created and the most extreme wheel position are analysed, these are due to suspension movement, steering angle and setup changes (Camber and Toe angle).

Here below it is inserted the results of this geometrical boundary condition analysis for the front upright. As we can see, the piece is really bulky and heavy in this phase because this is just the starting volume of a following topology optimisation process.

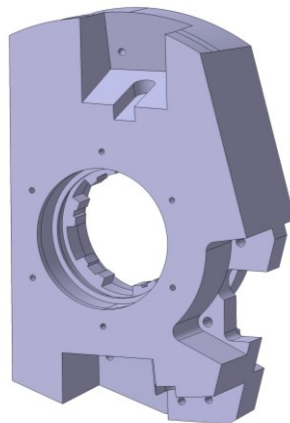
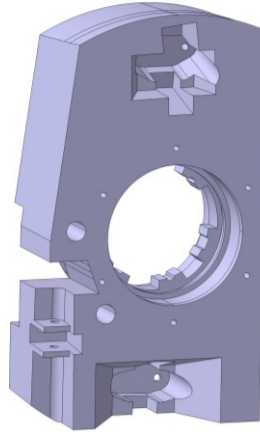


*Figure 17 – SC21 Front upright starting volume CAD*






Here instead the starting volume of the rear upright is inserted. There are some evident differences in the suspension attachments zones. Meanwhile, the motor and transmission geometry linkages are identical to the front upright being exactly the same components in all the four wheels of the car.



*Figure 18 – SC21 Rear upright starting volume CAD*

In order of being able to perform the Topology Optimisation process of the components and then the Finite Element Method (FEM) Analysis it is necessary to define the various load cases to which part will be subjected in its working application. The load cases are used to simulate some distinct instances that could arise during testing and race events. Of course, to be sure to design a safe component, each load cases is studied to simulate vehicle performance in perfect conditions, exploiting the maximum braking capability of the tires, the maximum lateral acceleration due to the best aerodynamic condition possible and so on.

The load cases used in 2021 designing phase were five:

-  **Pure Acceleration (PA):** as suggested by the name, this is a pure straight acceleration case with no acceleration along the axis perpendicular to the direction of movement of the vehicle.
-  **Pure Braking (PB):** same as PA load case but in case of braking and so, negative acceleration along x axis.
-  **Pure Lateral (PL):** this is a case that simulates a constant speed turn. It is characterized by having a value of acceleration different from zero only along y axis which is the axis parallel to the radius of curvature of the turn.
-  **Acceleration in turn (AIT):** this is one of the two load cases that are called combined. Here we will exploit an acceleration both in x and in y direction, it simulates the phase of acceleration when exiting from a corner.
-  **Braking in turn (BIT):** this is the second combined load case. Same as in AIT we will have acceleration both in x and in y direction but, due to the braking action, the acceleration along x direction will be negative.

Here below a table with the specific accelerations values for each load case is inserted, it is noticeable that not only the magnitude of the acceleration is changing from load step to load step, but also the vehicle speed is different.

	$a_x \left[ \frac{m}{s^2} \right]$	$a_y \left[ \frac{m}{s^2} \right]$	$v \left[ \frac{m}{s} \right]$
<b>PA</b>	1,6 g	\	10
<b>PB</b>	-2,5 g	\	22,22
<b>PL</b>	\	- 2 g	22,22
<b>AIT</b>	1 g	- 1,5 g	15,28
<b>BIT</b>	- 1 g	- 1,5 g	15,28

*Table 4 – SC21 Detailed load cases*

The loads that are generated from these accelerations cases are studied by the Vehicle Dynamic Division of the Team and are passed to the mechanical designers in the form of forces along the three main axes of the vehicle (x, y and z). These forces are applied to the tire contact patch, then the designer will decide how to transpose them in the position needed for its particular component and he will consider all the transport moments generated.

Further details related to the topics discussed in this Section will be examined in depth in section 3.2 and section 4.3 , in which the 2022 Solution is analysed more precisely in every aspect.

### 2.3. Topology optimisation and FEM analysis

When studying a component for high performance application, such as Formula Student prototype, is important to carry out a topology optimisation process. Topology optimization is a computational design method used to optimize the material distribution within a given design space to achieve specific performance goals. It is commonly applied in engineering to find the most efficient and lightweight structure for a given set of constraints.

The goal of topology optimization is to determine the optimal layout of material within a structure, while considering factors such as strength, stiffness and weight. By analysing the loads and boundary conditions applied to the structure, the algorithm redistributes material in order to minimize stress concentrations, improve structural integrity, and reduce unnecessary material usage.

The optimization process starts with an initial design space, which represents the volume or region where the optimized structure will be located. This design space is then discretized into smaller elements, such as finite elements, forming a mesh or grid.

During the optimization process, the algorithm iteratively removes material from the design space, redistributes it, and analyses the resulting structural performance. The material removal is typically performed by applying a set of mathematical or computational techniques, for example a density-based method.

The optimization algorithm evaluates the performance of the structure based on predefined objectives and constraints. These objectives can include minimizing the structural weight, maximizing stiffness, minimizing stress or deformation under specific loads, or a combination of multiple criteria.

Throughout the optimization iterations, the algorithm progressively refines the material layout by removing less critical or redundant material. This iterative process continues until a convergence criterion is met or the desired performance goals are achieved.

The output of topology optimization is a material distribution or density map that indicates the optimal layout within the design space. Thanks to Altair Inspire software it is possible to directly convert this material distribution in a solid component through some commands that, following the direction of the distribution output, reconstruct a shape far more production oriented and simpler.

This “fitting” command could be used only if an additive manufacturing production method is adopted because the geometry obtained, even though simplified, will still be practically impossible to be created by a standard CNC-Milling machine. In section 4.4 the solution to this issue will be discussed.

In Section 2.2 the overall “design” space allowed by geometric constraints were explained. When speaking of “Topology optimisation” the name “design” space indicates exclusively the fraction of volume that can be influenced by the optimisation algorithm. Here below there are three pictures useful to understand, starting from the overall volume of **Figure 17** (on the left) the subdivision between non-design space (in grey in the middle), and design space (on the right in dark red colour).





*Figure 19 – SC21 Front upright design and non-design space*

The non-design space is mainly related to the transmission housing and the suspension attachments as well as to the braking calliper mounting holes. This part is used also to apply the constraints and loads of the model, these are needed to perform both the optimisation as well as the FEM analysis of the final component.

In 2021 it has been decided to apply a single constraint on the transmission outer bearing raceway, being the only support used in the model it had to prevent motion and rotations along and around the three axes, thus blocking all the 6 d.o.f. of the component.

Similar to Altair HyperMesh, in Inspire there are some elements called “connectors” that could be defined as rigid or flexible type and they are used to create a linkage between surfaces/holes/faces of the component and a single point in the space. In section 4.3 a more in depth analysis related to these two types of connector elements will be performed. For now, it is only useful to know that for supporting the model, by applying a constraint, rigid connector type are required.

Here below it is inserted the picture that highlights the position of the support, in the centre of the outer bearing (“outer” because further away from vehicle middle line) and connected to the bearing outer raceway by a rigid connector.

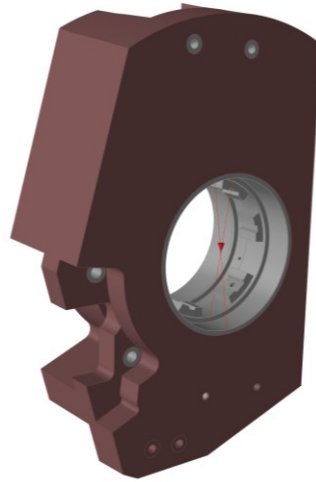


*Figure 20 – SC21 Model support and connector*

After the definition of the constraints of the model, it is necessary to define the load application method. As mentioned before the Vehicle Dynamic division provides the mechanical designers with a set of Forces applied on the contact patch of the tire for each load case. For the 2021 season, the choice has been to apply the loads acting on the upright in these specific points:

**Suspension Hardpoints:** these points are 3 defined position where the suspension universal joints are placed, being a double wishbone layout these three points will be defined as:

- **UCAO:** Upper control arm outer
- **LCAO:** Lower control arm outer
- **TIEO:** Tie rod outer

**Inner Bearing:** the forces at the tire contact patch were applied at the inner bearing taking into account with the connector only the half of the raceway interested by the direction of the force, to better simulate the pressure of the bearing.

**Calliper centre point:** in PB and BIT load cases the braking force to apply at calliper pads is added.

**Motor torque:** the motor delivers a peak torque of 21 Nm, that is applied to the 6 circumferential screws of the motor plate.

For all the points mentioned above, flexible type connectors have been used.

A MATLAB code has been used to calculate, for each point listed, the force and moment to be applied which are derived from the contact patch forces and motor torque data. In Section 4.2 a deeper analysis will be done related to the 2022 solution loads calculation and

application, which will share some points in common and some other in contrast with the 2021 one.

Here below the Pure acceleration (PA, on the left) and Braking in turn (BIT, on the right) load cases are presented, the model is very complicated to be understood from pictures due to the high number of forces, moments and connectors used. The dark red design space has been hid to better visualize the connectors present in the brake calliper and suspension zones.

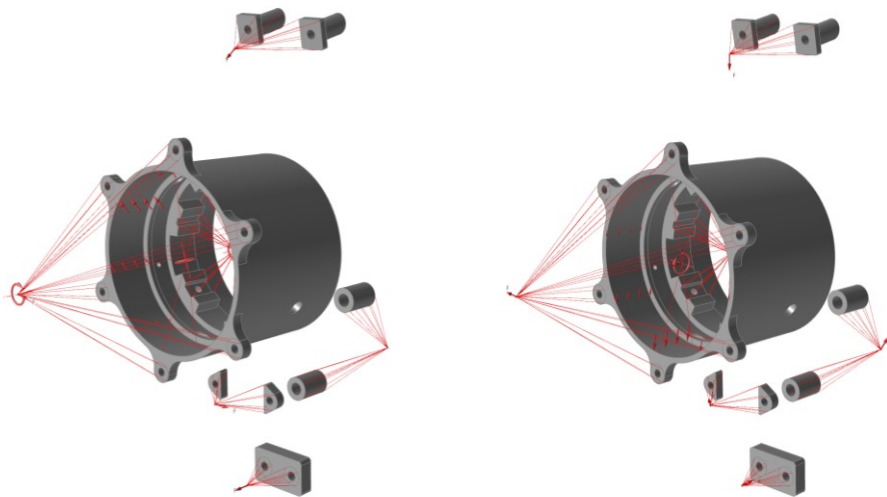


*Figure 21 – SC21 Model PA and BIT load cases*

After that all the loads and constraints are applied the optimization process can almost begin, the only aspect missing is the mesh settings. The term “mesh” refers to the discretization of the design volume into a finite element mesh. Altair Inspire, has two main parameters to be set to let the software know how the user wants the mesh to be:

**Average dimension:** the target dimension of each mesh element. This was set to 2 mm.

**Minimum dimension:** in the case of small curvature radius or complex geometry zones the software will lower the dimension of the mesh elements to better follow the shape of the component; the minimum dimension is simply the lower limit of this procedure. This was set to 0,5 mm.

It is important to underline that the mesh settings affect a lot the optimisation and analysis outcomes both in terms of accuracy and in terms of computational complexity. The uprights are in general quite big mechanical parts (around 300 x 185 x 80 mm) and so it is needed to compromise a little bit the accuracy of the results to have a feasible computational time.

When starting a topology optimisation process it is necessary also to set the target of the optimisation, being it maximising component stiffness or minimising the mass. In general, when dealing with a critical component, such as the upright for the wheel assembly, the objective is always to maximize stiffness to lower the overall displacements. Other shape control commands can be applied but, being the production process an AM technique, it is possible to leave maximum freedom to the software. In the case of CNC-Milling it is practically mandatory to use the shape control function to avoid too complex geometry outcomes.

Here below a comparison between the initial design volume and the result after the first topology optimisation iteration. Further iterations have been performed in order to improve the geometry.

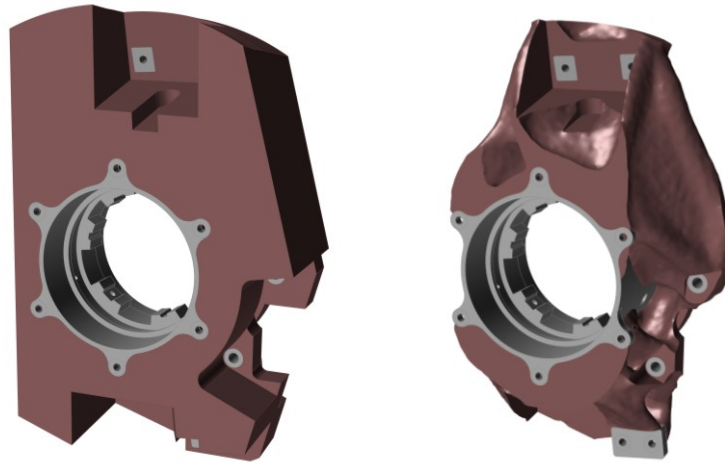


*Figure 22– SC21 topology optimisation first iteration results*

Altair Inspire, after performing a topology optimisation, let the user start a quick FEM analysis on the optimised geometry. This is done in order to understand if the behaviour of the component under load is still acceptable even with the reduced volume. This iterative process of reducing mass is repeated until the performance targets are satisfied.

At the end of the iterations the material distribution needs to be reconstructed and transformed in a solid part. This is done with the help of the fitting and wrapping commands of Altair Inspire, as explained before.

The most critical areas to be handled, during this reconstruction phase, is the linkage between the optimised design volume and the original non-design space. Non-design space has a defined geometry that can't be changed, meanwhile the design space has received an optimisation and reconstruction process that gave him very complex shaped, extremely not canonical. Having a smooth transition is a key factor to achieve reliable analysis results and moreover good performances of the produced component.

Down here a focus on some transition points of the 2021 front upright is showed by using a visualization method that put in evidence only the sharp edges of the model (black solid lines).

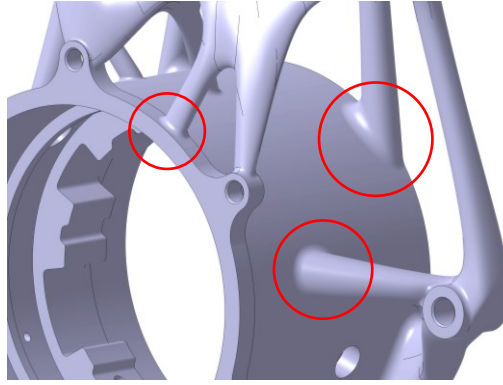


*Figure 23 – SC21 front upright geometry transition zones*

When the reconstruction is completed, an FEM analysis is conducted to determine the results of the designing process in terms of stresses and displacements under load. The same load cases and constraints as the topology optimisation procedure are used. To obtain truthful results of the static stress analysis, it's crucial to use a fine resolution of the mesh. Compared to the topology optimisation process, FEM is less critical from the computational effort point of view and so it is possible to decrease the mesh settings, such as lowering the average dimension target to 1 mm. Here below an overview of the FEM models used for the front and rear upright of SC21 is inserted.

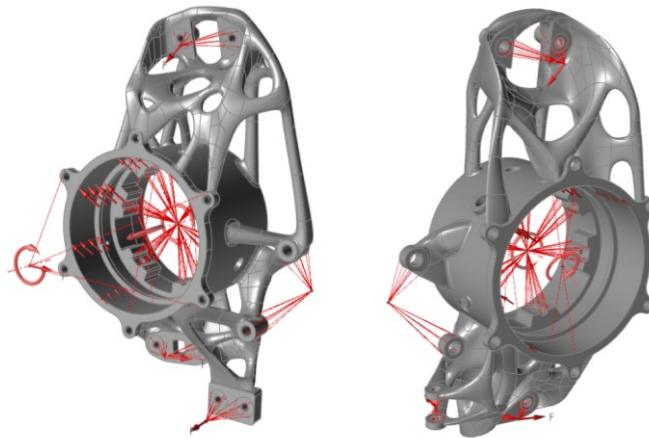


*Figure 24 – SC21 FEM Model front and rear*

In the following section, the FEM results are presented as well as some production images and issues emerged during testing phase of the final components.

## 2.4. Final component outcomes

In this section, the FEM results are presented as well as some production images and issues emerged during testing phase of the final components.

At this stage the final geometry of the front and right uprights are defined. The design phase takes place considering one side of the prototype that, thanks to its intrinsic symmetry, it is sufficient to mirror the components on the vertical mid plane of the car.

Here below the final components are shown from three different angles.

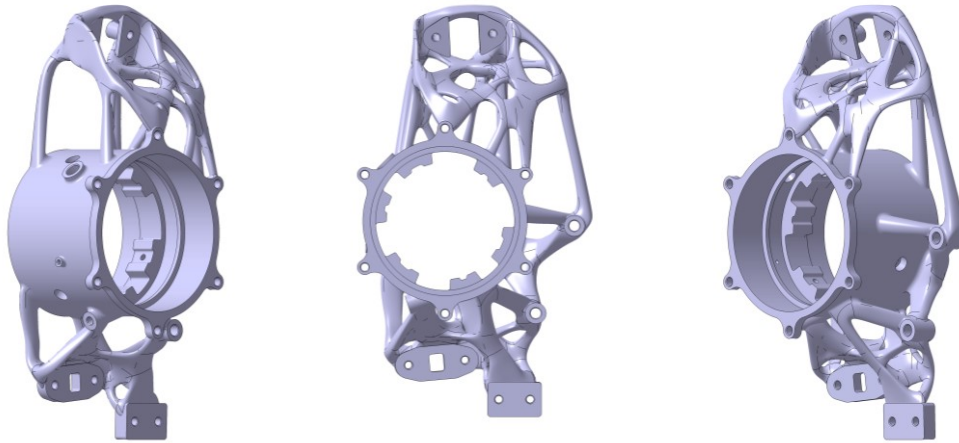


*Figure 25 – SC21 Front Upright*

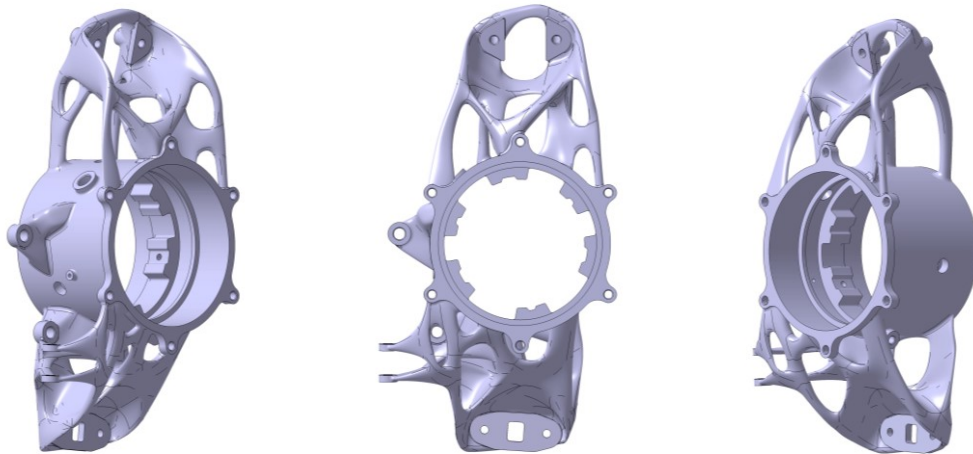


*Figure 26 – SC21 Rear Upright*



It's interesting to take a look also at the 2021 wheel assembly, it's easy to say that the upright is one of the biggest components and, surely, the only one which is linked with all the sub-assemblies present in this complex zone of the prototype. For a better visualization the uprights colour has been set to bright yellow.

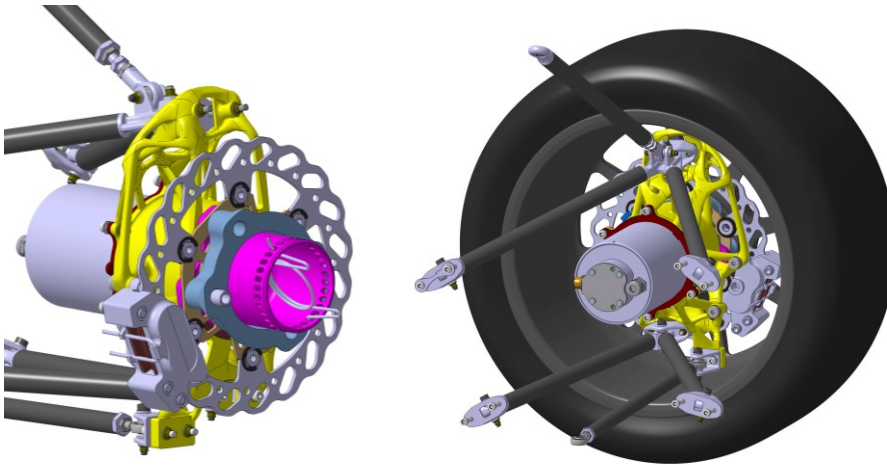


*Figure 27 – SC21 Front wheel assembly*

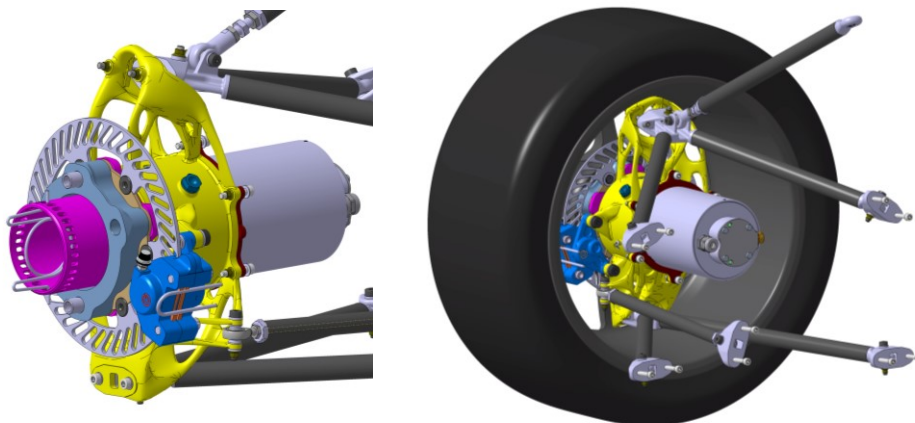


*Figure 28 – SC21 Rear wheel assembly*

In Laser Powder Bed Fusion (LPBF), and in a vast majority of AM processes, in order to be able to create such complex geometries, supports are needed. They are structures that are printed along with the main component being fabricated. These supports serve several important functions:

- Stability:** Supports provide stability and prevent deformation or warping of the component during the printing process. They help to anchor the component to the build plate and ensure it remains in the correct position as layers are added.
- Overhangs:** LPBF supports are particularly crucial for supporting overhangs of the component that extend beyond the previous layer without any underlying support.

**Heat Dissipation:** Supports can assist in dissipating heat generated during the laser melting process. By conducting heat away from the component, they help prevent thermal stress and improve the overall quality of the printed part.

It's important to note that supports are designed to be removable, as they are not intended to be a permanent part of the final component. After the printing process, supports are typically removed through mechanical means (sandblasting for example), as in this case, or other techniques, such as heat treatment or chemical dissolution, to reveal the completed component.

Altair Inspire software helps in designing supports in a semi-automatic way. Here below two pictures of the front upright just after the printing process, supports are still present.



*Figure 29 – SC21 Production process*

Here below another view of the support structures from the bottom plane.

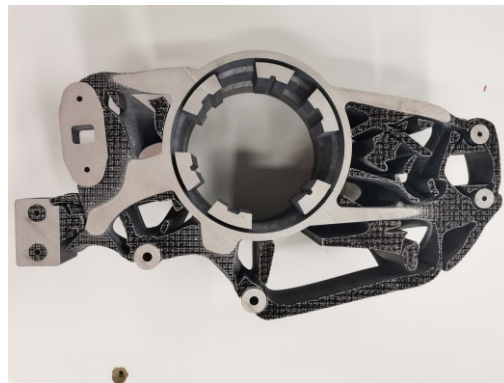


*Figure 30 – SC21 Support structures*

Now the FEM analysis results will be presented both visually and numerically. Usually the key factors that are analysed are the stress distribution and peak value as well as the maximum displacement occurring in the component. Knowing the stress peak value and yield strength of the material it's possible to calculate a Safety Factor (S.F.), this will be valid in static conditions. Fatigue analysis are usually not conducted for time reasons during the design of the upright assembly parts in the Team, however a post-design fatigue analysis has been carried out for the 2022 solution and will be discussed in chapter 6.

For stress analysis the Von Mises criterion is adopted and selected in the software. Von Mises stress measures the combined stress state experienced by a material under load. It is widely used in structural analysis to evaluate the potential for yielding or failure in materials. It's based on the concept that materials yield when a specific equivalent stress level is reached,





regardless of the individual components of stress (tensile, compressive, or shear). It provides a single scalar value that represents the combined effect of these stresses.


The formula for calculating von Mises stress is:

$$\sigma_v = \sqrt{\frac{(\sigma_1 - \sigma_2)^2 + (\sigma_2 - \sigma_3)^2 + (\sigma_3 - \sigma_1)^2 + 6(\tau_{xy}^2 + \tau_{yz}^2 + \tau_{zx}^2)}{2}} \quad (2.1)$$

Where:

  $\sigma_v$  = Von Mises stress

  $\sigma_1, \sigma_2, \sigma_3$  = Principal stresses (tensile or compressive stresses along the three mutually perpendicular directions)

  $\tau_{xy}, \tau_{yz}, \tau_{zx}$  = Shear stresses in the xy, yz, and zx planes

The von Mises stress criterion states that yielding or failure occurs when the von Mises stress exceeds the yield strength or ultimate strength of the material. When calculating a safety factor, it is common to use the yield strength rather than the ultimate strength of the material.

The yield strength represents the point at which a material begins to deform plastically and so, using it, ensures a margin of safety by considering the onset of plastic deformation rather than the point of failure. Safety factor equation is the following:

$$S.F. = \frac{R_{p0.2}}{\sigma_v} \quad (2.2)$$

Here below the visual results of the FEM analysis on the front upright are presented. Only the most critical load case, upon the 5 analysed (PA, PB, PL, AIT, BIT), is inserted: in case of the Von Mises stress distribution the higher peak value has been found in pure braking; meanwhile, looking at the maximum displacement, the peak values are practically identical in PB and Braking in turn load cases.

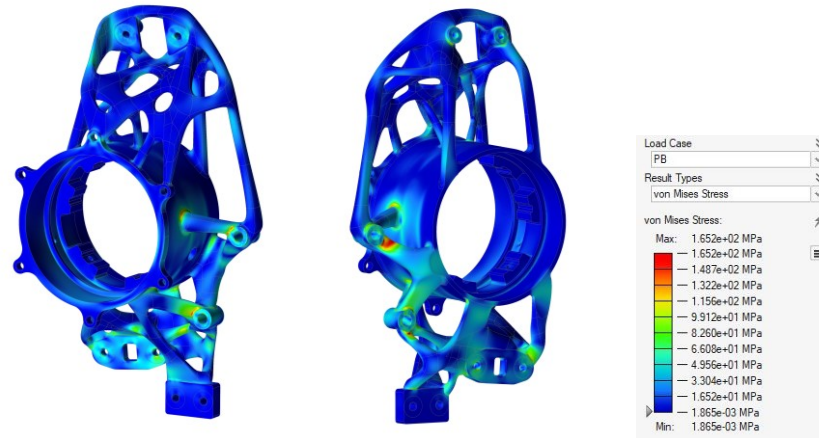


Figure 31– SC21 Front upright PB Von Mises

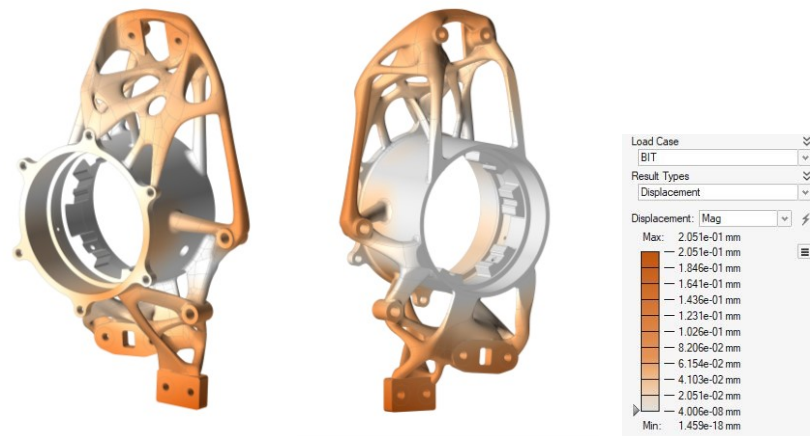


Figure 32– SC21 Front Upright BIT Displacement

Now the rear upright results are inserted, in particular for both Von Mises stresses and displacements the AIT load case has proven to be the most critical one. This difference with respect to the front upright can be explained by the fact that on the rear wheels the torque generated during acceleration is far more severe than the torque applied during a braking manoeuvre, opposite than what happens for the front wheels.

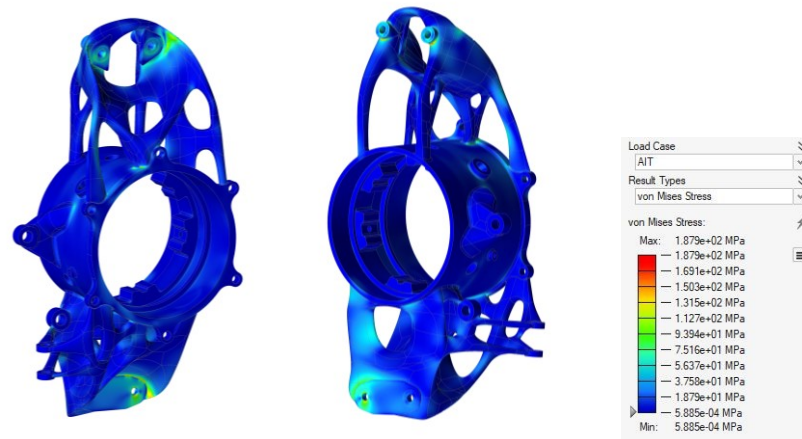


Figure 33– SC21 Rear upright AIT Von Mises

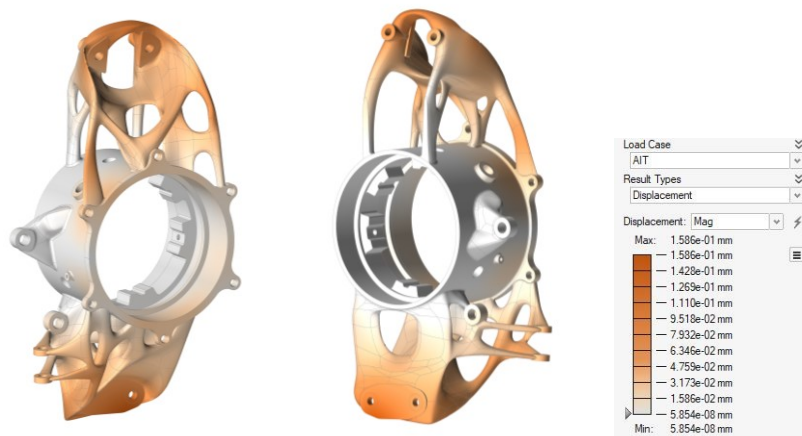


Figure 34– SC21 Rear upright AIT Displacement

Here below a table with the numerical results and calculated safety factors is presented. To calculate the S.F. the datasheet yield strength has been used because the experimental results were not robust enough to constitute a solid reference, the datasheet imposed a minimum value of  $R_{p0.2}$  equal to 250 MPa.

	Max Displacement	Critical load case (displacement)	Peak Von Mises Stress	Safety Factor	Critical load case (S.F.)
<b>Front Upright</b>	0,205 mm	BIT	165,2 MPa	1,51	PB
<b>Rear Upright</b>	0,159 mm	AIT	187,9 MPa	1,33	AIT

Table 5– SC21 FEM numerical results

The results showed really good performances in terms of stiffness, having maximum values of around 0,2 mm in such a big component is impressive, especially considering the high g-forces involved. Speaking about safety factor it is hard to say that the results are impressive or convincing. It is important to say that these low values of S.F. are restricted to areas where the geometry is hard to be meshed correctly and so, they could be not fully truthful. Further considerations will be carried out in Chapter 5.

## 2.5. Track testing failure

This section of the work is one of the key points that started and slightly changed my design phase. Unfortunately during some track testing performed in October of 2021, the front right brake disk and upright have undergone a critical failure.

In particular, the brake disk cracked in 2 pieces and the upright failed in the lower attachment holes of the brake calliper. Fortunately no one was hurt and the rest of the wheel assembly didn't have any damage, the car stopped safely using the other discs as well as the regenerative braking torque of the motors. Here below there are some picture of the failure.



*Figure 35 – Upright and brake failure*

The failure happened on the front right wheel during braking, of course the front axle is mainly stressed by braking actions; as demonstrated by the FEM results in which the PB and BIT load cases were the most critical ones.

Unfortunately, being the upright a very expensive component, no spare were available, thus forcing the Team to interrupt track testing for 2021.

Many considerations and analysis were performed to understand what caused the issue and moreover, which component was the first one to fail. The concept behind this last sentence is that, being the brake calliper and brake disc in contact, a failure of the disc may cause a movement of the brake calliper that could snap the supports on the upright and, vice versa, a rupture of the upright will cause a movement of the calliper that may damage the disc.

The analysis performed led to the assumption that the disc was the first to suffer the failure and consequently the upright. The most likely failure type seemed to be thermo-mechanical fatigue due to the uneven temperature distribution on the disk surface and the drastic temperature rise during an heavy braking manoeuvre.

In particular the studies that have been carried out on the failure are:

#### **On the upright:**

- **Tomography:** to better visualize the internal structure of the component's material
- **Optical microscope:** in order to take a deeper look at the failure surface details and potential porosities

#### **On the brake disk:**

- **Microscope:** to take a look at the beach lines and fracture propagation
- **Liquid penetrant:** to highlight defects and visible cracks

Irrespective of the component responsible for the damage, this unforeseen incident significantly altered the 2022 design objectives for both the brake and uprights assemblies. In the context of a Formula Student car, the primary concern lies in achieving reliability. Once this concern is adequately addressed, it makes sense to embark on the optimization processes, pushing them to their limits in order to reduce the mass of the components. It is far more advantageous to possess a car that is 5 kg heavier but capable of running 1000 km without encountering issues, as opposed to a prototype with a low Safety Factor (S.F.) resulting from its extreme design. The exploration of extreme solutions only becomes worthwhile and meaningful after years of designing and manufacturing dependable vehicles, and even then, it is essential to subject them to thorough bench testing.

### 3. Design Specifications

In this Chapter the 2022 design specifications for the Upright assembly will be discussed.

In particular the design steps followed for SC22 season were the same as in the previous year and the general targets for the upright assembly didn't change massively. The prototype suspension and transmission layout was the same, as well as the braking assembly didn't suffer major changes, especially for what concerns the linkage points on the upright.

The main difference was the production method, and consequently the material used. The 2022 uprights have been produced using Ergal (Al7075-T6) and CNC-Milling machine.

Design choices fine tuning has been performed in various spots:

- ✍ **Transmission positioning screws:** the orientation of the whole transmission assembly has been changed around y-axis. This was done for being able to insert all the three positioning screws of the ring gear. In 2021 this was geometrically not feasible because the screw was blocked by a part of the upright itself.
- ✍ **Camber setup:** in the UCAO attachments, between the bracket and the upright, thin metal setup plates are inserted to change the camber angle of the wheel. These plates have been slightly modified to allow an easier and faster setup change.
- ✍ **Ackermann setup:** this change was done to allow steering characteristic setup. In particular, by changing the length and attachment points of the tie rods, on the front axle, the steering geometry can be varied slightly. On the upright, a buttonhole was created in the tie rod attachment point and an insert was designed with an off-centre hole for being able to rotate it by 180° and have a different TIEO point.

In section 5.4 pictures of these solutions are present.



### 3.1. What was to be changed from 2021?

As already explained in section 2.5 the 2022 design phase was guided by the common desire to have a very “safe” component in terms of S.F.

Despite the analysis performed on the 2021 failure were more oriented to a failure by the brake disc, the whole Team and especially the technical director wanted to have a far more reliable solution both in terms of upright assembly and in terms of braking system.

The choice of changing again the production method, returning to the 2019 solution process, was done and with that also some tweaks to the optimisation process had to be made.

### 3.2. Static load cases

In order to perform a good design of any mechanical component it is mandatory to have a correct estimation of the loads that the part will undergo when installed and assembled in the designated spot.

As already mentioned the load cases for the whole team are carried out by the Vehicle Dynamics division, in particular every year a vast work of tuning and tweaking the loads is performed to better simulate the components during the design process.

Despite clocking very low kilometres during 2021 season competitions and testing, the vehicle showed some very impressive performances in terms of longitudinal and lateral accelerations. These performances, both in braking, acceleration and lateral instants, are at the basis of the five load cases which are taken into account for by the vehicle dynamics division first, and mechanical designers later on.

More in general, every year of development of the Team’s vehicle, is more or less translated into better overall performances. This is why every year the load cases studied become little more complex and severe. The big jump made between 2021 and 2022 seasons in terms of load cases difficulty is justified also by the failure suffered in October 2021.

Here below there is the same table as previously used for the 2021 solution with the five load cases detailed.

	$a_x \left[ \frac{m}{s^2} \right]$	$a_y \left[ \frac{m}{s^2} \right]$	$v \left[ \frac{m}{s} \right]$
<b>PA</b>	1,6 g	\	10
<b>PB</b>	-3 g	\	27,8
<b>PL</b>	\	- 2,5 g	22,22
<b>AIT</b>	1 g	- 1,5 g	16,7
<b>BIT</b>	- 1 g	- 1,5 g	16,7

*Table 6 – SC22 Detailed design load cases*

Here it’s inserted the variation with respect to 2021 season for each load case.

	$a_x \left[ \frac{m}{s^2} \right]$	$a_y \left[ \frac{m}{s^2} \right]$	$v \left[ \frac{m}{s} \right]$
<b>PA</b>	\	\	\



<b>PB</b>	- 0,5 g	\	+ 5,6
<b>PL</b>	\	- 0,5 g	\
<b>AIT</b>	\	\	+ 1,4
<b>BIT</b>	\	\	+ 1,4

*Table 7 – Load cases comparison 2021-2022*

It's important to notice the variation applied to the PB load case, which already was the most severe one in 2021. Passing from -2,5 g of longitudinal acceleration to -3 g equals to a 20% increase, added also to the speed variation of 5,6 m/s, describes a very difficult condition for the whole wheel assembly.

To better understand and visualize these variations and, in particular, how this acceleration values are imposed it is useful to take a look at the G-G-V plot here below. This data are taken by some track testing activities carried out at the end of the 2021 season.

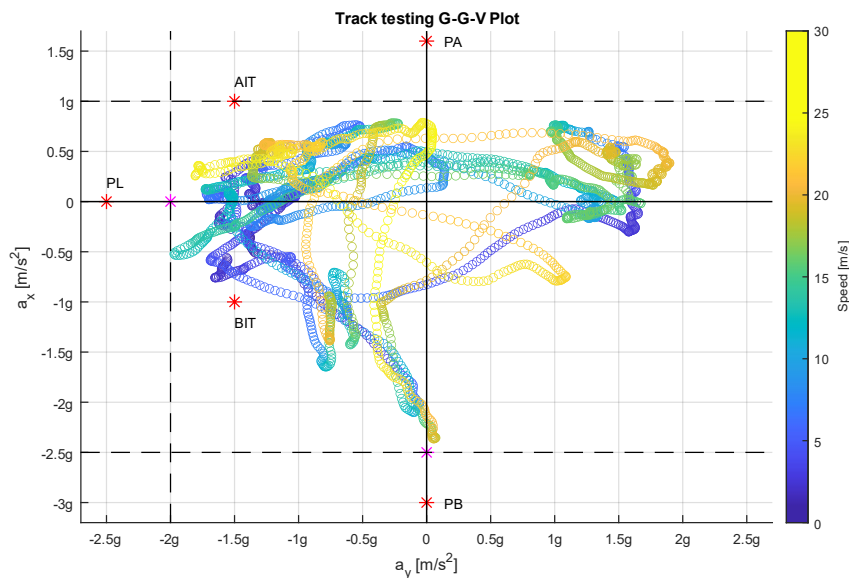


*Figure 36 – G-G-V plot*

This is a scatter plot that is sometimes defined as the vehicle's performance envelope in motorsport. On the X axis there are shown the lateral acceleration values, meanwhile on the Y axis, the longitudinal ones are inserted. Then, there is a colour bar on the right showing the speed of each point of the diagram.

This plot describes the accelerations exerted by the driver-vehicle package in a single lap during an endurance test. The dotted lines are set to be near the limit values of acceleration registered by the sensors and the asterisks are the 2022 design load cases; an intrinsic safety factor is correctly inserted when defining them. This is done to anticipate the desired increase in performance of the prototype the following year. In magenta colour there are also the asterisks corresponding to pure lateral and pure braking 2021 load cases, that have been logically increased for the 2022 design phase. As it can be seen, leaving them unchanged, would have been risky for the new season hoped performances.

Another load case that has been taken into account in the optimisation process was PA0 which is a pure acceleration load case simulated with a  $0^\circ$  camber setup. From the point of view of  $a_x$  and  $v$  nothing changes but the contact patch coordinates are different due to the

varied position of the wheel assembly, this implies different transport moments applied on the upright itself. This was done to better simulate the acceleration event, speaking in general the camber angle helps the car increasing lateral grip and sacrifices the longitudinal grip which is, instead, the key factor of an acceleration event.

Some additional load cases were then used to verify the safety of the component in extreme situations. These cases were not adopted also for the optimisation process because, in theory, they should never happen in real application. They have been analysed to have a complete understanding of the capabilities of the uprights and wheel assembly more in general.

These cases are three:

**Bump:** this case is divided into 4 sub-cases which simulate a bump of 70 mm hit on a straight line section. The bump has been simulated by an inclined plane with height 70 mm and 45° angle. The wheel hitting the obstacle will result in some additional  $F_x$  and  $F_z$  to be summed to the canonical ones extrapolated by the vehicle speed and acceleration. The 4 sub-cases are used to simulate different speeds and longitudinal accelerations.

**Curb:** this load step has been used to simulate the hit of the wheel with a curb on track. Usually Formula Student circuits doesn't imply the standard curbs that we are used to see in Formula 1, despite this, for us, it was interesting to simulate the components behaviour in the remote possibility of hitting one. The same 70 mm ramp was used and the additional forces generated were summed to the 5 canonical load cases.

**Extreme braking:** analysing the log files from the 2021 season track action some very high values of deceleration were found. After doing some filtering action and deeper study, these high values were defined as outliers and sensor spikes; nevertheless an FEM analysis was performed using those extreme braking deceleration values ( $a_y = -3,5 \text{ g}$   $\text{m/s}^2$ ). It's important to notice also that this load case is simulated at 120 km/h (maximum speed of the vehicle), where the aerodynamic forces reach their peak values.

Here the table with all these additional load cases is inserted.

		$a_x \text{ [m/s}^2\text{]}$	$a_y \text{ [m/s}^2\text{]}$	$v \text{ [m/s]}$
<b>BUMP</b>	<b>Slow</b>	1,6 g	\	10
	<b>Medium</b>	1 g	\	16,7
	<b>Fast</b>	0,5 g	\	25
	<b>Superfast</b>	\	\	33,3
<b>CURB</b>		Obstacle Forces summed to canonical load cases		
<b>EXTREME BRAKING</b>		- 3,5 g	\	33,3


Table 8 – SC22 Additional load cases


### 3.3. Targets: weight, reliability, stiffness

The 2022 aims can be summed up in the word: "reliability".

As already explained in many sections previously, the reliability of a component such as the upright is a key factor for every FS Team. The uprights failure will cause the failure of the whole wheel assembly, starting from the carbon fibre suspension and arriving to the delicate outboard motor. This is why, for this year design, the performance targets such as weight and maximum displacement had far lower importance.

Speaking more in general, the two main performance targets to be satisfied when designing an upright are:

 **Weight:** of course needs to be minimized. Being a not sprung mass, the entire wheel assembly will have a critical impact on vehicle dynamic performances. Since unsprung masses are integral parts of the suspension system, they directly influence its response. Higher unsprung masses can increase the overall inertia of the suspension system and affect the car's responsiveness and its overall grip, making the car less responsive and less agile. In particular, the upright is a big component with respect to all the others involved in the wheel assembly. This means that there is a greater potential for weight reduction in terms of the overall percentage of the vehicle's mass.

 **Displacement:** when speaking of vehicle dynamic performances, displacements play a key role, same as said for the weight, especially in the wheel and suspension assembly. Displacements in the upright will result in changes of the wheel characteristic angles: camber, toe and caster. Wheel angles will change dynamically throughout the lap, making the effect of the displacement of suspension parts even more detrimental and unpredictable from the driving point of view. It is like having infinite instantaneous setup changes during every instant of a lap, especially in braking and cornering, where the loads on the wheel assembly are higher and consequently the displacements bigger. Of course, this behaviour was explained to arrive to the conclusion that the displacements needs to be lowered as much as possible.

In the performance targets the safety factor has not been included because cannot be defined as a real performance indicator of a mechanical piece. Usually the safety factor must be reached in any case, if it isn't the component will not be declared as finished and so it will not be produced. Instead, the performance targets are more oriented to the engineering design trade-off point of view. In particular, having a very low weight will imply higher displacements than having a bulkier component; a sweat spot needs to be found.

## 4. 2022 Solution analysis

This chapter is entirely dedicated to the design process of the 2022 upright assembly of the Squadra Corse PoliTO Team's car. A lot of topics will be discussed and deepened, starting from the production method, passing through the topology optimisation and finishing with the FEM analysis.

An important point to have in mind is that Formula Student has technical and sporting regulations, as any other motorsport championship. The rules are mainly focused on the safety of the vehicle, mainly regarding the electric parts of it. Meanwhile, regarding suspension assembly and upright in particular, no specific rules are present, apart from the critical fasteners matter. Critical fasteners rule is applied to the whole vehicle and defines the minimum diameter of screws used and the type of positive locking mechanism installed.

This is why the design process of the upright assembly is usually one of the most custom components produced by the Team.

### 4.1. 2022 Production technology and material

As anticipated in the previous chapter, the production technology adopted in 2021 was abandoned for the uprights, CNC-milling has been chosen instead.

Here's a comparison of the advantages and disadvantages of CNC milling and additive manufacturing:

#### Advantages of CNC milling:

- **Material selection:** CNC milling offers a wider range of material options when speaking about metals.
- **High accuracy and precision:** CNC milling machines are capable of producing highly accurate and precise parts with tight tolerances. This makes it suitable for applications that require precise dimensions as the uprights. This is why CNC milling has been used also in 2021 after printing the rough component.
- **Surface finish:** CNC milling can produce parts with excellent surface finishes, especially when compared to certain additive manufacturing processes. This is advantageous for parts that require smooth surfaces such as bearing housings.

#### Disadvantages of CNC milling:

- **Limited complexity:** CNC milling has limitations when it comes to producing complex geometries, internal channels, or intricate designs. Some geometries may require multiple setups or specialized tooling, increasing the complexity and cost.

- **Material waste:** CNC milling is a subtractive manufacturing process, meaning that excess material is removed from a larger block. This can result in material waste, especially for parts with complex shapes or when working with expensive materials.

It's important to consider the specific requirements of the project of interest when choosing between CNC milling and additive manufacturing. Each method has its strengths and limitations, and the most suitable choice will depend on factors such as part complexity, desired material properties, production volume, time constraints, and budget.

While additive manufacturing offers unique advantages in terms of rapid prototyping, customization, and complex internal geometries, CNC milling remains a preferred choice for many applications that require superior material properties, high precision, strength, and cost-effective production on a larger scale.

In our specific case, CNC milling was chosen for 2022 to avoid as much as possible any uncertainty derived from the complex setup of LPBF 3D printing process. Another big point in favour of CNC milling, related to our 2022 targets, was the possibility of using Ergal as material choice. Ergal properties were already well-known from the Team because it has been used in many other mechanical components for many years. The 2019 uprights were also produced using this material.

Ergal, also known as Al 7075-T6, is a high-strength Aluminium alloy with excellent mechanical properties. Here are some characteristic features of it:

- ✍ **Strength:** Ergal is known for its high strength-to-weight ratio, making it suitable for applications where lightweight materials with excellent strength are required. It has a tensile strength of around 570 MPa, which is significantly higher than standard Aluminium alloys.
- ✍ **Hardness:** Ergal exhibits good hardness, typically ranging from 150 to 160 Brinell hardness (HB). This makes it resistant to wear and suitable for applications that require durability and resistance to surface damage.
- ✍ **Fatigue resistance:** Ergal has excellent fatigue resistance, making it appropriate for components subjected to cyclic loading or repetitive stress. Its fatigue strength is higher compared to many other aluminium alloys.
- ✍ **Corrosion resistance:** Ergal has good resistance to corrosion, particularly when compared to other high-strength aluminium alloys. However, it is not as corrosion-resistant as some other materials like stainless steel or titanium. Proper surface treatments or coatings may be applied to enhance its corrosion resistance further, as will be detailed later on in this section.
- ✍ **Machinability:** Ergal is generally considered to have good machinability, although it can be more challenging to machine compared to lower-strength aluminium alloys. Specialized cutting tools and techniques may be required to achieve optimal results.

In general, Ergal's combination of high strength, light weight, and good fatigue resistance makes it suitable for various applications in the aerospace and automotive industries. It is commonly used in aircraft structures, racing car components, bicycle frames, and high-performance equipment.

Here below the Ergal chemical composition and mechanical properties are detailed.

Chemical Composition (% - Weight)								
Si	Fe	Cu	Mn	Mg	Cr	Zn	Ti	Al
≤ 0,40	≤ 0,50	1,20 – 2,00	≤ 0,30	2,1 – 2,9	0,18 – 0,28	5,1 – 6,1	≤ 0,50	Res.
Tensile Strength							530 R <sub>m</sub> [ MPa ]	
Yield Strength							450 R <sub>p0,2</sub> [ MPa ]	
Young Modulus							71,7 E [ GPa ]	
Elongation at break							11 A [ % ]	
Density							2,81 g/cm <sup>3</sup>	
Hardness							150 HRB	

*Table 9 – Ergal (Al7075-T6) Chemical composition and mechanical properties*




As it is possible to notice, Ergal mechanical properties are far above the ones of AlSi10Mg produced by LPBF, adopted in 2021. If we take a look at the yield strength, one of the key parameters to take into account when designing a mechanical part, the difference in favour of Ergal is huge: + 80%. This increase in yield strength, fortunately, isn't translated in an increase in density, which is practically unchanged from AlSi10Mg.

Al7075 T6 compared to AlSi10Mg [% variation]	
Tensile Strength	+ 22 %
Yield Strength	+ 80 %
Young Modulus	\
Density	+ 6 %

*Table 10 – Material comparison*

Ergal is the commercial name for Al7075-T6, this means that the after treatment process is already considered when speaking about this material's properties and characteristics. In particular, the T6 heat treatment is applied.

The T6 treatment for Ergal involves a series of steps:

-  **Solution Heat Treatment:** The material is heated to a specific temperature range, typically between 480°C and 520°C, and held at that temperature for a period of time. This allows the alloying elements to dissolve and form a homogeneous solid solution.
-  **Quenching:** After the solution heat treatment, the material is rapidly cooled by quenching it in a suitable medium, such as water or air. This rapid cooling helps to retain the desired microstructure achieved during the solution heat treatment.
-  **Aging:** The quenched material is then artificially aged at a lower temperature, typically between 120°C and 160°C, for several hours. This ageing process allows for the precipitation of fine particles within the aluminium matrix, which significantly increase the material's strength and hardness.

It is interesting to notice how the same heat treatment (T6) changes when applied to different materials, in section 2.1 the T6 treatment was described for AlSi10Mg and the temperatures used were different.

The T6 heat treatment for Eral (7075-T6 aluminum) is typically performed before the CNC milling process. The T6 treatment is applied to the raw material, which is in the form of a block or billet, before it is machined into the desired shape using CNC milling techniques.

To avoid losing the T6 heat treatment effects when CNC milling an Eral component, it's important to take certain precautions:

- ✍ **Coolant and lubrication:** Use an appropriate coolant or lubricant during the CNC milling process. This helps dissipate heat generated during machining and reduces the risk of localized overheating that could affect the T6-treated material.
- ✍ **Optimize cutting parameters:** Adjust the cutting parameters, such as cutting speed, feed rate, and depth of cut, to ensure efficient material removal without generating excessive heat.

After the completion of the milling process, the component can undergo to several post-processing options that can be considered to further enhance the component or achieve specific surface characteristics. Some common post-processing techniques for Eral include:

- ✍ **Surface Finishing:** This involves techniques such as polishing, sandblasting, or brushing to improve the surface smoothness, remove burrs, and enhance the aesthetic appearance of the component.
- ✍ **Anodizing:** Anodizing is a popular surface treatment for aluminum alloys, including Eral. It involves creating an oxide layer on the surface of the material, providing increased corrosion resistance, improved wear resistance, and the option to add color or decorative finishes.
- ✍ **Painting or Powder Coating:** Applying paint or powder coating to the surface of the Eral component can provide additional protection against corrosion, enhance the appearance, or provide specific functional properties.

For the upright application, the anodizing post-process has been chosen and in particular the aesthetic one is been used to improve the overall resistance of the component against corrosion, wear, abrasion, and external impacts. Hard anodization was not necessary for this application, it is instead obliged by the rules for the wheel nuts due to their continuous tightening and unscrewing actions.

The machine used to perform all the machining operations was a 5 axis one from Haas.



## 4.2. 2022 Boundary conditions

As already said in previous sections, the overall vehicle layout didn't change in a significant way passing from 2021 to 2022; the 2022 prototype can be described as a fine tuning of the 2021 studies and solutions.

In particular, for what concerns the upright assembly, the following changes and carry-over has been done:

- ✍ **Brake calliper:** the model and position of the brake callipers, for both front and rear wheels, remained exactly the same as in 2021. The mounting holes were slightly modified to increase their thickness, thus enhancing their safety factor.
- ✍ **Electric Motor:** the motors used were carried over from 2021 prototype and also the motor-plate, used to connect the motor to the uprights, was the same; as it is possible to understand, the upright design was maintained unchanged in this portion.
- ✍ **Transmission and wheel hub:** being the transmission strictly related to the motor and being the most expensive wheel sub-assembly, the layout was unchanged and so, also the upright internal geometry had to be the same.
- ✍ **Suspension assembly:** for this sub-assembly a different explanation needs to be made. The suspension assembly technology remained the same but the spatial positions of the outer attachment points were changed from the vehicle dynamics' division to fine tune the car dynamic behaviour. Furthermore, some modifications were made in the upright geometry of these attachments, to avoid the usage of redundant brackets and try to save some additional weight.

As it is possible to notice from the list above, no critical modifications were made in the boundary conditions of the uprights. Being also the rim and tires used the same, the design starting volume was basically created by varying the suspensions attachments point in the 2021 ones presented in section 2.2.



### 4.3. FEM Model

In this section, the FEM model used for both the topology optimisation and static analysis will be detailed and explained meticulously, differently from what was done in Section 2.3, in which the 2021 model was practically only mentioned.

The first thing to do when starting any design process and, in particular, when creating a model is to decide and define the reference systems of the sub-assembly. In this case, the main reference system is the car reference frame and it is defined as follows:

- /// **Car reference frame origin O (X,Y,Z):** it is placed in the middle point of the front wheels axle.
- /// **X axis:** parallel to the ground and dividing the car into two symmetrical sides, right and left. The direction of positive X values is towards the rear of the car.
- /// **Z axis:** perpendicular to the ground pointing towards the sky.
- /// **Y axis:** this axis completes the right-handed coordinate system of the whole vehicle. It is horizontal to the ground, passes through the front wheel hubs and points towards the car's right side.

Here below some pictures detailing the car reference system are inserted.

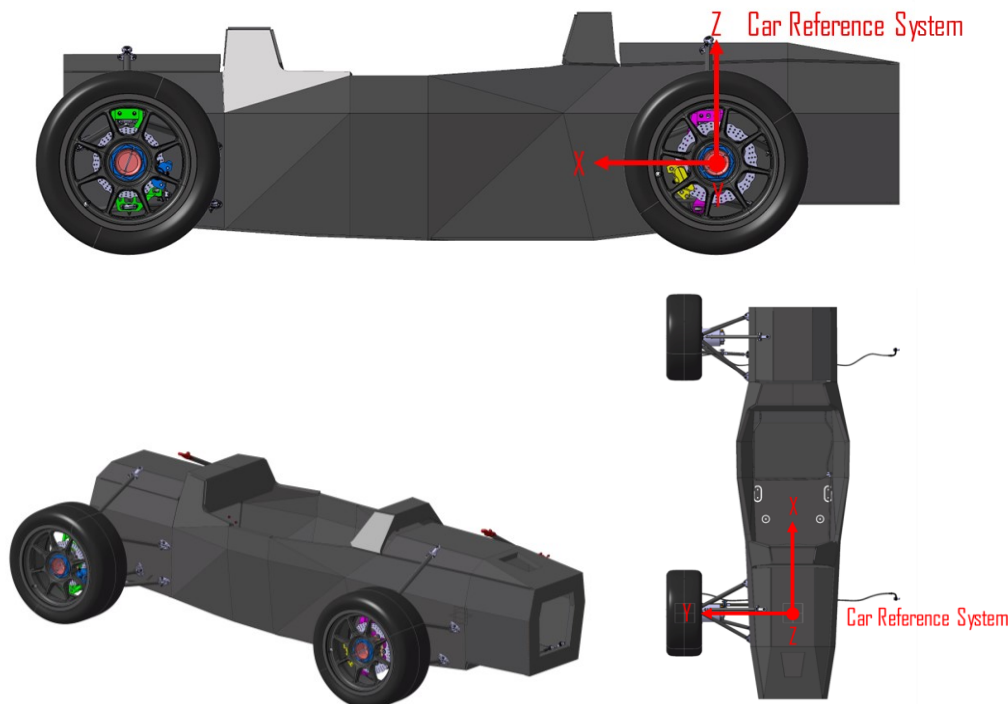


*Figure 37 – Car Reference System*

The vehicle dynamics division outputs, to the mechanical designers of the Team, the forces at the wheels applied to a fictitious contact patch centre point which had the coordinates  $(X_{cp}, Y_{cp}, Z_{cp})$  expressed in the Car reference system, as detailed in the images below. This is not completely correct from the tire-ground theory point of view because the forces are in

reality distributed as pressures in the whole contact patch area with a non linear distribution. The need to concentrate the pressure distribution into a triad of forces is dictated by the already complex analysis that the mechanical designers need to perform. It is desirable and plausible that having the forces concentrated in one single point will result in more difficult load conditions for the whole wheel assembly.

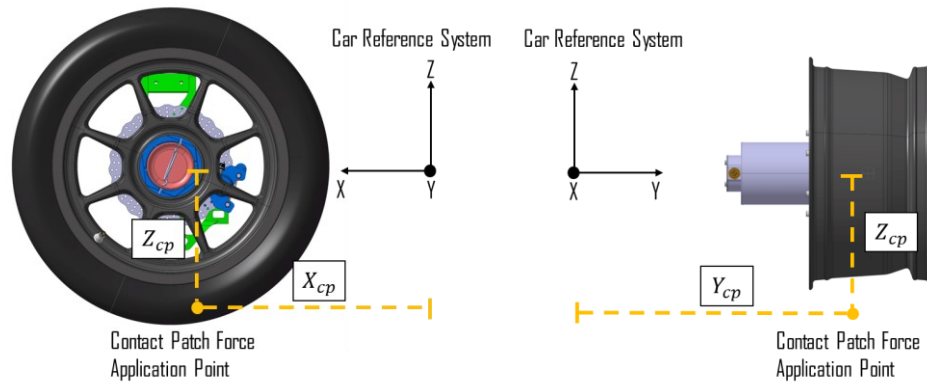


Figure 38 – Contact patch coordinates in Car Reference System

It is needed now to convert the CP coordinates from Car to Upright reference frame; the rear upright is taken into account in this case but the procedure is the same for the front one. The upright reference system has the same axis directions and orientations as the car's one but it is translated into the centre of the upright itself. In particular it has the origin in the centre of the wheel hub on the most outward point of the upright.

The formula used to shift the CP coordinates from one reference system to the other is:

$$\begin{cases} x_{cp} = X_{cp} - X_u \\ y_{cp} = Y_{cp} - Y_u \\ z_{cp} = Z_{cp} - Z_u \end{cases} \quad (4.1)$$

Where:

$(X_u, Y_u, Z_u)$ : are the upright reference frame origin position expressed in the car reference system.

$(X_{cp}, Y_{cp}, Z_{cp})$ : are the contact patch position expressed in the car reference system.

$(x_{cp}, y_{cp}, z_{cp})$ : are the contact patch position expressed in the upright reference system.

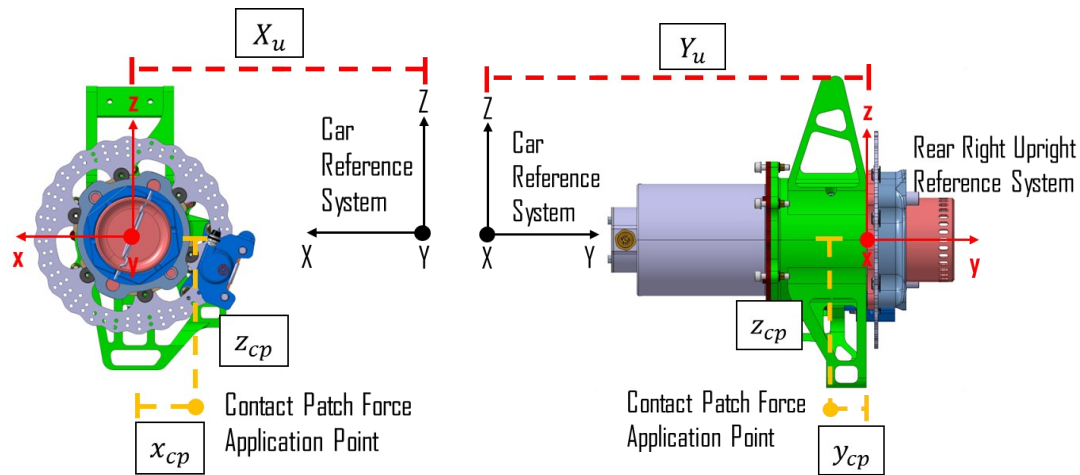


Figure 39 – CP coordinates in upright reference system

The situation is now the one described by the image below: 3 forces applied in one single point (in orange) with known coordinates in the upright reference system (in red). It is needed now to define the upright FEM model itself by deciding the constraints and how to apply the forces.

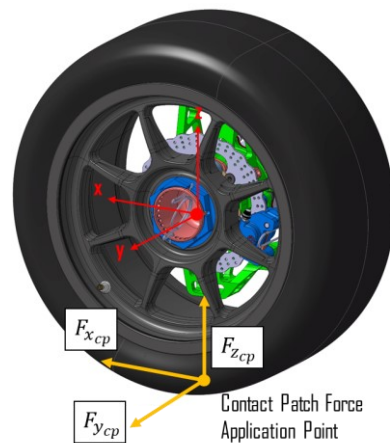


Figure 40 – CP forces representation

Before to proceed it is needed to perform a meshing operation on the upright or on the starting volume, if we are about to start a topology optimisation. The meshing operation was performed using Inspire which gives less control to the user but it is highly faster than doing it on HyperMesh, the upright has some very complex shapes that can be tricky to be meshed correctly avoiding quality index errors.

Also the topology optimisation, as it will be explained in following pages, it has been set up on Inspire. Meanwhile the FEM analysis and the topology optimisation calculation process were completed on HyperMesh.

When the geometry is meshed correctly it is possible to proceed applying loads and constraints.

Starting from the constraints, differently from what done in 2021, the upright was blocked in 3 different points corresponding to the suspension arms outer universal joints: UCAO, LCAO, TIEO.

The constraints were applied using “rigids” connectors present in HyperMesh which are defined also as RBE2 connectors. Meanwhile RBE3 connectors have been used to apply all the loads of the model.

In HyperMesh, "Rigid" and "RBE3" are different element types used to model connections between nodes in finite element analysis. Here's a comparison of the two:

### **Rigid Elements:**

- Represent completely rigid connections between nodes
- Connected nodes do not deform relative to each other and have no relative displacement or rotation
- Suitable for modelling connections that are rigid, such as fixed supports or connections that have negligible flexibility
- Displacement and rotation of one node connected by a rigid element will be directly transferred to all other connected nodes

### **RBE3 Elements:**

- Used to model connections that have flexibility or variable stiffness between nodes
- They allow for different stiffness and mass properties at each node connected to the element, providing flexibility in modelling complex connections

In summary, the main difference between rigid elements and RBE3 elements in HyperMesh lies in the behaviour they represent. Rigid elements are difficult to be used correctly without altering the simulation outputs because they add, as the name says, rigidity to certain zones of the geometry which is not completely true to reality. Rigid elements are needed to apply the constraints to the model because the dependent node of an RBE3 system cannot be directly constrained, as this would lead to a double-dependency for that node.

Here below an image describing the two connection methods is present.

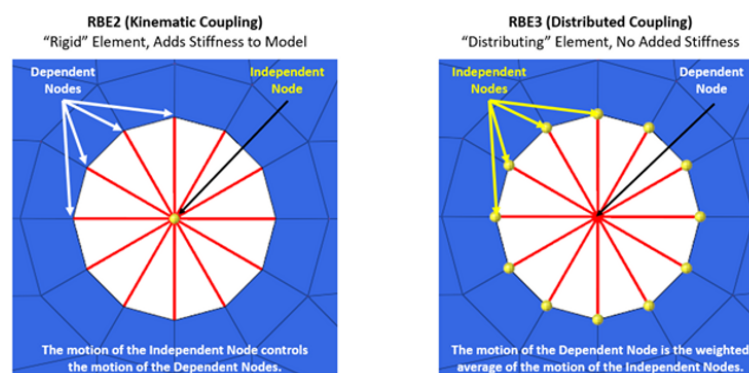


*Figure 41 – RBE2 (Rigids) and RBE3 Comparison*

The universal joints of the suspension outer points have defined coordinates, decided by the Vehicle Dynamics division, and correspond to the independent node of the rigid coupling. Here a constraint is placed blocking only the three translations along the 3 axes, meanwhile

the rotations are left free due to the intrinsic property of the universal joints used in the real vehicle.

In the image below the whole picture of the rear upright with the constraints applied is presented.

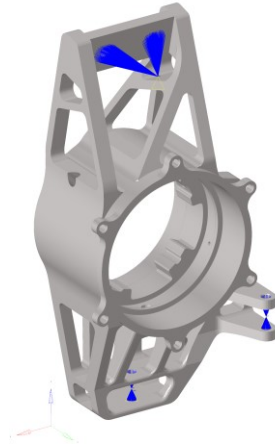


*Figure 42 – Rear upright constraints*

The tie and lower control arm outer points are directly mounted on the upright itself. This linkage is done using some shoulder screws and so the rigids' dependent nodes are distributed on the holes' internal surface to simulate the shear load applied from the screw to the upright. The pictures are self explanatory.

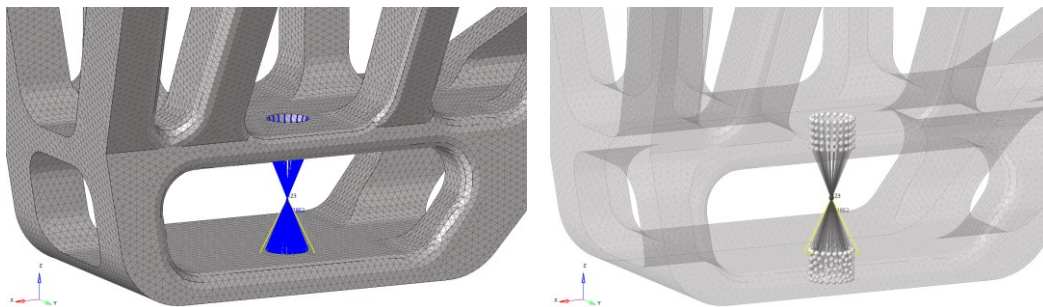


*Figure 43 – LCAO constraint*

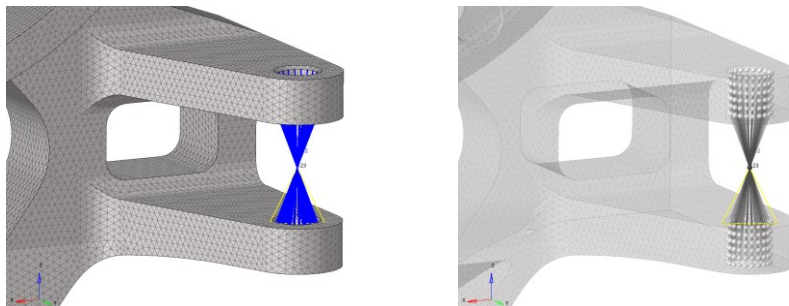


*Figure 44 – TIEO constraint*

A different solution is applied to the UCAO, where the universal joint is not directly linked to the upright but there is a bracket in between the two. This bracket is needed to easily

perform setup changes in camber angle by inserting setup calibrated plates between the upright and the bracket surfaces, as it will be delighted later.

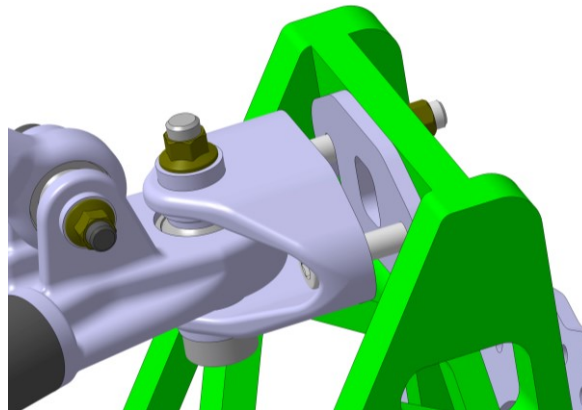


*Figure 45 – UCAO Bracket detail*

The reaction force applied to the upright mounting holes in this case does not produce shear stress but it is distributed on the contact surface. This is simulated by applying the dependent nodes in two circular areas around the bracket mounting holes, on the two upright surfaces perpendicular to the holes axes.

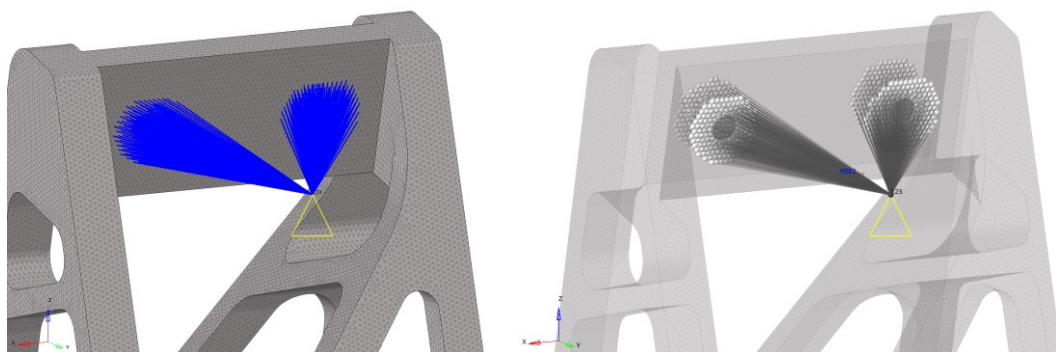


*Figure 46 – UCAO constraint*

The forces applied to the upright will be derived from the 3 fundamental ones which are applied to the CP. From them, a set of the 3 forces and 3 transport moments will be calculated and applied in various points and zones of the upright. There will be also some other considerations to be performed regarding mainly the braking cases, the most complicated ones.



To simulate the transmission rigidity and connection to the upright two rings are inserted in the position of the transmission bearings. The two rings (red in picture below) are connected to the upright using a freeze contact which blocks the two components together. The rings are made of the same steel as the bearings used in the transmission assembly: 100Cr6.

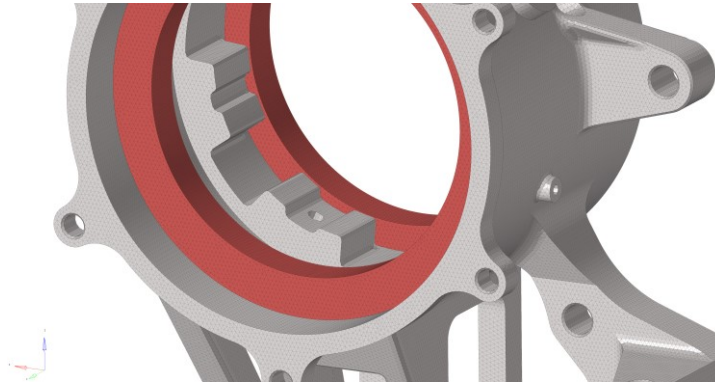


*Figure 47 – Transmission bearings*

The freeze contact is represented by the small pyramids blue and white in the pictures below.

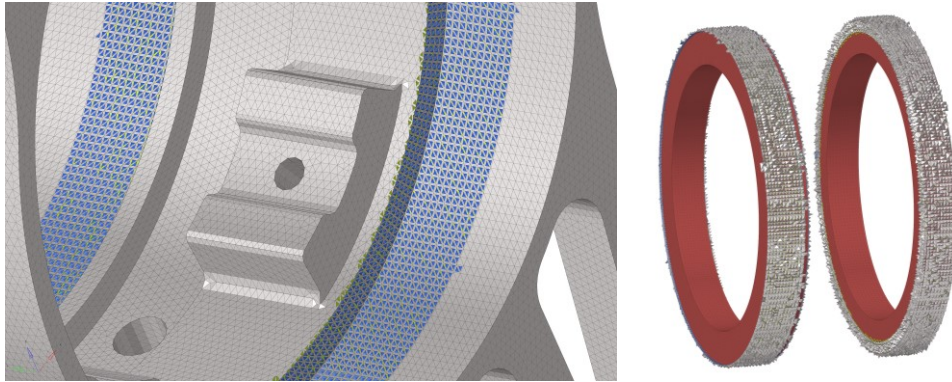


*Figure 48 – Freeze contact transmission bearings*

Most of the forces and moments applied to the upright pass through the bearings, this is due to the fact that the tire and the upright are connected by the rim, the wheel hub and the transmission gears.

To apply the load to a single point an RBE3 system is used, the dependent node is placed in the middle point of the two bearings on the wheel axes. The coordinates expressed in the upright reference system are:  $\{x, y, z\} = \{0, y_b, 0\}$ . The independent nodes are all the ones present on the bearings inner raceway.

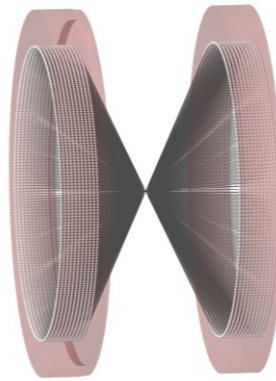


*Figure 49 – Bearings RBE3*

Motor torque is applied to the upright as the reaction of the mounting screws. The motor is attached using 6 screws to one of the faces of the upright, an RBE3 set is used and the dependent node is in the centre of the wheel hub, as it is visible in the images below. The motor stator and cooling jacket are attached here.

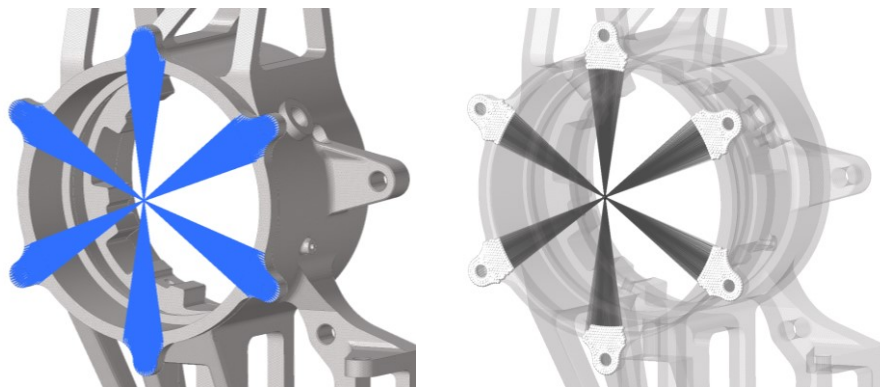


*Figure 50 – Motorplate RBE3*

For the torque around the y axis 2 sets of RBE3 elements are created, one for the positive values of torque and one for the negative ones: this is done to distinguish which sides of the ring gear teeth are in contact with the upright teeth seats.

In the images below the master nodes selected and the two coloured RBE3 sets are visible.

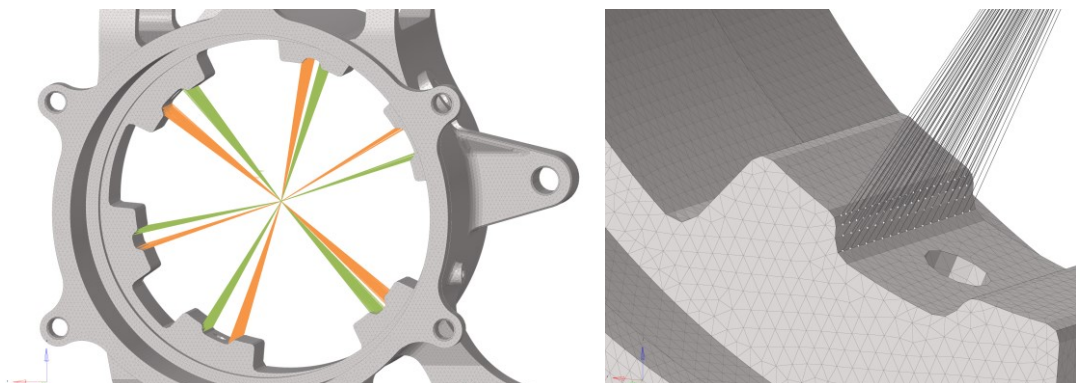


*Figure 51 – Ring gear RBE3*



Here the elements used to connect the brake force application point to the brake calliper mounting holes on the upright are visible. As we can see the application point is located slightly shifted towards the outside of the upright where the brake disk is placed, and the position is dictated by the pads centre point. The elements used are RBE3 and the master nodes are placed inside the mounting holes to simulate a shear effect due to the brake forces. The master nodes selected are only the ones which give a compression stress to the upright to better estimate the stress created.

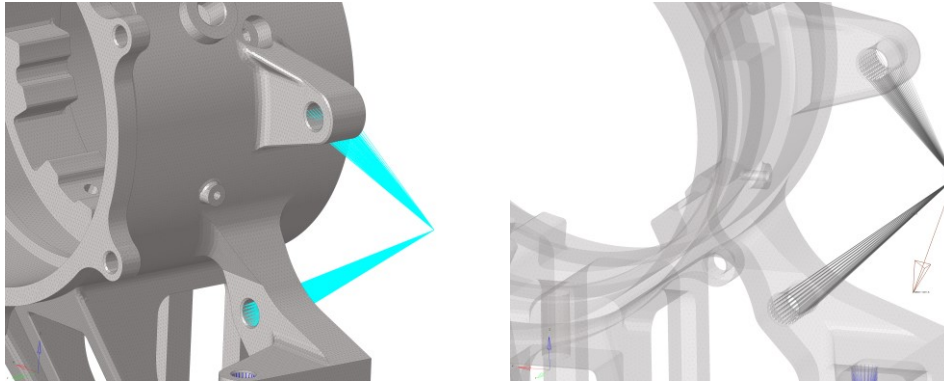


*Figure 52 – Brake calliper RBE3*

It is now possible to begin the calculations that are needed to change the forces application point to the desired ones created by the numerous RBE3 sets discussed above. When doing so, a transport moment needs to be calculated and applied to not change the resultant action on the component itself. One of the first points to be discussed is the bearing centre application point: here the three forces and two transport moments will be applied ( $F_x, F_y, F_z, M_x, M_z$ ). The transport moment around y axis it is not applied here because the bearings are free to rotate around this direction and so they will not “see” this torque applied.

Here below a schematic representation of the bearings RBE3 application point is inserted,  $y_b$  is the upright bearings central point coordinate in Upright Reference System.

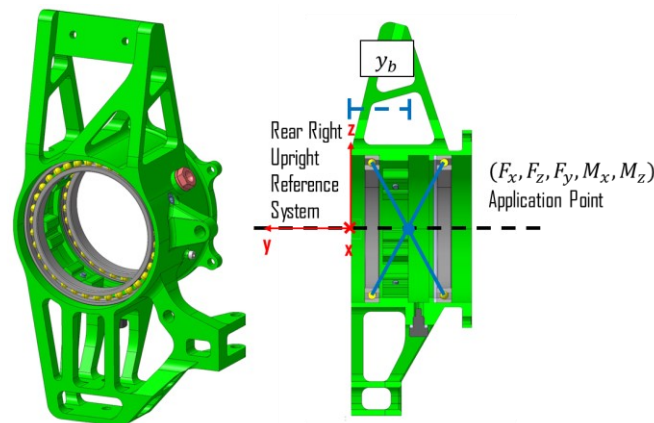


*Figure 53 – Bearing centre application point*

To calculate the transport moments arising from the variation of application point of the forces is sufficient to calculate the moment generated by the forces in their original position with respect to the new position.

This is done by knowing the CP coordinates expressed in the upright reference system, already calculated in some paragraphs before.

The formulas used to do so are the following:

$$\begin{cases} M_x = F_{z_{cp}}(|y_b| - |y_{cp}|) + F_{y_{cp}}|z_{cp}| \\ M_z = -F_{x_{cp}}(|y_b| - |y_{cp}|) + F_{y_{cp}}x_{cp} \end{cases} \quad (4.2)$$

All the terms inserted in the equations above have been already explained before. Here below there is a representation of this calculation steps.

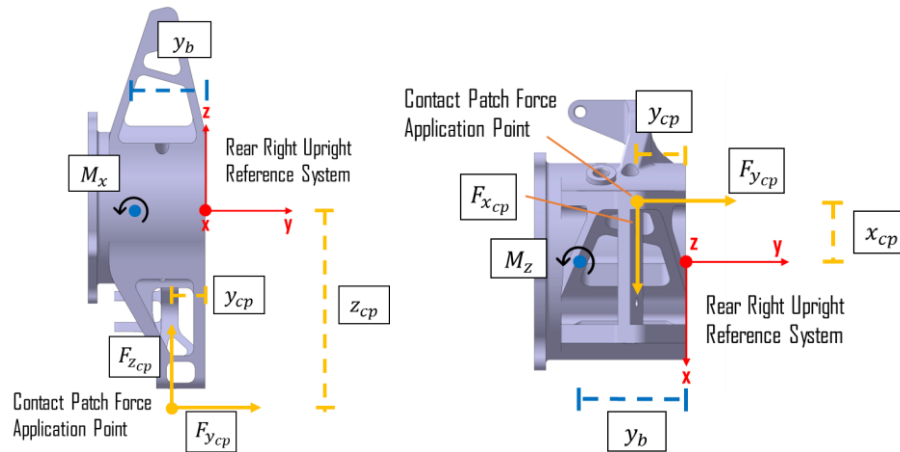


Figure 54–  $M_x$  and  $M_z$  calculation

The transport moment around  $y$  axis is applied to the ring gear centre point. This is due to the fact that the ring gear of the transmission is not free to rotate around  $y$  axis but, instead, has a toothed connection with the upright.

It can be calculated using the following formula:

$$M_y = -F_{z_{cp}}x_{cp} - F_{x_{cp}}|z_{cp}| \quad (4.3)$$

It's important to underline that in the braking load cases (PB and BIT) the contribution of  $F_{x_{cp}}$  to  $M_y$  has been cancelled due to the fact that it is already taken into account in the braking forces and moments that will be explained in the following paragraphs.

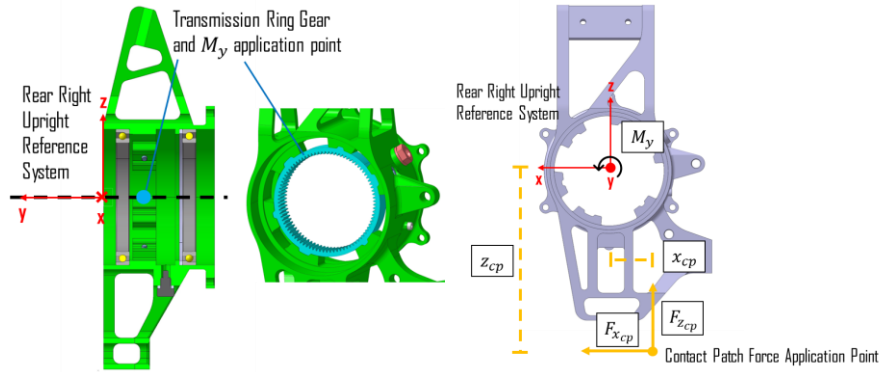


Figure 55 –  $M_y$  transport moment calculation

The motor applies to the upright, through the transmission, a torque which can be calculated from the transport torque around y axis, coming from the contact patch forces. It's important to consider in the calculations the fixed transmission ratio that the Team's car have on all the 4 wheels. This motor torque will be limited to the maximum possible one that the motors can output and will be considered only in traction phases, in braking phases the calliper forces will be inserted instead.

$$M_{motor} = \frac{M_y}{\tau} \quad (4.4)$$

Where:  $\tau = 14,69$  = Transmission ratio (constant)

The direction of the moment is related to the reaction torque that the upright “sees”, which is opposite to the actual direction of the torque applied to the wheel.

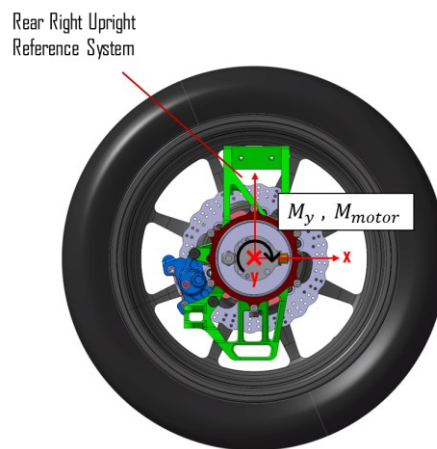


Figure 56 – Motor torque calculation

A little bit more complicated study needs to be done when considering the braking forces and moments applied to the uprights. The calliper position plays a big role when calculating the direction of the resultant force. The calliper position is opposite in the front and in the rear uprights; this is done to centre the masses of the car and lower them as much as possible. This is why it is needed to present the two cases separately.

Starting from the rear one. In this case the calliper is placed towards the front of the vehicle (on the right in the pictures below). The braking force applied to the calliper mounting holes has been calculated from the longitudinal force between tyre and ground. Of course the upright will receive the reaction force and so the direction will be the opposite with respect to the real braking torque applied to the disk and consequently to the wheel.

Here below the scheme of the forces acting on the calliper mounts is presented.

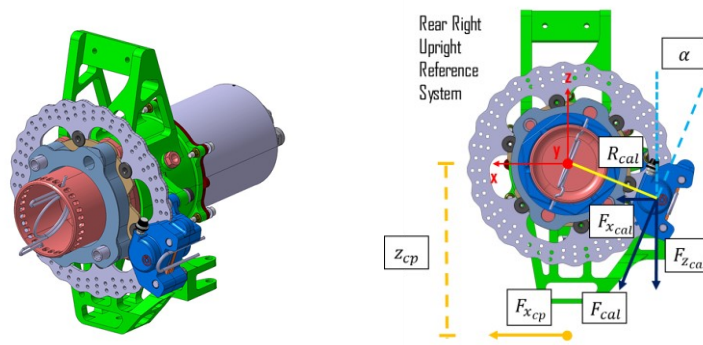


Figure 57 – Rear calliper force calculation

The calculations coming from the image above are the following:

$$M_{b_{cp}} = M_{b_{cal}} \rightarrow F_{x_{cp}} z_{cp} = F_{cal} R_{cal} \rightarrow F_{cal} = \frac{F_{x_{cp}} z_{cp}}{R_{cal}} \quad (4.5)$$

$$F_{x_{cal}} = F_{cal} \sin \alpha \quad (4.6)$$

$$F_{z_{cal}} = -F_{cal} \cos \alpha \quad (4.7)$$

Where:

$R_{cal}$  = Rear Brake force application radius (half of the disk braking band)

$\alpha$  = Rear Brake Force inclination (tangential to the disk)

$M_{b_{cp}}, M_{b_{cal}}$  = Braking torque at the contact patch and at the calliper respectively.

The front upright will undergo the same calculations but with different force directions. The calliper in this case is placed towards the rear of the vehicle, on the left in the picture below.

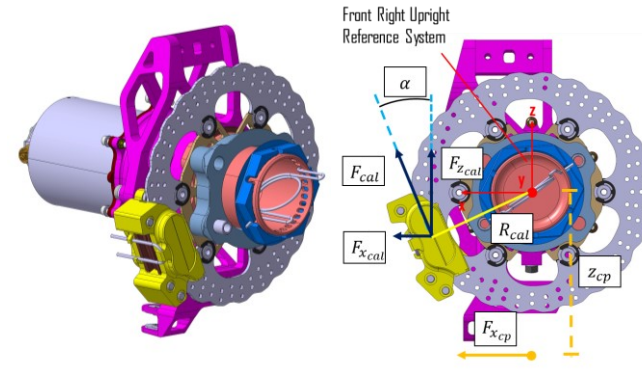


Figure 58 – Front calliper force calculation

The formulas used for calculating  $F_{cal}$  are the same but  $\alpha$  and  $R_{cal}$  have different values, as easily predictable from simple dynamic studies. The front brakes are bigger both in disk size and in calliper number of pistons. The equation 4.6 is again used also in this front case, meanwhile the equation 4.7 is changed in sign.

$$F_{z_{cal}} = F_{cal} \cos \alpha \quad (4.8)$$

Moreover, to conclude the FEM model explanation, it is necessary to apply some additional internal forces that balance the braking forces of the calliper  $F_{x_{cal}}$  and  $F_{z_{cal}}$ . These two forces are opposite to the ones applied on the calliper and are positioned in the centre of the bearings of the upright. By doing so it is also necessary to apply a transport moment around x and z axes. Here below the equations and images valid both for front and rear cases.

$$y_{disk} = y_b + y_{calliper} \quad (4.9)$$

$$M_{x_b} = F_{z_{cal}} y_{disk} \quad (4.10)$$

$$M_{z_b} = -F_{x_{cal}} y_{disk} \quad (4.11)$$

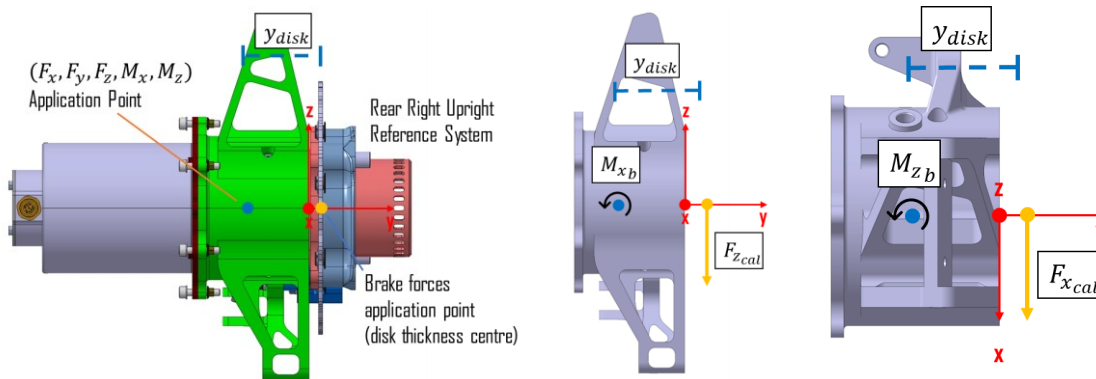


Figure 59 – Internal braking balancing forces and moments

The FEM model explanation is finished and it is now time to explain, in the next section, the topology optimisation settings and procedure.

It is important to underline that the model explained in this section has been applied firstly to the starting volume, discussed in section 4.2, to perform the optimisation process and only afterwards to the completed component to verify it and evaluate its performances. In this pages the finished rear, and sometimes front, uprights have been adopted to present the model for easiness and commodity because the starting volume has far bulkier geometry and it is more complicated to understand the zone analysed in the pictures.

## 4.4. Topology optimisation

As done in 2021 the topology optimisation is the first analysis to perform on the starting volume to obtain the final geometry. The analysis has been set up using Inspire, then it has been exported in HyperMesh and the real calculation process has been performed using this program.

The loads and constraints applied on the starting volume are the same as the ones described in section 4.3 and the load cases used for the optimisation were six: PA, PB, PL, AIT', BIT' and PA0 as presented in Section 3.2.

In 2022 the upright production method selected was CNC and so it is needed to add some additional settings to the topology optimisation setup to make the result suitable for CNC milling operations. It is mandatory to apply a shape control to limit the geometry complexity of the results obtained by the software. The strategy adopted in this study was to proceed in 3 steps:

- 1. Topology optimisation only in **Y-direction** starting from the original volume and subsequent reconstruction of the geometry.
- 2. Topology optimisation only in **X-direction** starting from the previous step geometry result and then reconstruction of the new geometry.
- 3. Final optimisation and reconstruction in **Z-direction**.

As done in 2021, the starting volume was divided in design and non-design space, so that the optimisation process and reconstruction was related only to the design space.

The shape control cards in Inspire allow to easily set the optimisation direction as shown in the image below, in this case the Y-direction was selected.

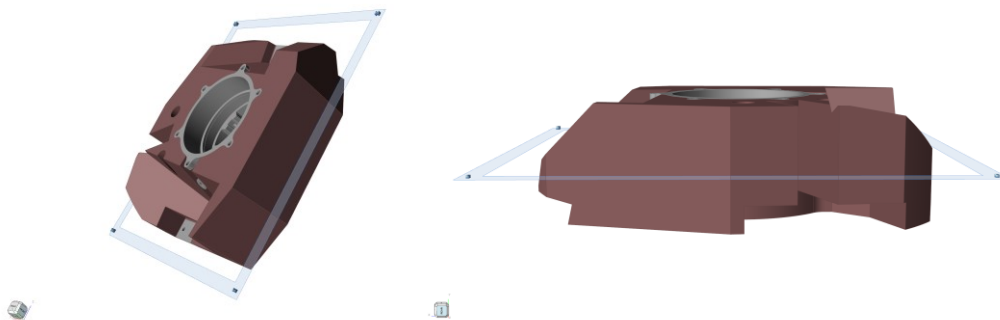



*Figure 60 – Topology optimisation shape control*


The optimisation objective was set to be “maximise stiffness” as done in 2021 but some additional parameters related to the minimum and maximum thickness of the material left after the optimisation were added.

The output result of the topology optimisation run with HyperMesh is an “.stl” file, a distribution or density map of the material. It is also possible, using a slider on Inspire or a parameter in HyperMesh, to check the quality of the optimisation process. This can be done by changing the density map visualization by gradually removing the material at the edges of

the optimised shape. But, to continue with the steps, the optimisation in the following direction, an “.stp” file is needed instead.

STL and STP are two common file formats used in the field of computer-aided design (CAD) and 3D printing. Here's a brief overview of each format:

 **STL** (Standard Triangulation Language): file format commonly used for 3D printing and rapid prototyping. It represents 3D geometry as a collection of connected triangles (mesh). STL files store the coordinates of the vertices and the surfaces' normals of each triangle.

 **STP** (Standard for the Exchange of Product model data or STEP): file format used for exchanging 3D CAD models between different software applications. It supports the representation of not only geometry but also other design information, such as product structure, assembly relationships, and metadata.

While STL files are primarily used for 3D printing and represent the surface of an object as a mesh, STP files are more comprehensive and include a richer set of information about the 3D model, making them suitable for design collaboration, data exchange, and interoperability between CAD systems.

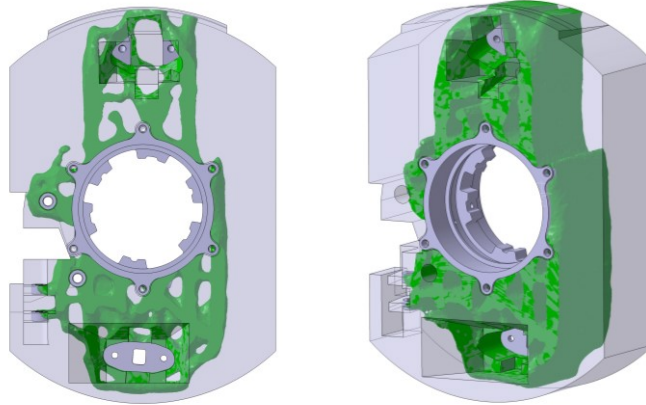
To pass from STL file, output of the optimisation process, to the STP file needed to continue the design phase the procedure adopted is different with respect to the one used in 2021. In particular using Inspire and designing a component for 3D printing, wrapping and fitting tools work really well, instead for CNC milling a more canonical geometry is needed to allow the machine to work faster and cheaper.

The procedure adopted is the usage of a CAD program such as CATIA. The STL file is imported and superimposed to the starting volume STP file. The starting volume is then set to have a degree of transparency (such as 50%) to allow the visualization of the density distribution related to the STL file.

In this way, manually, it is possible to copy the geometry on the starting volume by creating pockets and chamfers where needed. It is crucial and trivial that the objective is not to copy every little detail of the simulation output, doing so would result in a very complex and not continuous geometry. Both from production and performance point of view is far better to have a linear and defined geometrical shapes than having continuously varying thickness and angles.

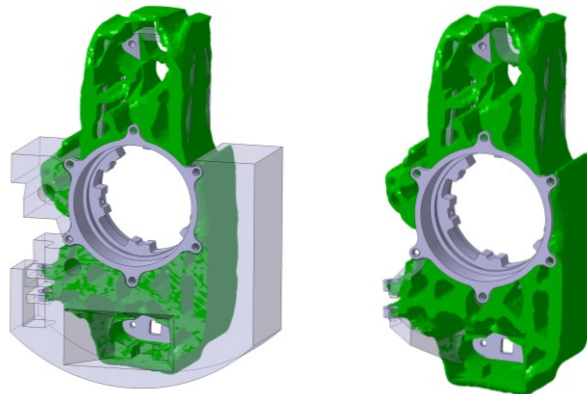


Here below there is an example of “reconstruction process” in various steps. In these first two images below, it is clearly visible the optimised density map (in green), the non design space (in solid grey colour) and the design space starting volume (in transparent grey). These pictures represent the first step of the optimisation process, Y direction.



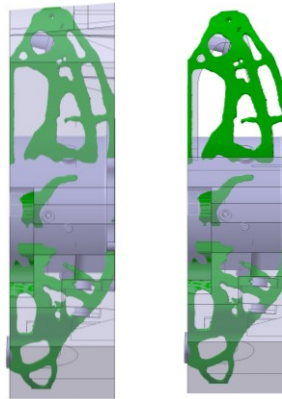
*Figure 61 – Rear Upright Y Direction optimisation*

After having imported the optimised STL file and set the correct transparency level, it is possible to begin with the proper reconstruction procedure. Here below are presented two instants of the work.






*Figure 62 – Rear Upright Y Direction reconstruction*

The reconstructed geometry will be then re-analysed and optimized in the other direction (X in this case). Here below the files superimposed in the CAD software.



*Figure 63 – Rear Upright X Direction reconstruction*

It is fundamental to keep in mind these three simple things, all strictly related to each other:

-  When performing an engineering design of a complex component as the upright, it's mandatory to use the software outputs as an help and do not substitute them to the engineering thinking of each designer. This is why, experience plays a big role in this industry. And this enhance the importance of projects such as Formula Student!
-  Some pockets and holes are ignored by the mechanical designer because may be redundant and too expensive;
-  It is not always needed or mandatory to perform the optimisation also along the third direction (Z in this study case). Sometimes the geometry output of the two main directions is already quite intricate to manage in a CNC machine.

Another example of utilising the software in a smart way is the LCAO solution applied in 2022, which differs from the one applied in 2021. In 2021 the LCAO used a bracket between the universal joint and the upright, this was done for both UCAO and LCAO. In 2022 the bracket for the LCAO was substituted by creating the bracket geometry directly on the upright itself.

This was decided after performing the topology optimisation and so, in the results presented above was not present. The bracket material was Ergal in 2021 and so, the same dimensions were used on the upright in 2022. T

he solution was then analysed using FEM, of course. Instead, for the UCAO, the bracket is still present because it's needed to be able to make camber adjustments using calibrated shims.

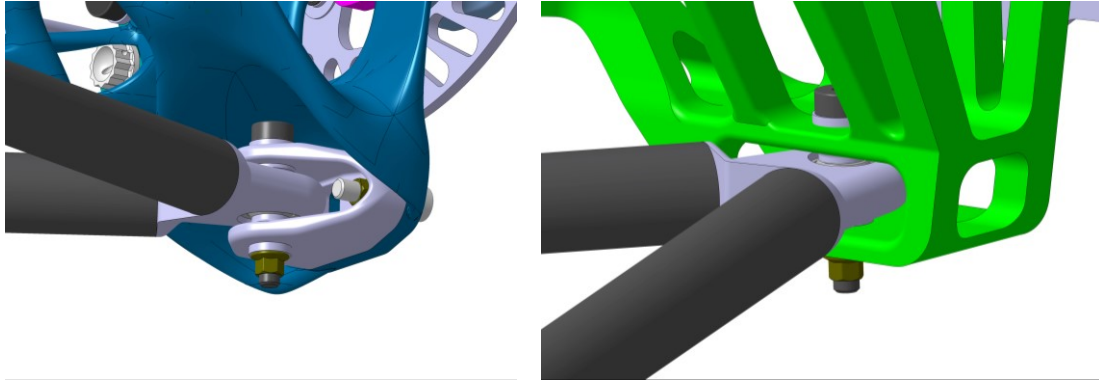


*Figure 64 – LCAO 2021/22 comparison*

This solution could save some weight and increase the performance of the upright in that area by creating a parallelepiped geometry. It's hard to judge the exact weight difference between the two solutions because the entire geometry is affected. For sure, two bolts, knuts and washers are taken out from the assembly.

In the next chapter the final geometry and, consequently, final FEM analysis are presented in detail.

## 5. Results and testing

In this chapter the final uprights geometry as well as the FEM analysis results will be presented and discussed. There will also be a small section devoted to some discrepancies that have arisen between the CAD file and the manufactured components. Other two sections will be dedicated to the test phase and the additional components designed and produced to enhance the vehicle's setup changes.

Speaking of final components, here below are inserted the screens of the finished geometry. After reconstructing it, some little modifications has been made such as some additional chamfers and fillets.

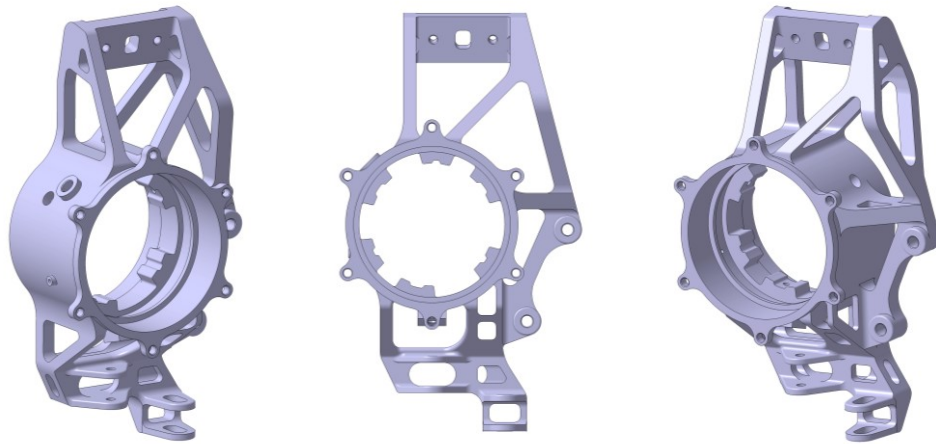


*Figure 65 – SC22 Front upright*

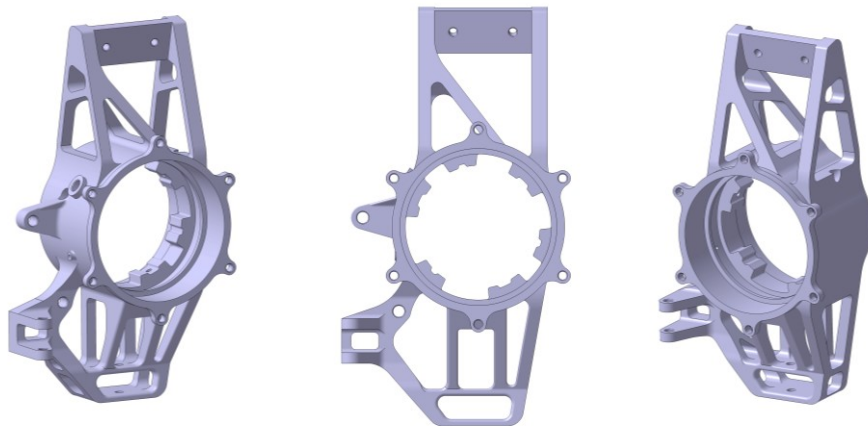


*Figure 66 – SC22 Rear upright*

The front upright is obviously more complex due to the limitations dictated by the steering action that needs to be possible. This is why the LCAO design is a lot different with respect to the one of the rear upright. The TIEO of the front upright is differs as well due to an additional setup change that has been studied this season. In particular the steering Ackermann characteristic can be varied using a flip chip insert placed in correspondence of

the tie outer point and adjusting the length of the tie rod itself. More details regarding the flip-chip will be given in section 5.4.

It is noticeable, looking at both the uprights, how the geometry around the cylindrical shape of the non-design space is really simplified. This has been done to lower the production costs and speed up the process. Also the internal radii have been “standardize” as much as possible to avoid the tool change procedure.

In particular, this has been done in late design phase after receiving the quotation of the production costs related to the first version of the rear upright. Slight modifications were then made, and statically analysed, to reduce the costs of the components.

Here below are inserted two pairs of images in which one of these modifications is highlighted. In the second version (in grey colour), it is sufficient to perform the holes using two principal directions of milling (Y and Z), there is no need of combined movements.

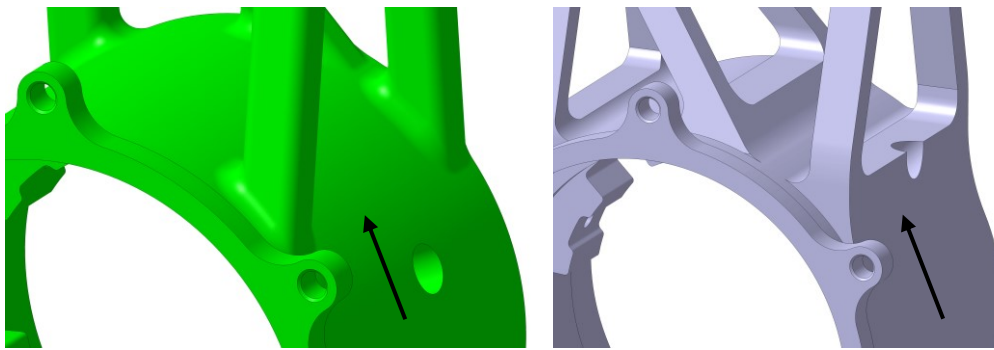


*Figure 67 – Rear upright version 1 and 2 comparison (1)*

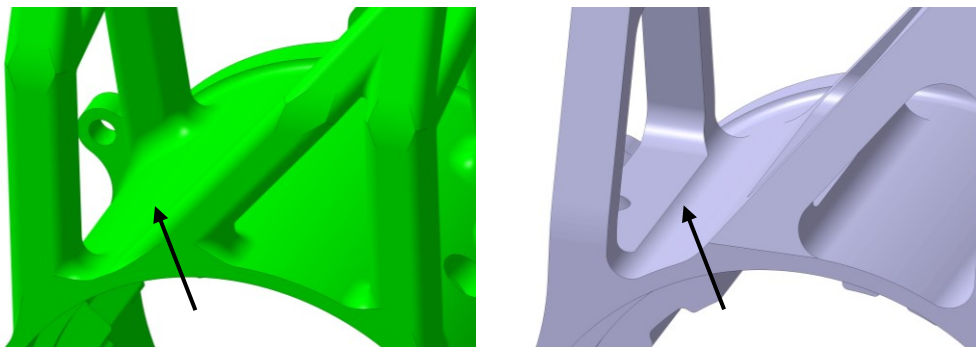


*Figure 68 – Rear upright version 1 and 2 comparison (2)*

The most important thing to do, after having decided the final geometry of the component, is to do the engineering drawings. These are used by the manufacturer to program the instructions to pass to the technician that will follow the CNC-machine during the process. On the engineering drawings, all the tolerances, such as form control and orientation control of a particular feature or hole, are detailed. In the uprights, the most stringent tolerances are found on the transmission bearings raceway, to ensure a correct installation of them, which is done by press-fitting. It's fundamental to know that, in legal terms, the 2D drawings are still the only valid document in case of issues with the produced components, despite the spread use of 3D file (such as STEP format), which are necessary for the correct use of CNC machines.

This final geometry has been obtained after the topology optimisation and reconstruction iterative process, and finally, after FEM analysis, the results of which are presented in the next section.

## 5.1. FEM results

In this section the static analysis results will be presented. Firstly, the design load cases will be inserted and discussed for both front and rear uprights. After that, it will be the turn of additional load cases described in section 3.2.

Before to start with the results, it is mandatory to explain one simple concept that has been applied to all the analysis performed. The vehicle dynamics division studies the load cases by simulating a right turn (when needed, not in PA or PB of course), due to the lateral load transfer the higher forces will be on the left side of the vehicle. This can be demonstrated by simple lateral dynamic equations.

The unfortunate thing is that, usually, mechanical designers are used to adopt the right side of the vehicle as their design space. This means that, to perform FEM analysis and topological optimisation there are two ways:

- ✍ Mirror the geometries of the components to obtain the vehicle's left side assemblies and apply loads on that.
- ✍ Use the right side parts but change the sign accordingly to the forces in the load cases (simulating a left turn instead of the original right one).

In this work, the first option has been adopted, this is why the following images will have a mirrored geometry, different from what has been presented up until now.

Starting with the canonical load cases, presented in **Table 6**:

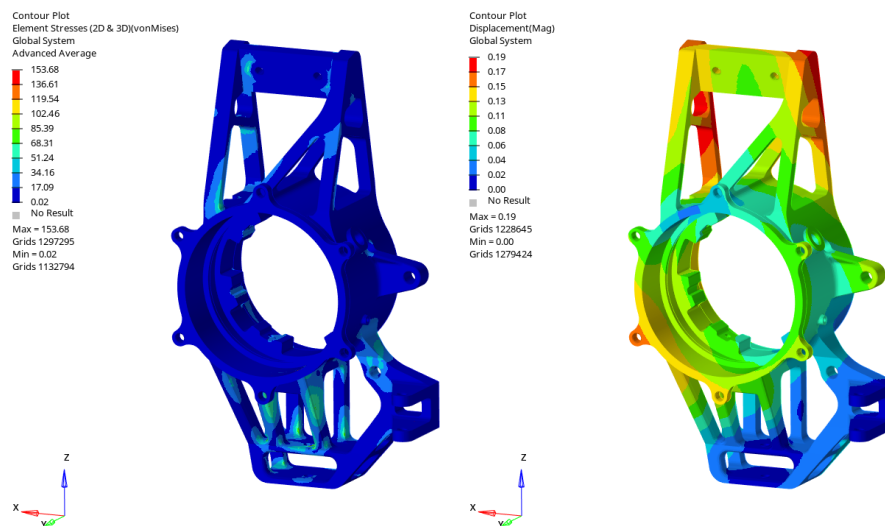
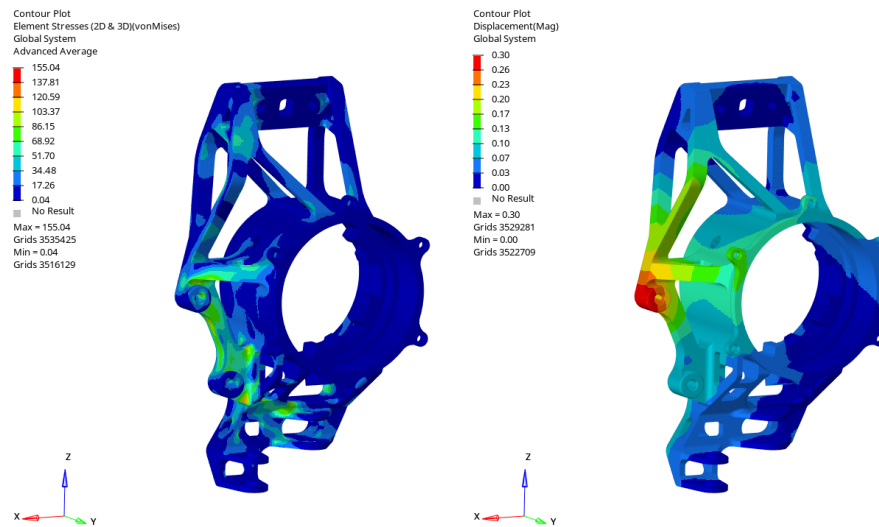


Figure 69– SC22 Rear upright AIT load case





*Figure 70 – SC22 Front upright PB load case*

In these images both front and rear most severe load case FEM result is inserted.

As for the 2021 solution analysis, the stresses method calculation is Von Mises. Here below a table which summarizes the results obtained.

	Max Displacement	Critical load case (displacement)	Peak Von Mises Stress	Safety Factor	Critical load case (S.F.)
<b>Front Upright</b>	0,30 mm	PB	155,04 MPa	2,90	PB
<b>Rear Upright</b>	0,19 mm	AIT	153,68 MPa	2,93	AIT

*Table 11 – SC22 Uprights design FEM results*

As it can be seen from the table, the safety factors are really high for a Formula Student component, especially if compared to the ones of the 2021 season. In the last chapter a more precise comparison will be delivered. It is interesting to notice that for the front axle the pure braking capability of the prototype are more severe than the traction phase, which is instead prevailing for the rear axle. This behaviour was expected and, logically, it appeared also in 2021.

As always, these maximum values tend to be localized in small portions of the component and, as it will be present later, there can be some outliers values due to some meshing or modelling errors in the calculation process. It is logical to state that, the safety factor calculated using this maximum values, without any filtering process applied, can be considered as already having an intrinsic safety factor. This last sentence is useful to further reassure the mechanical designer regarding its components.

Passing now to the additional load cases, presented in **Table 8**, the first one inserted is the pure braking extreme event. Even though the displacement results will be shown, they are not be taken into account in a deep way, because for these situations the only logic target is

to now have a failure in the component. These cases describe really demanding situations in which the whole vehicle is unsettled by the bump or curb and so, the variation of the wheels characteristic angles coming from mechanical components compliances are negligible.

Here below the results for the extreme braking case, a deceleration of 3.5 g at 120 km/h is simulated. The results show a really good behaviour of the designed components, the safety factor remains really high, even for the front upright, which is the most affected between the two, as expected. Safety factors values of all these additional load cases will be presented in a table at the end of this section.

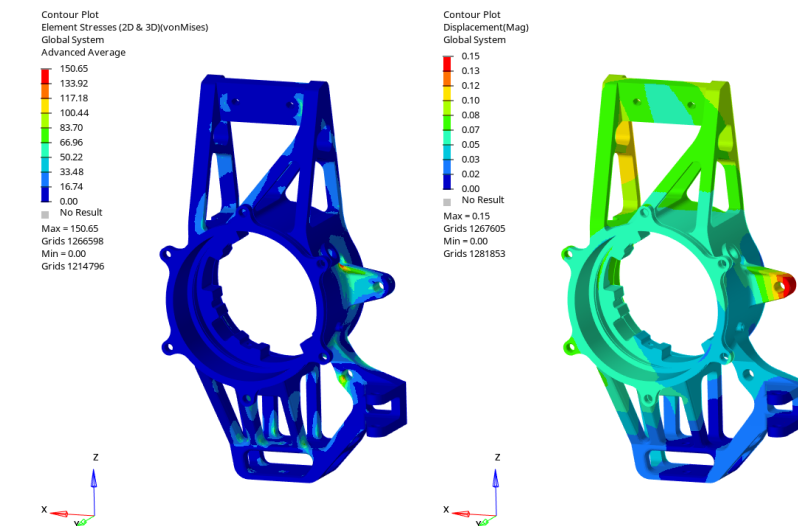


Figure 71 – SC22 Rear upright extreme braking load case

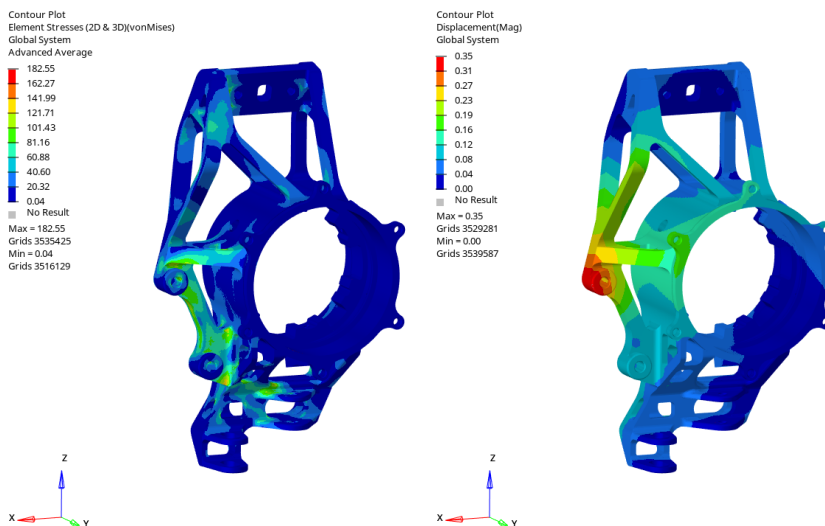


Figure 72 – SC22 Front upright extreme braking load case

Moving on to the following load scenario, the bump one. As a reminder, this load case simulate a bump of 70 mm caught by a wheel at various speed and acceleration combinations. The most severe was found to be the one at vehicle max speed (around 120 km/h) with null longitudinal acceleration (Superfast case), as imaginable by being at top speed.

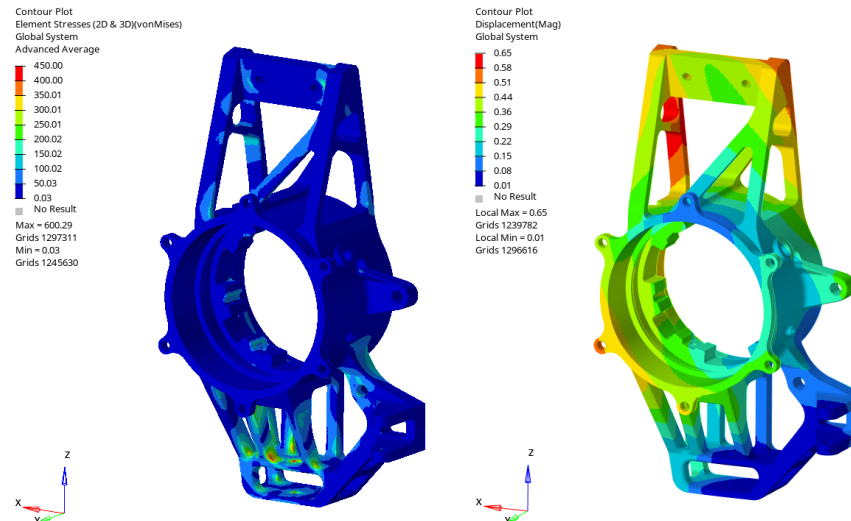


Figure 73 – SC22 Rear upright superfast load case

It's important to notice how the colour scale is set to have as maximum value 450 MPa, which is exactly the yield strength of the material. This has been done because there were some misleading results in the model, resulting in around 600 MPa of peak stress. These results can be explained by two plausible reasons:

- ✍ Too coarse mesh: being such a big component, when meshing the upright a compromise has to be found. As already explained in some chapters before, having a too fine mesh will result in huge computational time and power. Having a more large mesh size will allow to perform simulations and analysis easily but could arise some issues around very complex zones of the component, such as sharpe edges or holes.
- ✍ RBE2 rigidity: this type of connectors, needed to apply a constraint to a node, have infinite rigidity. This aspect will result in very strange behaviours when the connectors are applied to small hole edges. The small mesh element, of a defined material, will be in contrast with the infinite rigidity of the connector and stresses will increase drastically.

This aspect of the results analysis described above is another example of using the software in a smart manner, by having an engineering mind.

Similar results have been seen for the front upright, in the same load case scenario.

Again, the maximum stress value in the scale is set at 450 MPa for the same reasons described above.

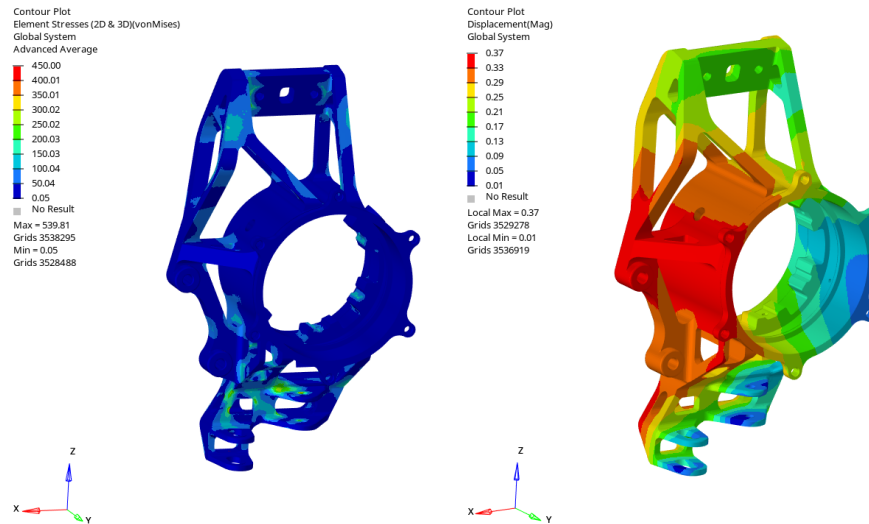


Figure 74 – SC22 Front upright superfast load case

Here below there is a clear representation of what is happening around sharp edges and holes for both the rear (on the left) and front (on the right) uprights.

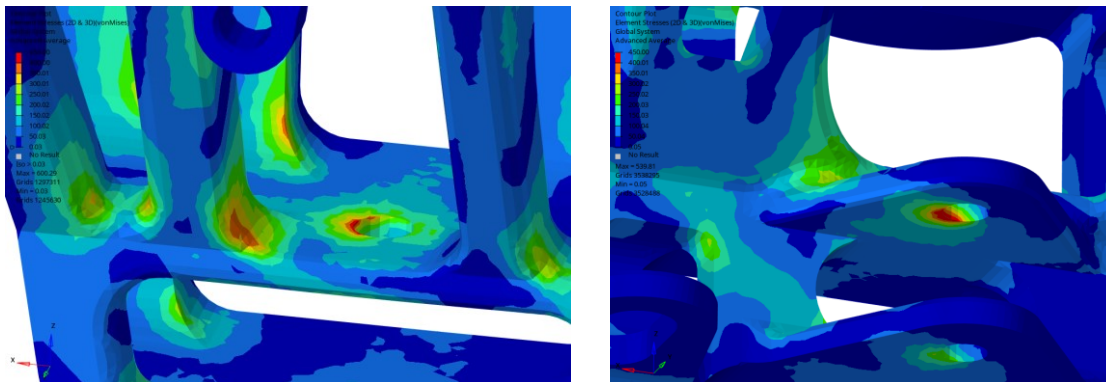


Figure 75 – Stress concentration around sharp edges and holes

The last but not least load cases added to the static analysis are the curb ones. In these scenarios, the curb impact is simulated by adding the obstacle forces to the canonical design load cases forces.

The most critical case found was the pure braking (with curbs) for both the front and rear uprights. The fact that also for the rear upright the most critical case is pure braking can be easily explained by looking at the speed at which the forces are calculated: PB velocity is set at 100 km/h, the highest among all the load cases. Thus, resulting is huge obstacle forces.

Again, for both front and rear upright, the maximum stress is set at 450 MPa for the same issues as the case presented before, as it can be observed in **Figure 78**.

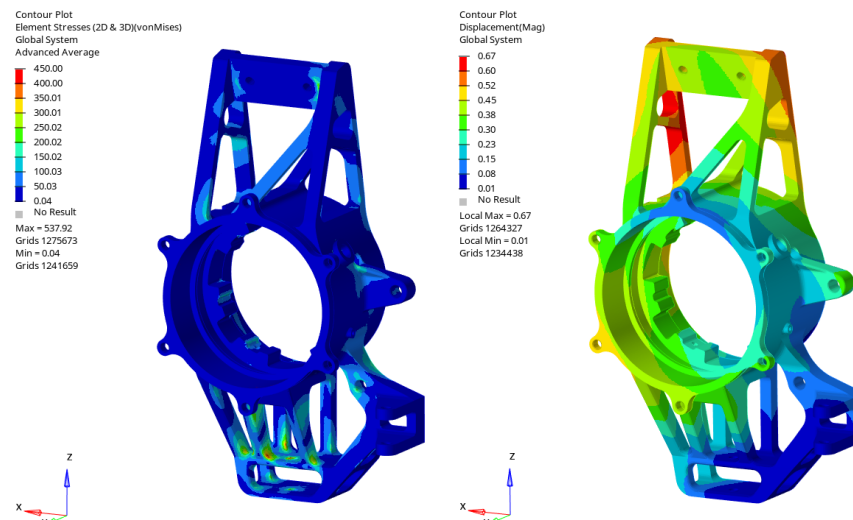


Figure 76 – SC22 SC22 Rear upright curbs (PB) load case

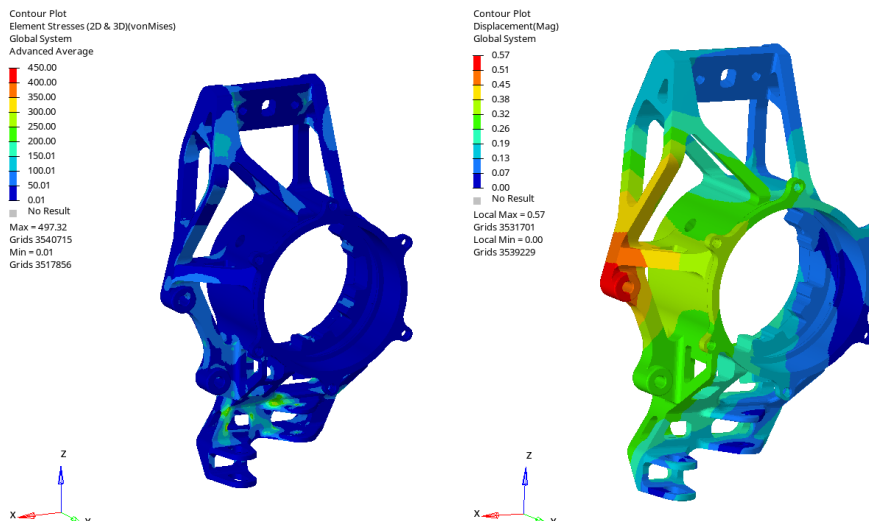


Figure 77 – SC22 Front upright curbs (PB) load case

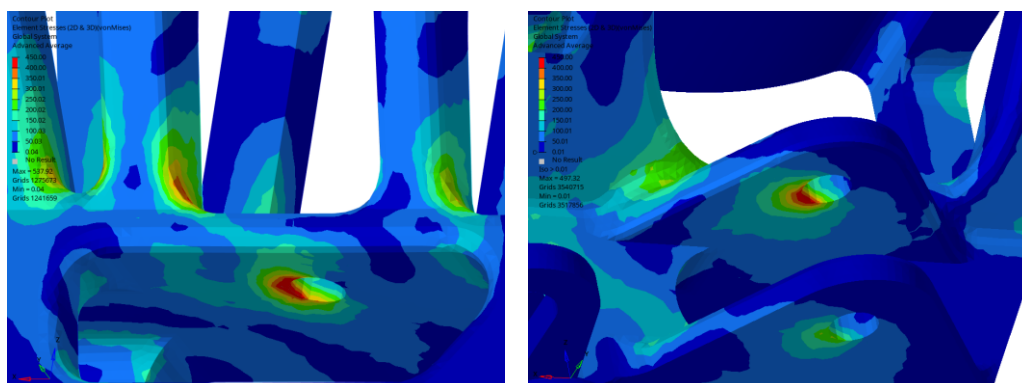


Figure 78 – Curbs (PB) edges stress concentration

To conclude this section, it is admissible that the results found for the additional load cases are really encouraging if we speak about the safety level of these components. Despite some

meshing errors that lead to the strange behaviour already discussed, the overall results are acceptable.

It is important to remember that, these load cases, are very extreme and weren't taken into account during the design phase.

## 5.2. Production-CAD discrepancies

In this section a brief comparison between the produced uprights and the final CAD geometry will be given.

Here below some pictures of the produced uprights are present.

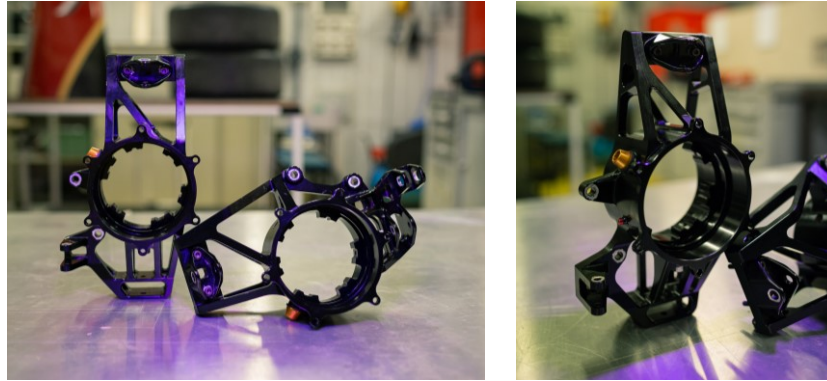


*Figure 79 – SC22 produced uprights*

It is interesting to perform the comparison between the predicted weight, calculated by the CAD software using the volume of the component and the density of the material selected, Ergal in this case, and the real one of the components after production. It is important to note that the weight estimated by the CAD is based on theoretical and ideal values, while the actual weight of the produced part is influenced by multiple real-world factors. Therefore, it is normal to have some discrepancy between the two values. If the weight difference is significant and may affect the performance or functionality of the part, it is necessary to analyse the causes of the discrepancy and make any necessary modifications to the production process or CAD model.

In the table below the singular weights and percentage differences are listed.

<b>UPRIGHT S</b>	<b>CAD weight [g]</b>	<b>REAL weight [g]</b>	<b>Difference [%]</b>
<b>Front Left</b>	895,0	901,4	+ 0,7
<b>Front Right</b>	895,0	899,5	+ 0,5
<b>Rear Left</b>	858,0	853,3	- 0,6
<b>Rear Right</b>	858,0	854,5	- 0,4

*Table 12 – Weight comparison CAD vs REAL*

As it can be seen, the differences are really low, under 1%. This means that no critical issues were found in the geometry during the production phase, in terms of impracticality for the machine to remove the material from the starting billet.

Some small differences are still noticeable between two components of the same axle, front left and right for example. This can be explained by the presence of variations in actual



density or material composition of the alloy and also by the production tolerances. During the manufacturing process, tolerances can affect the dimensions and thickness of the part. Even small variations in dimensions can have an impact on the final weight.

The only small feature that was not possible to replicate using the CNC-machine was the one highlighted in the picture below. More precisely, the necessary tool to perform it should have been a particular, very long, one and it wasn't available for the specific machine used. The feature was cut from the side, using a shorter tool, and it was not possible to remove completely the material.

It's important to underline that the feature in question is not critical nor for the safety nor for the performances of the components; it was just designed to lower the parts' overall weight.

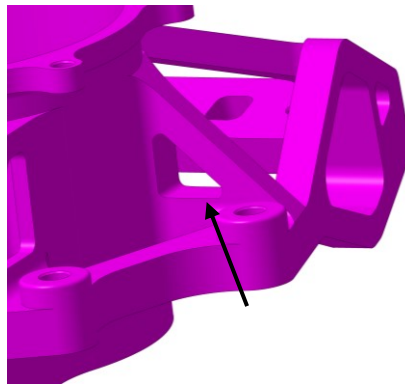


*Figure 80 – Front upright feature's detail*

### 5.3. Assembly and testing

The uprights are connected to an handful of other sub-assemblies of the vehicle and so, it is interesting to take a look at the overall wheel assembly picture present here below.

On the left, the rear one, and on the right, the front one.

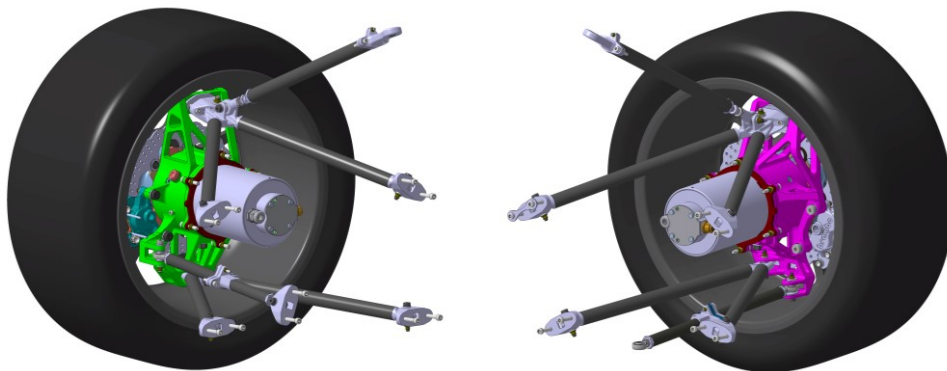


*Figure 81 – SC22 Wheel assemblies*

During the assembly itself, there were no particular issues related to the packaging of the components and of the tools needed to perform the locking and mounting operations. It seems like an obvious sentence but it is not.

When designing a component on the CAD software there are many possibilities to zoom in, zoom out and even take out some parts by simply clicking an icon: this is very powerful but really risky because it is easy to forget to re-visualize something.

This can lead to serious mounting and packaging issues, also because it's hard to understand the real dimensions of the components visualized on screen; sometimes the space required for an human hand to operate on a screw it's not trivial.

Speaking of testing and track action, monitor the upright assembly's performances using sensors is practically impossible. The only aspect that could be validated is the forces on the suspensions' arms, using strain gauges.

Despite this aspect, it is important to say that the components didn't suffer any visible damage or sign of possible failure. The 2022 testing and competition period has been characterized by some issues on the electric side of the vehicle that didn't allow the accomplishment of the target kilometres. Regardless of this aspect, the dynamic performances and maximum acceleration reached were a record for the Team's history.

## 5.4. Setup shims and flip chip

This section is the final one related to the 2022 solution description and analysis. As already mentioned before, apart from the 2 major components (front and rear uprights), other small parts have been designed and added or modified from the 2021 assembly.

In particular, two smart solutions have been applied to enhance setup changes and to increase and refine the adjustability of the vehicle behaviour.

The first one is related to camber adjustments, this characteristic angle is vastly used to vary the balance between longitudinal and lateral grip of the prototype. A short explanation is that, by increasing the camber value (always negative in race-cars) the lateral maximum grip exerted by the tires is higher. Meanwhile, having low camber values, also  $0^\circ$  in some conditions, will help the longitudinal grip of the vehicle.

It is straightforward to understand that, for the acceleration event, the camber is set very near to  $0^\circ$ , to exploit the maximum longitudinal performances. For the skidpad event, instead, the camber values are always negative but with high magnitude, in order to promote lateral grip. For the autocross and endurance events, the setup is a compromise between the two extreme ones described before, depending on track configuration, it can be beneficial to have higher lateral or longitudinal performances.

It is often required to perform a fast setup change between two events, thus designing an efficient way to do them, is crucial. The camber angle in the SC21 and SC22 is varied by changing the distance between the upright and the UCAO point, the LCAO is maintained fixed and so the entire wheel vertical axis is hinged there.

To change the distance in a repeatable manner, calibrated shims are used. In 2021, the shims were designed in a way that the two screws, holding the UCAO bracket and the upright, had to be taken out completely. This was resulting in a long and quite complicated procedure performed necessary by two people. For 2022 the plates were redesigned to allow their removal and addition without having to unscrew the wheel assembly. This resulted in an easier and faster procedure, as desired.

Here below some self explanatory images are inserted.



*Figure 82 – Camber setup shims 2021 (left) and 2022 (right)*

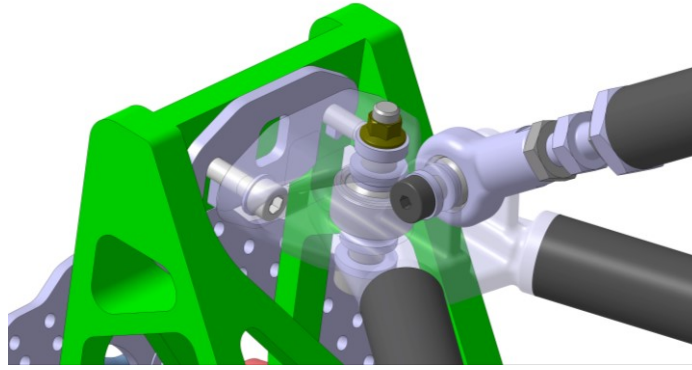


*Figure 83 – Camber setup detail*

An important change between 2021 and 2022 was the addition of the possibility to change the steering geometry characteristics.

In particular the Ackermann geometry can be now varied, passing from Anti-Ackermann, going all the way to Pro-Ackermann passing through the parallel Ackermann configuration. The steering geometry varies a lot the vehicle behaviour in turning manoeuvres; the Ackermann setup is in charge of defining the actual steering angle of each of the front wheels:

**Parallel Ackermann:** inner and outer wheel have the same steering angle

**Anti-Ackermann:** the outer wheel turns more than the inner one

**Pro-Ackermann:** the inner wheel turns more than the outer one

The choice of which configuration to use and how extreme it should be (usually in percentage of how much a wheel will turn more, in degrees, than the other one) relies on many vehicle and track factors such as: aerodynamic configuration, vehicle speed, vehicle load transfer, tire-ground friction coefficient and so on...

These changes are possible by changing the tie rod outer point, with respect to the wheel steering axis, and the length of the tie rod itself. Here below, a very simplistic graphic representation of this geometry changes is present.

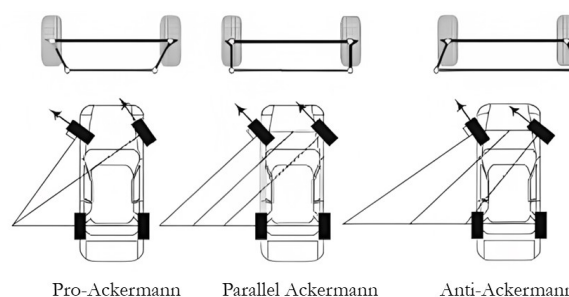


*Figure 84 – Ackermann steering geometries*

The position variation of the TIEO point needed to have small adjustments is very small, if compared to the hole needed for the correct linkage between upright and tie rod. This means that there wasn't the possibility to have numerous holes drilled directly on the upright itself, instead, a solution adopted mainly in mountain bikes damper adjustments was re-designed for the SC22. A flip chip with an off-centre hole was produced and inserted in the upright's

buttonhole. Doing so, it was possible to change the flip chips and have a near continuous regulation of the steering geometry, depending on how many pieces were produced.

Here below some CAD and real pictures of what these flip chips effectively are and were are installed in the assembly.



*Figure 85 – SC22 Flip chips*

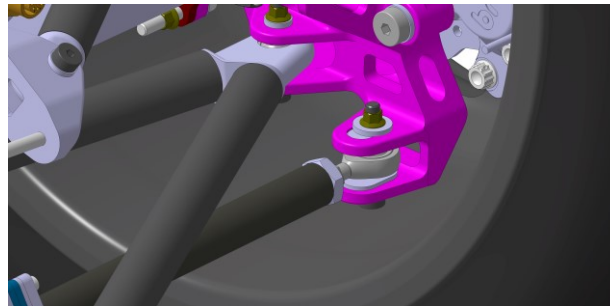


*Figure 86 – SC22 TIEO detail*

The very interesting outcome is that with a pair of flip chips, it is possible to achieve up to two configurations by simply rotating them of 180° around z-axis, as shown in the image below.

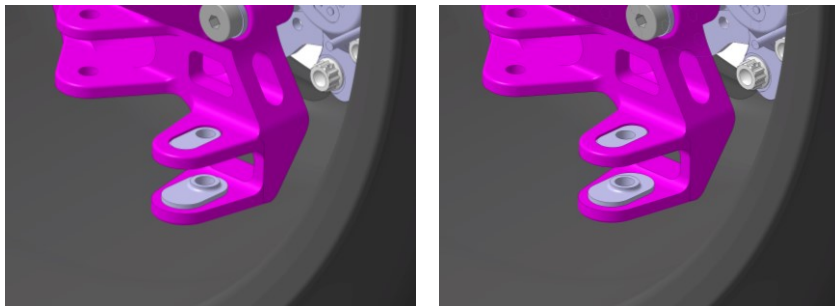


*Figure 87 – SC22 Different positions of TIEO point*

The other parameter to change, accordingly to the TIEO variation, is of course the tie rod length. If this was not the case, the entire wheel toe angle would vary a lot and the steering characteristic change would not be correct. This is done by simple calibrated shims placed on the tie rod itself, as done for the camber adjustments described before. In this work all the components related to the suspension assembly are not presented because are property of another member of the Team, the suspension designer.

## 6. Fatigue analysis

In this chapter the fatigue analysis performed is presented and discussed. Unfortunately this was not done during design phase of the components but has only been done afterwards, to have a clearer idea of parts' behaviour during testing. For the future, the team is already working on doing and integrating this type of analysis, alongside the conventional static FEM analysis, during the main design period.

Fatigue analysis is a process that focuses on understanding and predicting the behaviour of structures and components under cyclic loading conditions, it implies both the engineering's as well as material science's studies. Fatigue failure occurs when a material or structure experiences repetitive loading and unloading, leading to cracks and ultimately catastrophic failure.

Understanding and mitigating fatigue failures is crucial in industries such as aerospace, automotive, civil engineering, and many others, where components are subjected to cyclic loading throughout their operational lives. It is important to understand that, this last sentence is mainly applicable to standard automotive industry, meanwhile in motorsport world it is slightly different. Especially, speaking of Formula Student, the life of a single component is usually no more than 2/3 years and so fatigue analysis should be taken into account with the appropriate significance.

The primary goal of fatigue analysis is to estimate the number of cycles a component can endure before failure occurs and to identify critical locations prone to fatigue damage. This ensures the reliability, safety, and durability of mechanical systems, ultimately reducing the risk of unexpected failures.

Mechanical SN fatigue analysis, also known as stress-life fatigue analysis, is a widely used methodology for evaluating the fatigue performance of materials and components subjected to cyclic loading. SN refers to the S-N curve, which represents the relationship between the applied stress (S) and the number of cycles to failure (N). This analysis involves determining the fatigue strength, also known as endurance limit or fatigue limit, which is the maximum stress level that a material can withstand for an infinite number of cycles without experiencing failure.

After this brief introduction to fatigue analysis objective and theory, in the following sections there will be a deeper look at the procedure performed on the 2022 uprights.

## 6.1. Load spectrum

The first thing to do is to define the load spectrum to use. Fatigue analysis is based on a load scenario that is repeated cyclically up to the target life of the component.

To have a more realistic analysis, similar to what has been done to define the design load cases intensities, some log files coming from track testing sessions have been selected. More specifically, a single lap of the track in endurance event testing conditions has been selected, autocross event is in general more demanding but is it performed seldomly during a season. The majority of kilometres are done in these conditions, thus resulting in a logic fatigue analysis base cycle.

Here below it is inserted the satellite map of the circuit with trajectory plot and velocity colour bar.

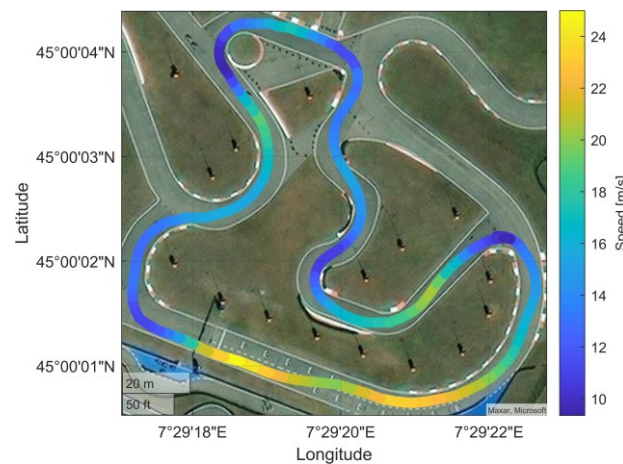


*Figure 88 – Cerrina Race Track SC22 trajectory and speed*

From the telemetry files of the vehicle, it is possible, using some MATLAB scripts to derive the forces exchanged between tires and ground surface at every logging instant; which are then used to calculate all the moments and forces acting on the upright, as already done previously for the static analysis. Unfortunately, on SC22 there are no strain gauges installed which could direct measure the forces, instead these are calculated using tires data (contained in a .tir file) and general vehicle data related to the load transfer, weight, geometry and suspension setup.

The lap is 31 seconds long and the sensors log at 100 Hz frequency, this means that one single lap will result in roughly 3100 instants, and, for each instant, a set of 3 forces ( $F_x$ ,  $F_y$ ,  $F_z$ ) per wheel are calculated.

Before to proceed with the discussion, it is important to mention that a moving average filter was applied on the forces calculated from sensors' raw data. More precisely a moving average filter has been used to clean sensors spikes and general noise. A time window of 30 instants has been used, corresponding to 0,3 seconds of delay: acceptable value, especially for this application.

For time reasons, it was decided to select the most severe wheel in terms of load spectrum and perform the fatigue analysis only on that particular upright. To do so, the resultant force was calculated at each time instant with the simple formula presented below:



$$F_{tot} = \sqrt{F_x^2 + F_y^2 + F_z^2} \quad (6.1)$$

Afterwards, for each wheel, the average value of  $F_{tot}$  has been computed.

Here below there is a figure with 4 subplots, one per wheel, containing both the raw and filtered force trend as well as the average values.

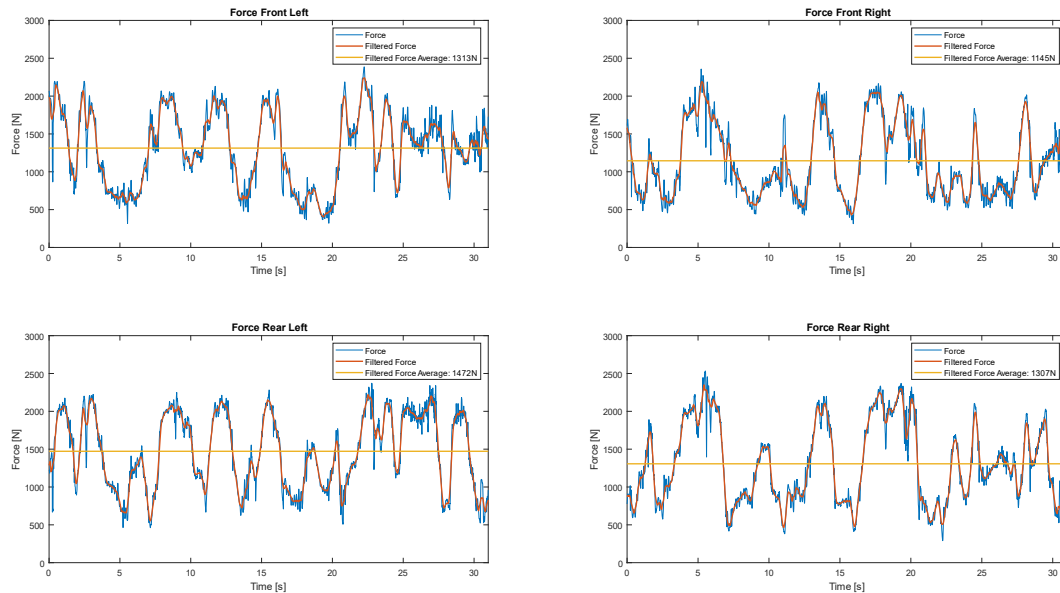


Figure 89 – Wheel forces during track test

Here a table with the filtered average force values is presented. The higher average force are present on the left side of the prototype, as expected from the track configuration. Indeed, as shown in **Figure 88**, the lap is clockwise and so the main cornering direction is right, thus, according to load transfer principles, most of the forces are shifted on the left side of the vehicle.

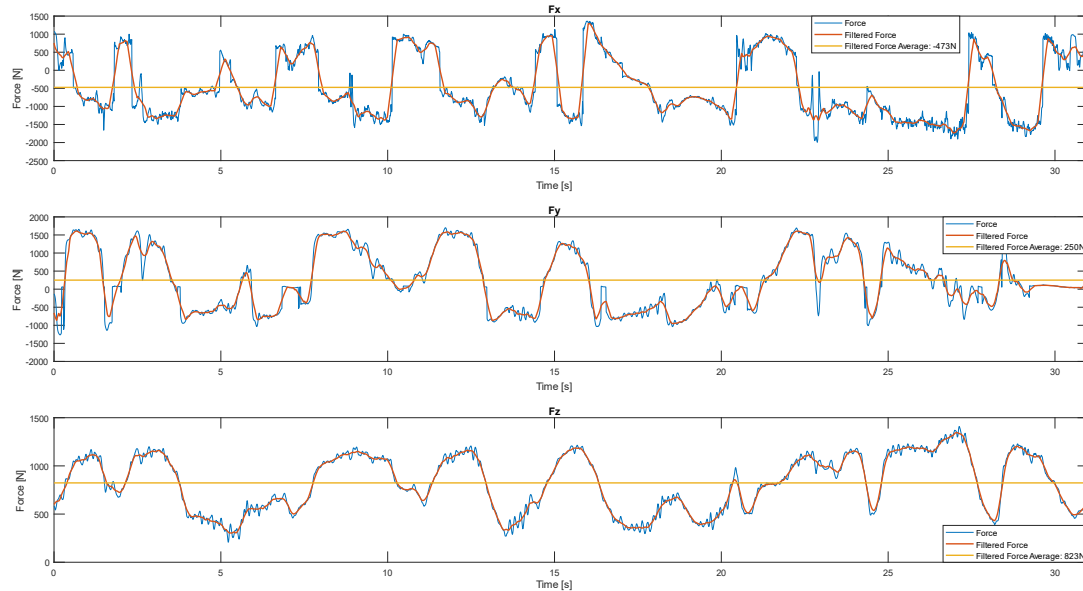
WHEELS	Filtered average force [N]
Front Left	1313
Front Right	1145
Rear Left	1472
Rear Right	1307

Table 13 – Wheels' filtered average force during track test

Between front and rear, left uprights, the choice is a little bit more tricky. It is not sufficient to compare directly the average forces but it's better to take a look also on the average forces used as input in the canonical FEM analysis and the resulting safety factor. If these last two

quantities are comparable between front and rear upright, then it is logic to choose the rear left upright as the one to perform the fatigue analysis on; as it is the case for this study.

Having chosen the upright to continue the analysis on, it is interesting to make some considerations on the single direction forces by taking a look at the figure below.



*Figure 90 – Real left upright forces during track test*

In the plots there are both the raw and filtered force trends and the average value calculated, for each direction, some points can be observed:

**$F_x$**  : the negative average value (- 473 N), indicating the presence of more severe and frequent traction phases than braking ones, can be easily explained by the fact that we are speaking of a rear wheel and so:

- Torque balance shifted to the rear and traction control mainly acting on the front axle, if needed.
- Brake bias shifted towards the front and so braking scenarios very light at the rear axle

**$F_y$**  : the average value is + 250 N and there is a visible unbalance in the force trend; mainly shifted to positive values. This is due to the track layout, as already explained, being clockwise and considering the left upright, the right turns will be more critical and frequent during a lap.

**$F_z$**  : as hoped and expected the values are always positive, meaning that the tire is never lifted from the ground. It is interesting to notice the average value (+ 823 N), which is pretty high if compared to the expected static value coming from vehicle plus driver weight. That value is explained from both the dynamic load transfer, that during traction phases is shifted to the rear as well as the downforce coming generated by aero pack. Considering the static weight balance a value around + 700 N had should have been found.

An additional consideration can be made by looking simultaneously at  $F_x$  and  $F_y$ , imagining drawing a vertical line connecting the two graphs. The relation between the two forces follows the elliptical model theory: when the lateral grip is maximum, the longitudinal one is zero and vice versa. The grip level is directly proportional to the output force, plotted in the figure. This behaviour can be seen also in the G-G-V plot of Figure 36. Here below there is the theoretical representation of this behaviour.

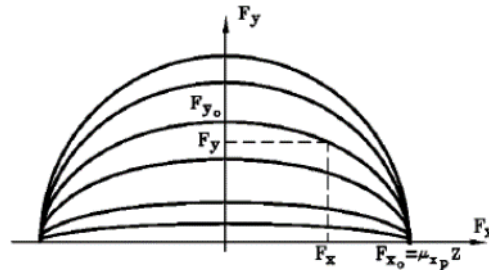


Figure 91 – Tyre elliptical model

In the next section, the setup and run of the fatigue analysis will be presented more in detail. For now, it is sufficient to say that, after having calculated transport moments, braking forces, traction torque and all the other quantities mentioned before in section 4.3, for each instant, it is needed to normalise them.

This process is easily performed on MATLAB, where each quantity's vector will be normalised with respect to its maximum value. Below, an example plot with the trace of  $F_x$ .

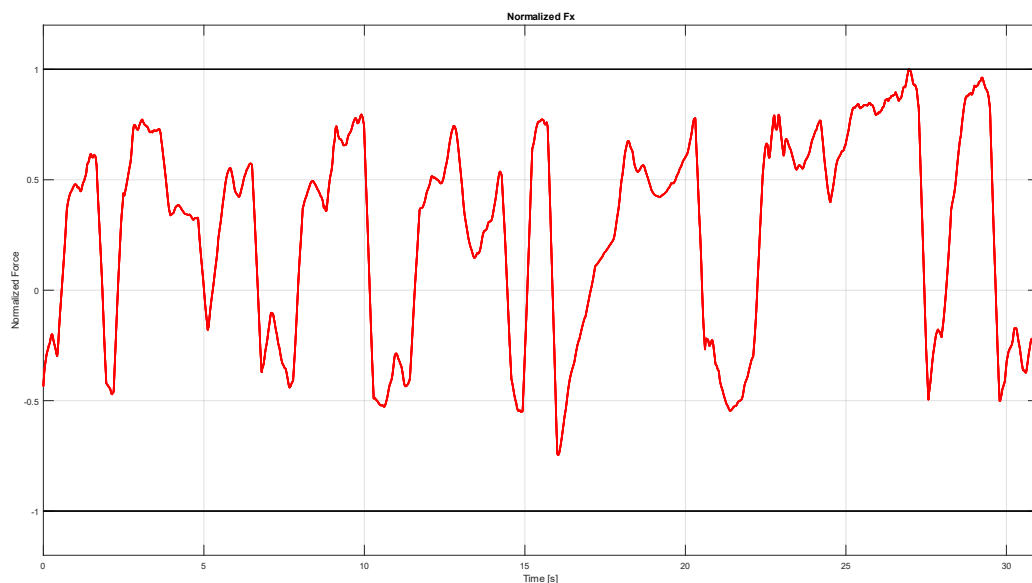


Figure 92 – Normalised  $F_x$

The last passage to be made using MATLAB is to prepare the input file for the fatigue analysis software. It has to be a .csv (comma-separated values) file, having on the first column the time instants and on the second column the normalised force values, as it can be seen on the example below.

```
0,-0.435101066190079
0.01,-0.407693512259307
0.02,-0.385917563651483
0.03,-0.368283147325908
0.04,-0.353378482475697
0.05,-0.341131307001886
0.06,-0.330215020782804
0.07,-0.320765409794729
0.08,-0.312361930348525
```

*Figure 93 – CSV example*

## 6.2. Fatigue analysis setup

In this section, the setup passages to perform a fatigue analysis from scratch will be explained. The software used is HyperLife, which is a powerful computational tool commonly employed in the field of structural analysis and durability assessment, developed by Altair, designed specifically for fatigue life prediction and optimization.

Through HyperLife it is possible to import finite element models and input load data, allowing the software to simulate the cyclic loading conditions. HyperLife then applies various fatigue analysis techniques, such as stress-life (S-N) and strain-life ( $\epsilon$ -N) approaches, to assess the fatigue performance of the structure.

The input file that is mandatory to have is an static FEM analysis similar to the one used in the design phase and already explained deeply in section 4.3. In reality, the FEM model needs to be slightly different in terms of load collectors and steps.

In the previous FEM analysis setup, there were only 5 load steps, corresponding to the 5 load case scenarios (PA, PB and so on). In each load step there were applied more load collectors, apart from the mandatory constraints (SPC), such as forces, moments, torque and so on. Instead, to correctly perform the fatigue analysis, the FEM model needs to have as many load steps as load collectors, as shown in the picture below.

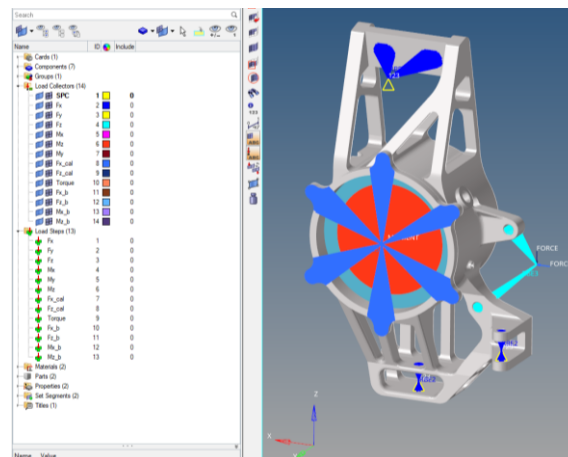


*Figure 94 – Modified FEM for fatigue analysis*

More specifically, every load step will have the SPC load collector (suspension hardpoints' constraints) and one force or moment load collector applied. The single load collectors have the maximum value of the quantity that they represent, for example the load collector named " $F_x$ " will have the value of force used for the normalisation procedure described in section 6.1. When the modified model is finished, a normal static analysis is performed using HyperMesh.

Passing now to HyperLife, the first thing to do is to upload both the FEM model and result files (.fem and .h3d) in the window below.

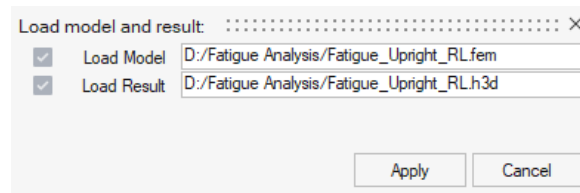


Figure 95 – HyperLife model and result loading

Afterwards, the stress life calculation method is selected, as well as some other parameters listed in the image below.

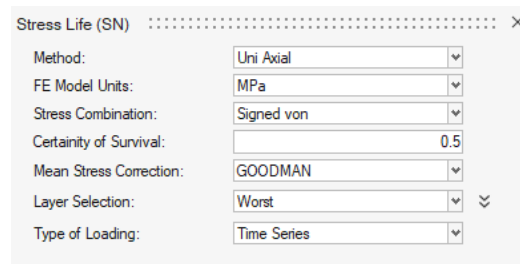


Figure 96 – Stress life (SN) setup

The method is Uni Axial because Multi Axial can't be applied to solid geometries yet in the software, units of the FE Model are MPa, and the stress combination selected is Signed Von Mises. The stress combination selected is recommended if the material is ductile, as the Aluminium alloy used. Signed Von Mises is very similar to the criterion adopted for static analysis but it adds the sign to the calculated stress, this is done because in the fatigue life calculation, it's important to know when there is a traction or compression stress state.

The Mean stress correction method chosen is the Goodman relation, this is necessary to correct the stress amplitude in relation to its mean value:

**Negative** (compression state): mean stress value ignored in the fatigue calculations

**Positive** (tension state): mean stress accelerate fatigue failure

The next step is to select the material, with its fatigue curve characteristics. As shown below, at this stage it is also mandatory to activate the fatigue calculation only for the components desired, only the uprights in this case. It is also possible to include a finish property, such as “machined” and a surface treatment, like aesthetic anodizing.

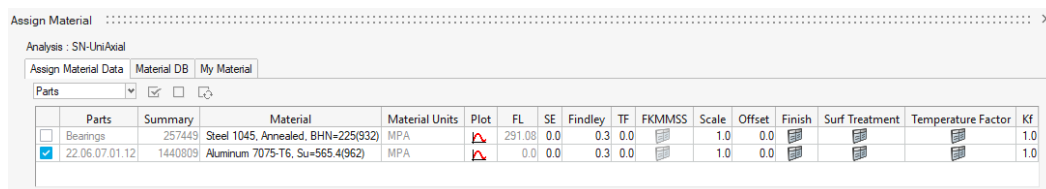


Figure 97 – HyperLife Material selection

HyperLife has a vast material library from which chose the correct one for the application, there is also the possibility to add a new material, if experimental data are available. In this case, the standard Al 7075 - T6 has been selected, here below there is a representation of the S-N curve.

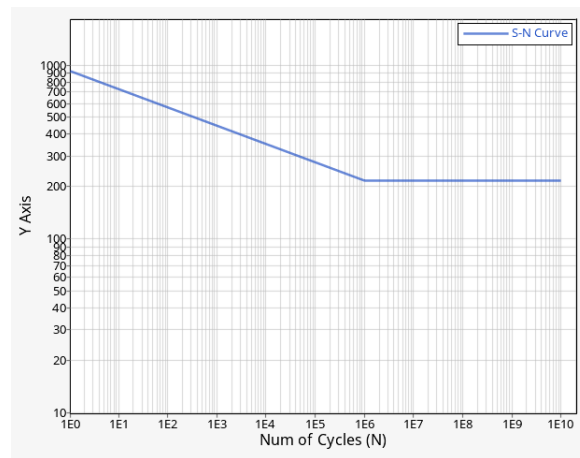


Figure 98 – Ergal S-N curve

Various studies showed that the Aluminium alloys behaviour differs a bit from steel, in terms of fatigue curve. More specifically it's not clear if the Aluminium alloys have an endurance limit, the stress amplitude limit below which, the material will never fail and have an infinite life. This is ignored by the software, which considers an endurance limit also for Aluminium alloys, as it can be seen in Figure 98. In reality, specifically for this application, this is not a problem at all because the target number of cycles life is far below the infinite life definition.

Penultimate step: load mapping. In this window it is needed to upload the .csv files prepared in the previous section, one for each load case (subcase in this software). Each file is linked to the corresponding subcase and they are all inserted in one single “Event”. This event will be the base cycle that will be repeated over and over up until fatigue failure or life target.

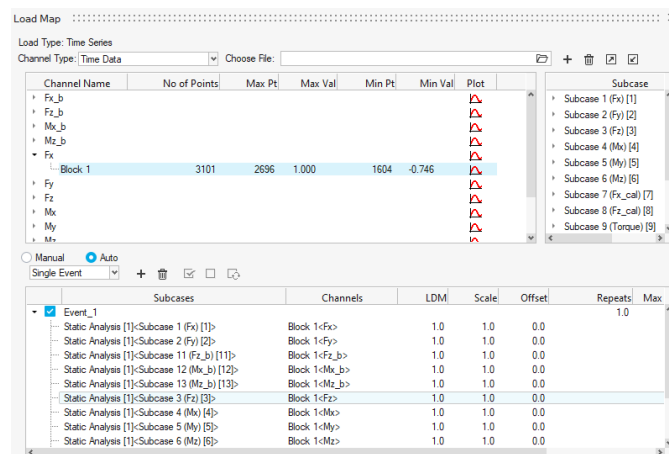
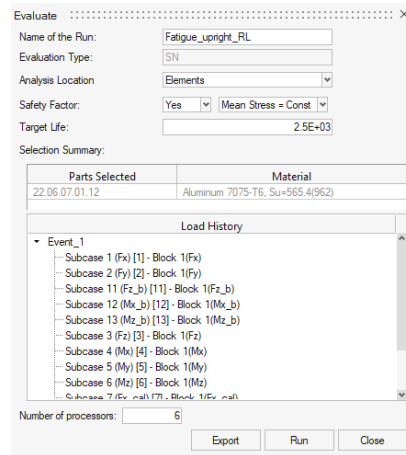


Figure 99 – HyperLife load mapping

Last step to begin the analysis, here the most important parameter to decide and set is the target life of the component. In order to enter a sensible number, it is necessary to analyse the objectives of the season and the design and production of the subsequent uprights.



Imagining to change uprights every season it is sufficient to take into account the target testing kilometres of a season and divide them by the length of the lap which was considered as base cycle. In a perfect season, 1000 km of testing is already a very ambitious target for Formula Student world. Considering a track length of approximately 450 metres, the calculated service life is 2222 cycles. Rounding up a little, the hoped target life is 2500 cycles.



*Figure 100 – Target life cycles and analysis start*

This window above is useful to check again the components' material and load history before to click “run” and starting the analysis, the results of which will be presented in the next section.

### 6.3. Fatigue analysis results

The results obtained from the fatigue analysis were really encouraging and satisfactory. In particular, at 2500 cycles, the upright didn't have quantifiable damage in fatigue terms as highlighted in the picture below.

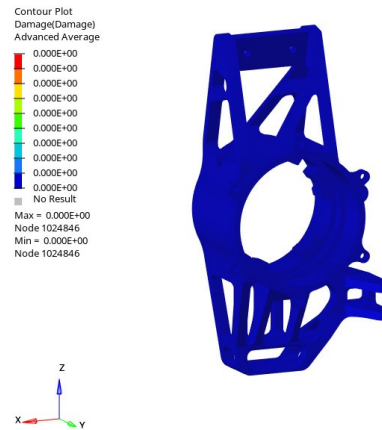


*Figure 101—Fatigue damage at 2500 cycles*

More over, the safety factor is also pretty high, with minimum value of 3,11. This is interesting also from a target setting point of view, if the uprights can sustain 2500 cycles with ease, they may be able to perform 2 or even 3 full seasons.

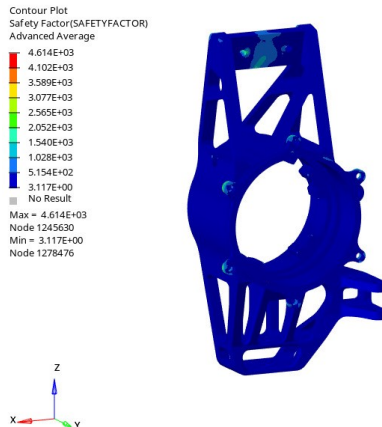


*Figure 102 – Fatigue safety factor at 2500 cycles*

Safety factor is calculated by the software based on target stress (at target life) against the stress amplitude from the working load history with a simple ratio between the two quantities; in this case, the constant mean stress method has been applied.

It has been performed another fatigue analysis by simply changing the target life, increasing it up to a million cycles, just for curiosity reasons. The results were impressive, with still no fatigue failure of the component and a safety factor of roughly 1,10. It is important to underline that, as already commented before, the material data proposed by the software are not really correct if high number of cycles are considered.

Overall, the fatigue analysis performed in this study is a good basis which needs a bit of work and deep study, especially on the material data and on the effectiveness of the software procedure and calculations.

## 7. Conclusions and future works

To conclude this thesis work it's interesting to take a fast look at the outcomes and analyse potential future works not necessary related to upright assembly.

First of all, a deep comparison between two very different production techniques has been done, additive manufacturing and CNC-milling. Each of these two has intrinsic advantages over the other one but not always it is easy to exploit them correctly. In particular, speaking of additive manufacturing, the shapes producible are really hard to design properly for a structural component such as the upright. Moreover, the upright-transmission-motor configuration of our Team's car is pretty standard and axial oriented, thus a standard production technology like CNC is already enough to satisfy these constraints. Some other teams try to take advantage of 3d printing by offsetting the motor with respect to the wheel; this is done to have a different transmission layout and lower the centre of gravity of the entire vehicle. This can be crucial for the wheel assembly itself, being an unsprung mass, it alters a lot the dynamic behaviour of the prototype.

Strictly correlated to production method, there is the choice and comparison between materials, Ergal and AlSi10Mg in this study. It was clear from the beginning that the two choices were not comparable in terms of mechanical properties and densities. The main reason that brought to the usage of AlSi10Mg for the 2021 solution was the possibility of avoiding the production costs due to a collaboration with a third party company. For sure there are better materials for both applications, especially for additive manufacturing, but the an objective of the competition is also to have a clear idea of the costs of the entire project. In particular, every decision must be justified, if, for example, a better material is chosen, and consequently the expenditure is higher, there must be a consequent and congruent increase in performance, which is directly related to the weight of the part produced for a structural element.

Interesting studies could be performed by trying to optimize and design an upright made of titanium alloy, which has incredible performances with a slightly higher density with respect to aluminium alloys. The interesting thing about titanium is that it could be both printed and machined, not without difficulties, especially on the machining process point of view, but it is possible. Another possibility is to use the Scalmalloy, which is a mix of scandium, aluminium and magnesium alloys, and has properties comparable to the ones of Ergal, but it is used in additive manufacturing.

For sure, deeper studies shall be performed about heat treatments, especially for 3d printing techniques. Many materials change drastically their properties if accurately treated, for example with a precipitation process through aging at elevated temperatures.

Speaking about FEM model and topology optimisation there are some bits that could be improved but the overall study conducted was challenging and satisfactory. The main improvement from previous years has been carried out on the model itself, on force application points and brake phases modelling for example. The transmission rigidity study is an important addition that has been made, and led to interesting results. Speaking of results, some deeper considerations can be made about mesh size and distribution, it could be interesting to try a meshing technique adopted for CFD (Computational Fluid Dynamics)

studies in which the mesh size varies a lot in relation to the geometry and position in the component. An additional load that could be inserted in the calculations is the wheel inertia, both considering the wheel itself as well as brake disc and motor rotor.

The last chapter, in which the fatigue analysis has been presented, is the one that leaves more hints and ideas for future studies. It has been one of the first fatigue analysis carried out in the team, and it showed really interesting results. The new Altair software, HyperLife, gives the possibility to perform very complicated analysis with not much effort and so, it could be possible to insert fatigue analysis into the canonical design phase process; especially for components subjected to simpler loading scenarios. For example, suspension brackets could be easily studied with a fatigue approach to lower costs and increase their carry over through seasons.

In conclusion, speaking more in general about the wheel assembly, one of the increasing trends in Formula Student is to use smaller tires and rims. Many teams are passing from 13 to 10 inches tyres. This, could set new challenges for the uprights design in terms of packaging and so, additive manufacturing could be exploited with real advantages.

# References

1. <https://www.matweb.com/>
2. <https://squadracorsepolito.com/>
3. <https://www.formulastudent.de/fsg/>
4. <https://www.primaadditive.com/it/>
5. <https://www.sciencedirect.com/>
6. [https://2021.help.altair.com/2021/hwsolvers/os/topics/solvers/os/user\\_guide\\_os\\_c.htm](https://2021.help.altair.com/2021/hwsolvers/os/topics/solvers/os/user_guide_os_c.htm)
7. <http://www.officinamassola.it/>
8. <https://www.fidelisfea.com/post/what-is-the-difference-between-a-kinematic-rbe2-and-a-distributing-rbe3-coupling-in-fea>
9. Course notes from Additive and Design for Additive - Politecnico di Torino, Department of Management and Production Engineering (DIGEP) – Prof. Alessandro Salmi
10. Course notes from Motor Vehicle Design - Politecnico di Torino, Department of Mechanical and Aerospace Engineering (DIMEAS) – Prof. Andrea Tonoli
11. Course notes from Driver Assistance Systems Design Part. B - Politecnico di Torino, Department of Mechanical and Aerospace Engineering (DIMEAS) – Prof. Nicola Amati
12. Course notes from Elements of Machine Design and Construction - Politecnico di Torino, Department of Mechanical and Aerospace Engineering (DIMEAS) – Prof. Francesca Curà
13. Hans B. Pacejka – Tyre and Vehicle Dynamics, Second Edition

# List of Figures

<b>Figure 1</b> – Formula Student Germany 2022 Panoramic Picture	8
<b>Figure 2</b> – Squadra Corse PoliTO 2005 Prototype (SC05)	10
<b>Figure 3</b> – Squadra Corse PoliTO 2009/10 Prototype (SC08H)	10
<b>Figure 4</b> – Squadra Corse PoliTO 2012 Prototype (SC12e)	11
<b>Figure 5</b> – Squadra Corse PoliTO 2022 Prototype (SC22, ‘Aurora’)	11
<b>Figure 6</b> – FSAA Award ceremony and celebration	12
<b>Figure 7</b> – Squadra Corse 2023 Team	12
<b>Figure 8</b> – Unsprung Masses 2021/22 Division	13
<b>Figure 9</b> – SC22 Unprung Masses Assembly	14
<b>Figure 10</b> – SC22 Front Wheel Assembly	14
<b>Figure 11</b> – LPBF Printing Process	18
<b>Figure 12</b> – Print Sharp 250 Prima Additive	18
<b>Figure 13</b> – DIN50125 Type A Specimen geometry	21
<b>Figure 14</b> – AlSi10Mg wrong specimens test results	21
<b>Figure 15</b> – AlSi10Mg specimen with correct rupture position	22
<b>Figure 16</b> – AlSi10Mg Stress Strain plot	22
<b>Figure 17</b> – SC21 Front upright starting volume CAD	24
<b>Figure 18</b> – SC21 Rear upright starting volume CAD	25
<b>Figure 19</b> – SC21 Front upright design and non-design space	28
<b>Figure 20</b> – SC21 Model support and connector	29
<b>Figure 21</b> – SC21 Model PA and BIT load cases	30
<b>Figure 22</b> – SC21 topology optimisation first iteration results	31
<b>Figure 23</b> – SC21 front upright geometry transition zones	32
<b>Figure 24</b> – SC21 FEM Model front and rear	32
<b>Figure 25</b> – SC21 Front Upright	33
<b>Figure 26</b> – SC21 Rear Upright	33
<b>Figure 27</b> – SC21 Front wheel assembly	34
<b>Figure 28</b> – SC21 Rear wheel assembly	34
<b>Figure 29</b> – SC21 Production process	35
<b>Figure 30</b> – SC21 Support structures	35
<b>Figure 31</b> – SC21 Front upright PB Von Mises	37
<b>Figure 32</b> – SC21 Front Upright BIT Displacement	37
<b>Figure 33</b> – SC21 Rear upright AIT Von Mises	38
<b>Figure 34</b> – SC21 Rear upright AIT Displacement	38
<b>Figure 35</b> – Upright and brake failure	40
<b>Figure 36</b> – G-G-V plot	44
<b>Figure 37</b> – Car Reference System	52
<b>Figure 38</b> – Contact patch coordinates in Car Reference System	53
<b>Figure 39</b> – CP coordinates in upright reference system	54
<b>Figure 40</b> – CP forces representation	54
<b>Figure 41</b> – RBE2 (Rigids) and RBE3 Comparison	55
<b>Figure 42</b> – Rear upright constraints	56
<b>Figure 43</b> – LCAO constraint	56
<b>Figure 44</b> – TIEO constraint	56



<b>Figure 45</b> – UCAO Bracket detail	57
<b>Figure 46</b> – UCAO constraint	57
<b>Figure 47</b> – Transmission bearings	58
<b>Figure 48</b> – Freeze contact transmission bearings	58
<b>Figure 49</b> – Bearings RBE3	59
<b>Figure 50</b> – Motorplate RBE3	59
<b>Figure 51</b> – Ring gear RBE3	59
<b>Figure 52</b> – Brake calliper RBE3	60
<b>Figure 53</b> – Bearing centre application point	60
<b>Figure 54</b> – $M_x$ and $M_z$ calculation	61
<b>Figure 55</b> – $M_y$ transport moment calculation	62
<b>Figure 56</b> – Motor torque calculation	62
<b>Figure 57</b> – Rear calliper force calculation	63
<b>Figure 58</b> – Front calliper force calculation	64
<b>Figure 59</b> – Internal braking balancing forces and moments	64
<b>Figure 60</b> – Topology optimisation shape control	66
<b>Figure 61</b> – Rear Upright Y Direction optimisation	68
<b>Figure 62</b> – Rear Upright Y Direction reconstruction	68
<b>Figure 63</b> – Rear Upright X Direction reconstruction	69
<b>Figure 64</b> – LCAO 2021/22 comparison	70
<b>Figure 65</b> – SC22 Front upright	71
<b>Figure 66</b> – SC22 Rear upright	71
<b>Figure 67</b> – Rear upright version 1 and 2 comparison (1)	72
<b>Figure 68</b> – Rear upright version 1 and 2 comparison (2)	72
<b>Figure 69</b> – SC22 Rear upright AIT load case	74
<b>Figure 70</b> – SC22 Front upright PB load case	75
<b>Figure 71</b> – SC22 Rear upright extreme braking load case	76
<b>Figure 72</b> – SC22 Front upright extreme braking load case	76
<b>Figure 73</b> – SC22 Rear upright superfast load case	77
<b>Figure 74</b> – SC22 Front upright superfast load case	78
<b>Figure 75</b> – Stress concentration around sharp edges and holes	78
<b>Figure 76</b> – SC22 SC22 Rear upright curbs (PB) load case	79
<b>Figure 77</b> – SC22 Front upright curbs (PB) load case	79
<b>Figure 78</b> – Curbs (PB) edges stress concentration	79
<b>Figure 79</b> – SC22 produced uprights	81
<b>Figure 80</b> – Front upright feature's detail	82
<b>Figure 81</b> – SC22 Wheel assemblies	82
<b>Figure 82</b> – Camber setup shims 2021 (left) and 2022 (right)	84
<b>Figure 83</b> – Camber setup detail	85
<b>Figure 84</b> – Ackermann steering geometries	85
<b>Figure 85</b> – SC22 Flip chips	86
<b>Figure 86</b> – SC22 TIEO detail	86
<b>Figure 87</b> – SC22 Different positions of TIEO point	86
<b>Figure 88</b> – Cerrina Race Track SC22 trajectory and speed	88
<b>Figure 89</b> – Wheel forces during track test	89
<b>Figure 90</b> – Real left upright forces during track test	90
<b>Figure 91</b> – Tyre elliptical model	91
<b>Figure 92</b> – Normalised $F_x$	91

<b>Figure 93</b> – CSV example	92
<b>Figure 94</b> – Modified FEM for fatigue analysis	93
<b>Figure 95</b> – HyperLife model and result loading	94
<b>Figure 96</b> – Stress life (SN) setup	94
<b>Figure 97</b> – HyperLife Material selection	94
<b>Figure 98</b> – Ergal S-N curve	95
<b>Figure 99</b> – HyperLife load mapping	95
<b>Figure 100</b> – Target life cycles and analysis start	96
<b>Figure 101</b> – Fatigue damage at 2500 cycles	97
<b>Figure 102</b> – Fatigue safety factor at 2500 cycles	97

# List of Tables

<b>Table 1</b> – Print Sharp 250 Prima Additive Technical Specifications	19
<b>Table 2</b> – AlSi10Mg Prima Additive Characteristics	19
<b>Table 3</b> – AlSi10Mg Experimental Mechanical Properties	22
<b>Table 4</b> – SC21 Detailed load cases	26
<b>Table 5</b> – SC21 FEM numerical results	38
<b>Table 6</b> – SC22 Detailed design load cases	43
<b>Table 7</b> – Load cases comparison 2021-2022	44
<b>Table 8</b> – SC22 Additional load cases	45
<b>Table 9</b> – Ergal (Al7075-T6) Chemical composition and mechanical properties	49
<b>Table 10</b> – Material comparison	49
<b>Table 11</b> – SC22 Uprights design FEM results	75
<b>Table 12</b> – Weight comparison CAD vs REAL	81
<b>Table 13</b> – Wheels’ filtered average force during track test	89

## Abbreviations

<b>FS</b>	Formula Student	<b>PA</b>	Pure acceleration
<b>SC</b>	Squadra Corse	<b>PB</b>	Pure braking
<b>g</b>	Acceleration of gravity	<b>PL</b>	Pure lateral
<b>d.o.f.</b>	Degree of freedom	<b>AIT</b>	Acceleration in turn
<b>FEM</b>	Finite Element Method	<b>BIT</b>	Braking in turn
<b>AM</b>	Additive Manufacturing	<b>E</b>	Young’s modulus
<b>R<sub>p0,2</sub></b>	Yield strength	<b>R<sub>m</sub></b>	Ultimate strength
<b>A</b>	Elongation at failure	<b>CNC</b>	Computerized Numerical Control
<b>LPBF</b>	Laser Powder Bed Fusion	<b>S.F.</b>	Safety factor
<b>UCAO</b>	Upper control arm outer	<b>LCA</b>	Lower control arm outer
		<b>O</b>	
<b>TIEO</b>	Tie rod outer	<b>PA0</b>	Pure acceleration at 0° camber
<b>CP</b>	Contact Patch		